

Development of Low-Field Flow ^{31}P NMR Spectroscopy for Reaction Monitoring in Organometallic Chemistry

Monographic dissertation

in partial fulfillment of the requirements for the degree of

***doctor rerum naturalium* (Dr. rer. nat.)**

of the Faculty for Mathematics and Natural Sciences

at the University of Rostock

submitted by

Laura Tadiello

born on 6th May 1996 in Busto Arsizio, Italy.

Leibniz Institute for Catalysis

at the University of Rostock

2024

Selbstständigkeitserklärung

Ich versichere hiermit an Eides statt, dass ich die vorliegende Arbeit selbständig angefertigt und ohne fremde Hilfe verfasst habe, keine außer die von mir angegebenen Hilfsmittel und Quellen dazu verwendet habe und die den benutzten Werken inhaltliche und wörtlich entnommenen Stellen als solche kenntlich gemacht habe.

Die vorliegende Dissertation wurde vom April 2021 bis März 2024 am Leibniz-Institut für Katalyse e.V. an der Universität Rostock unter Anleitung von Prof. Dr. Torsten Beweries erstellt.

1. Gutachter: Prof. Dr. Torsten Beweries, Leibniz-Institut für Katalyse e. V.
2. Gutachter: Prof. Dr. Björn Corzilius, Universität Rostock, Institut für Chemie

Tag der mündlichen Prüfung: 11.06.2024

Abstract

Benchtop low-field (LF) NMR spectroscopy is a valuable tool for reaction monitoring and its application in catalysis. It is particularly attractive thanks to its low-cost and portability (*i.e.*, the instrument can be installed right next to the fume hood). However, crucial quantitative results, *e.g.*, kinetic profiles, cannot be correctly determined the moment degradation of an air- and moisture-sensitive catalyst occurs. Therefore, inertness of the entire setup must be guaranteed.

In the first part of this thesis, it is demonstrated that this challenge could be overcome to meet the experimental requirements of highly oxygen-sensitive rhodium diphosphine complexes, relevant for homogeneous catalysis. Indeed, a commercially available benchtop LF NMR spectrometer has been evolved into an inert customized flow setup.

Catalytic hydrogenation monitoring *via* LF ^1H and ^{31}P NMR spectroscopy proved to be suitable with this flow setup despite the relatively low concentration of the investigated species (*ca.* 10 mM).

In the second part of the thesis, limitations due to the low magnetic field of the benchtop spectrometer (1.9 T) and the relative insensitivity of ^{31}P compared to ^1H nucleus have been faced. ^{31}P NMR signal-to-noise ratios (SNRs) have been improved using advanced pulse sequences. Sensitive Homogeneous And Resolved PEaks in Real time (SHARPER) enhances ^{31}P NMR signals by collapsing the target resonance into an extremely narrow singlet and eliminating the effects of field inhomogeneity. After demonstrating the advantage of this tool in static conditions (up to 10-fold enhancement factor on SNR), the customized *on-line* setup has been used to monitor a faster reaction (in the order of minutes), that could not be followed with traditional ^{31}P NMR sequences.

Acknowledgements

Thanks, Torsten, for your non-stop support. You helped me from the very beginning, when I was struggling with the new language and facing disappointments from experiments that, let's say, "were supposed to work". You continued to help me till the very end, always keeping your door open and being available for any questions or problems of mine. You always listened my ideas, even to the most bizarre ones (remember the sticky notes trick?) and you allowed me to pursue my callings. You, as great leader that you are, knew when I needed your direct assistance but also when I needed your trust, that I could take responsibility and deal with it on my own. In this way, I felt understood and strongly motivated to give back to you. These three years with you have been such an amazing journey. Please, keep motivating others like you did with me!

Thanks to Hajo. Thanks for your suggestions on how to get crystals suitable for X-ray and analysing them. Thanks for helping me out with German, especially at the beginning when my "luggage" contained only a couple of simple words... Danke, Bitte and Prost! Thanks for bringing the group together every year around Christmas time for a full afternoon. On these occasions, you taught me how to fold a German paper star as well as the basics of crochet. This helped me a lot when I found myself stressed at home. I could create some cute puppets for my nephew, relax and lift my spirit.

Thanks to Meghan. I know I was only three months there in UK, but I really appreciated your love for teaching. You reminded me how passionate a researcher can be. Programming has never been my strength, but I have learned so much from you and I am very grateful.

Thanks to Dr. Baumann for taking your time for my questions, it means a lot to me. As I have already told you, only by standing next to my poster at a conference I was asked about you. They recognized your $^{31}\text{P}\{^1\text{H}\}\text{-}^{103}\text{Rh}$ HMQC NMR experiment by a quick glance at it. Your expertise is recognized by the NMR community, so please, never forget how valuable you are.

Thanks to Fabian and Jonas. Fabian, you started a full internal lectures series out of nothing because I was asking you questions about DFT. I was fascinated by how this "new world" works and, despite I had no background knowledge on it, you taught me how to analyse some of my complexes. Jonas, I was moved by pure curiosity when I approached you and you were so kind and flexible to even change your course to English to allow me to follow. So much appreciated!

[DEU] Danke an meine gesamte Gruppe. Danke an Nora für die großartige Atmosphäre im Büro und deine nützlichen Tipps. Danke an Carmen für dein ständiges Lächeln! Es ist

unmöglich, jeden Tag gute Laune zu haben, aber mit deiner Einstellung ist es viel einfacher. Danke an Conny für deine Unterstützung im Labor, die Bereitstellung von Komplexen und die immer sehr schnelle Auffrischung trockener Lösungsmittel.

[DEU] Vielen Dank an das gesamte technische Personal des LIKAT. Vielen Dank vor allem an Matthias für die Erstellung des perfekt passenden Glasadapters und Andreas für die Unterstützung beim Bau des Strömungssystems.

Thanks to all LIKAT, with all my heart. Thanks to the analytical team, the purchasing team, human resources, and everyone else that contributed. Yes, as PhD representative I wanted to improve our institute even more, but LIKAT is already so great! I remember my first time here in Rostock, as a master student in Erasmus, fascinated by the high expertise we have in house and by the quality of the equipment (even by how white the corridors are!).

Thanks to the Deutsche Forschungsgemeinschaft (DFG) for funding my research.

Thanks to the University of York (UK) for hosting me for my three-months traineeship. I could improve the analysis on the benchtop spectrometers available there and bring back the knowledge to Rostock to apply it to our setup. On top of that, the whole experience of being in UK, in a very different atmosphere, helped me in my personal development.

Thanks to the University of Rostock and to the Graduate Academy of Rostock. I could learn German, at least at basic level, and start to feel integrated in a place far away from home. I could develop my soft skills, skills that I completely underestimated years ago. At conferences, I realised that some people have a great topic and fascinating results but because of their poor communications skills, their message does not reach the audience. This gave me the reason to improve my presentation skills, but I would have never been able to do that alone, without a great institution that offers such inspiring courses.

Thanks to the people I met people at conferences that gave me inspiration and motivation. Only being there helped me to open my mind, think differently and approach problems I was facing in the lab with a different perspective. Getting slots for orals, boosted my learning in a way I could not have imagined.

Thanks to Magritek for the support on the spectrometer. Thanks to Sanel for helping me with the first steps of setting up the spectrometer and later suggesting me the most suitable additional

package for my application. Thanks to Craig for the training on Spinsolve Expert and for your assistance with my requests (probably a bit too annoying, sorry!) about the PSYCHE sequence.

Thanks to HNP for assistance on the pump. Thanks to Carsten for being so excited about my paper on the setup evolution! We have not managed yet to couple the pump with the spectrometer in the way we wished but thank you very much for trying.

Thanks to my love, Richy. I often felt overwhelmed, getting too emotional and close to explode. Some days I just kept going down a deeper and deeper spiral, without even remembering what my trigger was. Every time you were there, at my side, giving me the strength to fight and the motivation to heal. I am so glad my initial plan to do my PhD in Italy did not go through. Staying here with you has given me so much more. I would have never felt so independent living abroad, but at the same time still extremely dependent from the people that really matters to me. I am so immensely grateful to you.

[ITA] Grazia alla mia famiglia per il sostegno incondizionato. Grazie nonna Carla per la tua passione, quella instancabile voglia di dare il meglio di te, per la tua immensa "grinta"! Grazie Luci per essere stato e per essere sempre uno splendido esempio per me. Grazie papi per esserti preso cura della mia educazione, anche se spesso non te l'ho riconosciuto.

[ITA] Grazie a miei cari amici, ai vecchi amici di infanzia, a quelli che ho conosciuto qui a Rostock e in Inghilterra. Grazie a Fabio per essere sempre così intrigante nei tuoi discorsi e per invitarmi in tutti queste belle serate per conoscere nuova gente. Grazie ad Andrea per avermi aiutato un sacco nei miei primi mesi qui a Rostock, presa dalle pratiche burocratiche e un po' persa fra l'ammettere di aver perso tanti cari amici e il trovarne di nuovi. Grazie a Barbara per avermi ospitato a York, per essere sempre piena di vitalità e per dividerla con le persone che ti circondano. Grazie a Leo per non aver mai smesso di credere in me e farmi ridere. Grazie a Dona e Ayaj per ricordarmi che qualche volta ci si deve lasciare andare e divertirsi. Grazie a tutti gli amici, lontani e vicini!

Table of contents

Abstract	v
Acknowledgements	vii
Table of contents.....	xi
List of abbreviation	xv
1. Introduction.....	1
1.1. Low-field vs high-field spectrometers	2
1.1.1. Applications of low-field spectrometers.....	3
1.1.2. Sensitivity loss of low-field spectrometers.....	4
1.2. Reaction monitoring	5
1.2.1. True and effective relaxation times.....	6
1.2.2. In-flow and out-flow effects	6
1.3. Phosphine ligands in catalysis	8
1.3.1. Phosphine ligands in catalytic hydrogenation	8
1.3.2. NMR analysis of phosphine complexes	8
1.3.3. NMR analysis of rhodium diphosphines complexes	9
1.4. Signal enhancement	11
1.4.1. SHARPER sequence.....	11
1.4.2. Selective SHARPER (sel-SHARPER)	12
1.4.3. Calibration of selective pulses	13
1.4.4. Multi resonance SHARPER (MR-SHARPER)	14
1.4.5. Pure shift methods	15
1.4.6. Transverse encoding	15
2. Objectives	17
3. Results and Discussion.....	19
3.1. Pathway to inertness – Setup evolution	20
3.1.1. First generation setup.....	20
3.1.2. Oxidation	21
3.1.3. Second generation setup	23

3.1.4. First step to inertness	24
3.1.5. Stepwise addition.....	26
3.1.6. Third generation setup	28
3.1.7. Inertness.....	30
3.2. Reproducibility – Setup details	32
3.2.1. Temperature remarks	34
3.3. Mass transfer – Flow vs static conditions	37
3.4. Limitations – High multiplicity signals	40
3.5. Catalysis – Styrene hydrogenation.....	46
3.6. Signal enhancement – SHARPER ³¹ P NMR sequence	50
3.6.1. Pulse calibration	54
3.6.2. Single-component solution <i>via</i> SHARPER	56
3.6.3. Simulated two-components solution <i>via</i> MR-SHARPER	57
3.6.4. Two-components solution <i>via</i> MR-SHARPER	58
3.6.5. Reaction monitoring <i>via</i> MR-SHARPER.....	60
3.6.6. Simulated two-component solution in flow conditions <i>via</i> MR-SHARPER.....	63
3.6.7. Reaction monitoring in flow conditions <i>via</i> MR-SHARPER.....	65
4. Summary and Outlook	67
5. Appendix.....	69
5.1. General remarks.....	69
5.2. General procedures	71
5.3. Phase cycling lists	72
5.4. Macros remarks.....	73
5.5. Macro of SHARPER sequence with NOE.....	74
5.6. Macro of sel-SHARPER sequence with NOE	85
5.7. X-ray structure determination	96
5.8. <i>On-line</i> registration of gas consumption under isobaric conditions.....	98
5.9. Additional HF NMR spectra in static conditions.....	100
5.10. Parameter screening – Presaturation power	103
5.11. Parameter screening – Echo time.....	105

5.12. Parameters screening in flow conditions	106
5.13. Additional LF NMR spectra in static conditions	110
5.14. Additional parameters of SHARPER and traditional ^{31}P NMR spectra	111
5.15. Academic Curriculum Vitae	115
6. References	117

List of abbreviation

1,2-DCE	1,2-dichloroethane	NOE	nuclear Overhauser effect
acac	acetylacetonate	PFG	pulse field gradient
BINAP	2,2'-bis(diphenylphosphino)- 1,1'-binaphthyl	pgo	pulse gated overheat
<i>ca.</i>	<i>circa</i> (around, about)	Ph	phenyl
CL	chunk length	ppm	parts per million
COA	cyclooctane	PSYCHE	pure shift yielded by chirp excitation
COD	1,5-cyclooctadiene	PTFE	polytetrafluoroethylene
COSY	correlation spectroscopy	Py	pyridine
Cy	cyclohexyl	r.t.	room temperature
DCM	dichloromethane	RF	radio frequency
DIPAMP	1,2-bis[(<i>o</i> - methoxyphenyl)(phenyl) phosphino]ethane	rxLat	receiver latency
DMSO	dimethyl sulfoxide	SC-XRD	single crystal x-ray diffraction
DPPB	1,4-bis(diphenylphosphino) butane	SHARPER	sensitive homogeneous and resolved peaks in real time
<i>e.g.</i>	<i>exempli gratia</i> (for example)	SNR	signal-to-noise ratio
ET	echo time	SPFG	single pulsed field gradient
FID	free induction decay	SS	stainless steel
FWHM	full width at half maximum	T	temperature
HF	high-field (spectrometer)	T_1	spin-lattice relaxation time
HMQC	heteronuclear multiple bond correlation	T_1^*	effective spin-lattice relaxation time
<i>i.e.</i>	<i>id est</i> (that is)	T_2	spin-spin relaxation time
ISTD	internal standard	T_2^*	effective spin-spin relaxation time
J	coupling constant	UV-Vis	ultraviolet-visible (spectroscopy)
LF	low-field (spectrometer)	<i>vs</i>	<i>versus</i> (compared with/as opposed to)
MeOH	methanol	δ	chemical shift
n.a.	not available		
NBD	norbornadiene		
NMR	nuclear magnetic resonance (spectroscopy)		

1. Introduction

Nuclear magnetic resonance (NMR) spectroscopy was first observed by Felix Bloch and Edward Purcell in 1946. For their discovery, they were awarded the Nobel Prize in Physics in 1952. Since then, NMR techniques have been continuously under development. Progress has been made in terms of multi-nuclear and multi-dimensional analysis, solvent suppression methods, high-throughput screening as well as user-friendly software.

NMR spectroscopy proved to be a versatile, non-destructive, technique. Indeed, it is a valuable tool in drug discovery as well as food science. For example, labelling experiments allow to characterise a protein while relaxation experiments allow to determine its binding to a target ligand.¹ The coupling of NMR methods with multivariate statistical analysis improved analysis of foods, complex heterogeneous matrices that are subject to adulteration.²

As an advanced analytical technique, NMR spectroscopy offers unique information to a chemist. It allows to elucidate complex macromolecules structures, identify, and quantify species in solution. Reaction monitoring experiments and characterisations of products of chemical reactions has been the focus of this thesis.

1.1. Low-field vs high-field spectrometers

High-field (HF) NMR spectrometers have a magnetic field higher than 7 T. Nowadays, instruments of about 300 or 400 MHz are commonly referred to as “middle-field spectrometers”. This trend is aligned with the advance in technology that made possible to reach higher and higher fields (*i.e.*, ultrahigh-fields, with a field strength over 1 GHz).³ These developments were driven by the need for high-resolution analytical techniques in the fields of analytical chemistry, biochemistry, and structural biology. HF spectrometers offer higher resolution, reducing issues with field homogeneity while changing temperature, and higher availability for different nuclei. Moreover, advanced pulse sequences^a are more commonly used on HF spectrometer, even though there is an increasing interest to extend those to lower fields. Drawbacks are mainly due to elevated upfront and maintenance costs of the large cryogen cooled superconductors. Additionally, the current worldwide helium shortage could determine the future application of these devices. Technologies have been developed to allow helium recapture, but further developments need to follow.

Low-field (LF) spectrometers has been defined with different ranges but in this thesis I refer to field strengths between 43 and 100 MHz (from 1 to 2.35 T).^{4,5} They are often called “benchtop spectrometer” because of their portability,⁶ which allows for example to set the spectrometer right next to the chemical reaction setup (*e.g.*, in a fume hood) or as part of larger automated reaction setups.⁷ They are much cheaper than the corresponding HF spectrometers, both in terms of upfront cost as well as maintenance. They are characterised by a permanent magnet and therefore do not require any cooling agents like liquid nitrogen or liquid helium. Those benefits improved the accessibility and broadened the range of applications in research and industry. Inherent challenges of LF NMR systems consist in drop in sensitivity and loss of chemical shift resolution, when compared to the HF NMR spectrometers.

The schematic illustration below highlights advantages and disadvantages of the different fields in NMR spectroscopy (Figure 1).

^a A pulse sequence is a set of radio frequency (RF) pulses applied to a sample to produce an NMR signal.

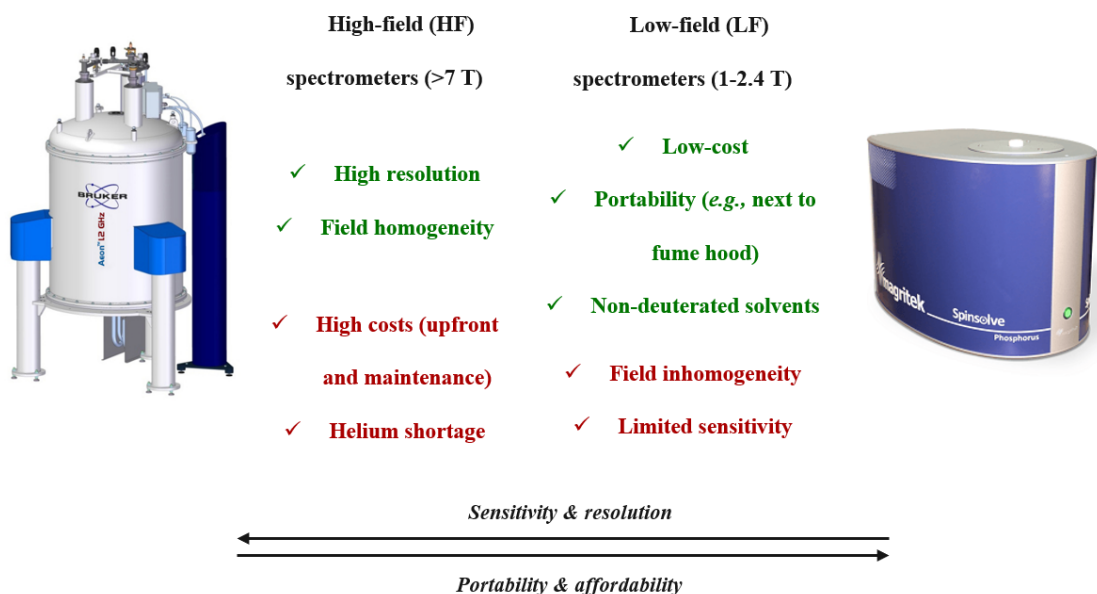


Figure 1. Simplified comparison between HF and LF spectrometers. Two devices from different suppliers (Bruker and Magritek) are shown as examples.

Non-deuterated solvents are more cost-effective than their deuterated counterparts. This is even more pronounced for *on-line* reaction monitoring, which requires significantly more solvent (about 5 mL for the herein described flow setup) than the classic amount that is used to fill a standard NMR tube (about 0.5 mL for a tube with a diameter of 5 mm). However, non-deuterated solvents typically generate broad and intense peaks in ^1H NMR that cause overlap with the desired signals of the analyte. Well established solutions,^b like presaturation^{8,9} or techniques based on gradients¹⁰ have been developed to overcome this issue. Fewer examples, but growing in number, has been specifically tested on benchtop spectrometers.¹¹

1.1.1. Applications of low-field spectrometers

LF spectrometers are mainly used for process control, after extensive studies have been conducted on HF instruments and the reaction under analysis has been already understood. Other applications include quality control and teaching purposes.^{12,13} More rare but relevant discoveries have been made using LF spectrometers in flow chemistry¹⁴ and lab automation.^{7,15} Even more limited are studies on heteronuclei such as ^{13}C , ^{19}F , or ^{31}P via LF NMR spectroscopy.^{16,17,18}

Temperature is key for many catalytic reactions, *e.g.*, to obtain selectively the desired product completely blocking an unwanted side reaction. However, temperature control is still considered a limitation for LF spectrometers. They mainly operate at room temperature (usually defined around 20–22 °C),¹⁹ but increasing efforts have been made to overcome this problem. There are

^b Presaturation is one of the most used solvent suppression methods, thanks to its simplicity and robustness. Thanks to a weak RF irradiation, it allows a full utilisation of the receiver dynamic range and therefore the analysis of the diluted analyte of interest.

a few commercially available benchtop spectrometers with an adjustable temperature capability. This technology allows reaction monitoring in a temperature range between 25 and 60 °C. However, they are defined as adjustable temperature spectrometers instead of variable temperature ones for a relevant reason: the magnet requires a relatively long equilibration time, when compared to HF spectrometers.

1.1.2. Sensitivity loss of low-field spectrometers

The sensitivity is a measure of the spectrum quality. It is related to the intensity of the observed signal, characterised by signal-to-noise ratio (SNR), which compares the level of the desired signal to the level of the background noise. Sensitivity should not be confused with resolution, correlated to the full width at half maximum (FWHM), or dispersion, which defines the separation of the signals.

The drop in sensitivity from HF to LF magnets is relevant and should always be taken into consideration before choosing the field. For example, changing the magnetic field from 400 MHz to 80 MHz results in a 11-fold loss in SNR.^c This is also aggravated by the active region consideration, which depends on the geometry of the coil^d of the spectrometer and can bring approximately 3-fold loss in SNR. SNR is further reduced moving from proton to heteronuclei, due to the lower magnetic field experienced (when comparing the same magnet), and moving from a singlet to a multiplet, due to the scalar couplings.

Those limitations are intrinsic for the LF spectrometers and cannot be changed, but it is possible to modify the conditions of the NMR experiment to enhance SNR in several ways. For example, increasing the concentration of the analyte or acquiring 2D NMR data will produce spectra with good SNR and provide a deeper understanding of the system of interest. To enhance the SNR in the present work, I decided to take advantage of advanced pulse sequences (please refer to [Chapter 1.4](#) and [Chapter 3.6](#) on signal enhancement).

^c The SNR is proportional to the square root of the cube of the magnetic field. This means that, for a 400 MHz spectrometer, the SNR is proportional to 8000. For an 80 MHz spectrometer, the SNR is proportional to 716. Finally, dividing 8000 by 716, the factor of 11 is obtained.

^d A coil is a wire through which current passes, thereby generating a magnetic field.

1.2. Reaction monitoring

Chemists are typically interested in understanding reaction mechanisms. Especially in the field of catalysis, it is important to understand the key steps of catalytic processes such as catalyst speciation, involving activation of the precatalyst, substrate coordination, product formation, and catalyst deactivation. The collection of data over time is thus an essential tool for understanding a catalytic transformation. Based on these data, it is possible to optimize catalytic reactions in order to ultimately contribute to more economically and ecologically viable processes. For an efficient and meaningful reaction monitoring it is desirable to conduct the analysis close to, or directly at the site of, the chemical transformation.

In general, *in situ* monitoring allows to insert the probe into the reaction vessel. In contrast, *off-line* monitoring analyses the sample after sampling. As a variation, *on-line* monitoring connects the reaction vessel directly with the analytical instrument: an aliquot of the reaction mixture is circulated between the external reaction vessel and the spectrometer (Figure 2).²⁰ In particular, our customized setup (Chapter 3.1) is characterised by a Schlenk flask (under the fume hood) from which the reaction solution is transferred *via* a pump into the NMR spectrometer, and back. To complete the flow setup a filter is inserted before the pump to protect the latter from clogging and a flow cell is inserted into the spectrometer to allow circulation of the reaction solution.

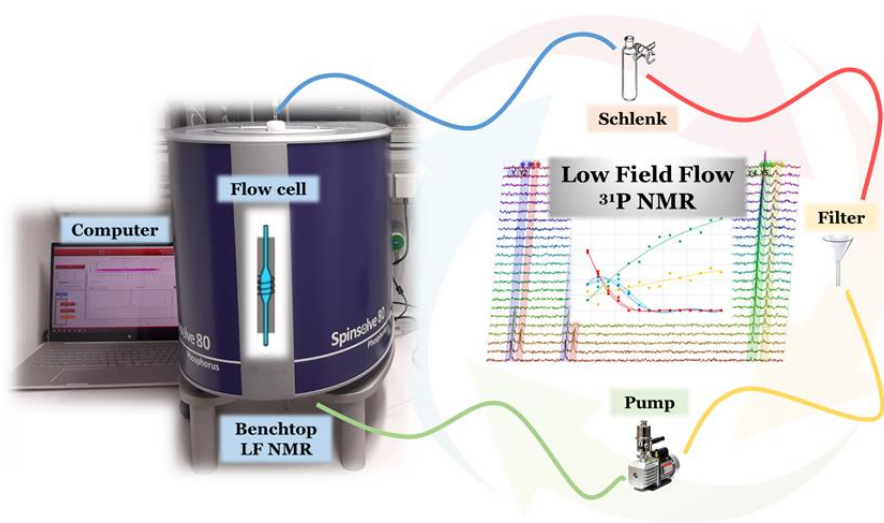


Figure 2. Schematic representation of our customized setup for low-field flow NMR monitoring.

NMR reaction monitoring is typically performed *in situ* (*i.e.*, inside the spectrometer and in static conditions) or *off-line*. Mass transfer²¹ is the main problem with the first choice while the second suffers from delays, which are not good for obtaining meaningful kinetic information and might cause alteration of the sample (*e.g.*, exposure to light, additional deuterated solvent, different temperature, solid precipitation). *On-line* NMR monitoring overcomes those limitations, and it is applicable to a wide range of conditions (*e.g.*, heating, cooling, inert or

reactive gas atmosphere).^{22,23} Homogeneous catalysis has particularly taken advantage of application of *on-line* techniques,^{24,25} despite the remaining challenges (Chapter 1.2.2),

1.2.1. True and effective relaxation times

The spin-lattice relaxation time (T_1) is also called longitudinal relaxation time because it describes the recovery of the Z component of the magnetization.^e The energy absorbed from the pulse is transferred to the surroundings (*i.e.*, the lattice). T_1 depends on different parameters, *e.g.*, concentration, temperature, and magnetic field. By using the inversion recovery method, it is possible to determine the true T_1 .^f However, in flow conditions the true T_1 becomes shorter, and it is called “effective T_1 ” (or T_1^*).²⁶ An increase in flow rate leads to decreased residence time (the time spent by the analyte inside the flow cell) and therefore a decreased T_1^* . A shorter T_1^* is both an advantage and a disadvantage: it allows to perform a faster NMR experiment, but the relaxation will be faster and therefore a lower SNR will be obtained. Paramagnetic relaxation agents, which further decrease the T_1 , have been added in some cases of reaction monitoring to allow faster acquisition.²⁷

The spin-spin relaxation time (T_2) is also called transverse relaxation time because it describes the decay of the magnetization within the transversal plane (*i.e.*, the XY plane). T_2 decreases too at higher flow rate. The impact of the flow rate on the “effective T_2 ” (or T_2^*), is sometimes considered minimal with respect to the one derived from instrumental limitations.²⁴ Such limitations are caused by the inhomogeneity of the field generated by the magnet as well as by the presence and the positioning of the flow cell inside the spectrometer in a non-symmetric way.

1.2.2. In-flow and out-flow effects

The integrals (and with them, the SNRs) of a nucleus of interest decrease going from static to flow conditions because of flow effects.²⁴ This effect is stronger in the case of nuclei like ^{31}P and ^{13}C when compared to ^1H and ^{19}F because of the longer T_1 (Figure 3). The schematic view shown here is for a HF spectrometer with the flow going from top to bottom through the instrument. The investigations of this thesis have been conducted using a LF spectrometer with flow in the opposite direction, but the same principles apply. Outside of the magnetic field, the spins have random orientation (A). Entering the magnetic field, they start to align along the Z axis, leading to a non-zero overall magnetization (B). In the designed probe area, the spins are

^e In an NMR spectrometer, the field is typically applied along the Z axis. Perpendicular to this axis, there is the XY plane, where the transmitter coil and the receiver coil are placed.

^f The inversion recovery method starts with a 180° pulse which rotates the Z magnetisation down to the $-Z$ axis. The magnetisation relaxes and returns toward equilibrium along the $+Z$ axis. Before it reaches equilibrium, a 90° pulse rotates the longitudinal magnetisation into the XY plane. After repeating multiple times this sequence changing the time between the 90° and the 180° pulses, T_1 can be determined.

fully influenced by the magnetic field (C). The higher the flow rate and/or the longer the T_1 of the nucleus, the smaller will be the integral. In both cases, there will be less time for a full build-up of the magnetization along the Z axis and therefore the detected signal along the XY plane will be smaller.

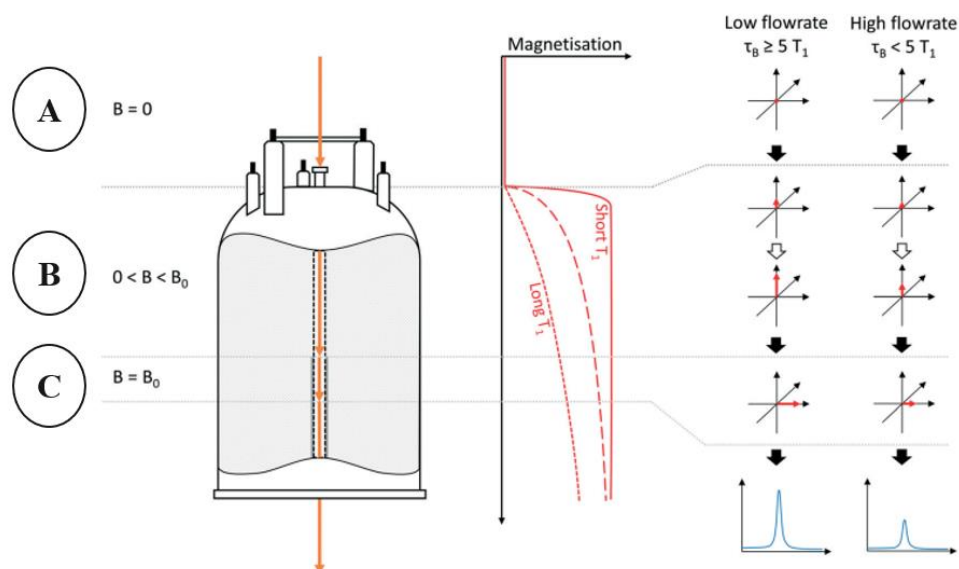


Figure 3. Flow effects, as explained by the Hintermair group.²⁴ Three sections (A, B, C) are schematically divided according to the field experienced by the nuclei during the NMR experiment in flow conditions.

Incomplete pre-magnetization produces in-flow effects. Out-flow effects are instead due to the constant refreshing of the sample. Indeed, nuclei that have been already subjected to the pulse sequence and therefore have an overall magnetization in the XY plane are constantly mixed with new sample that have just entered the magnet, with an overall magnetization along the Z axis. Both in-flow and out-flow effects cause integral loss.

Finally, there might be inhomogeneity in the magnetic field due to gas bubbles, introduced for example by stirring too fast the reaction mixture, by gas evolution caused by the reaction itself or by introducing gas as reactant (*e.g.*, in hydrogenation reactions).²⁸ In the last case, the solubility of the hydrogen in the selected solvent must be considered as well.²⁹

1.3. Phosphine ligands in catalysis

Catalysis improves reactions in term of reaction speed, reactivity and/or selectivity. Transition metal complexes are commonly used as catalysts in homogeneous catalysis and often rely on phosphorous-based ligands. Ligands play one or more key roles: stabilise the metal center, guarantee solubility of the complex, tune the reactivity through steric and/or electronic factors, actively participate in catalysis as proton shuttles or as labile ligand. Among others, phosphine ligands, tuned in highly different ways, have been applied in homogeneous catalysis and keep being developed nowadays.³⁰

1.3.1. Phosphine ligands in catalytic hydrogenation

Hydrogenation catalysts are fundamental tools in chemical synthesis. One of the milestones is the development of chlorido-tris(triphenylphosphine)-rhodium, $[\text{Rh}(\text{Cl})(\text{PPh}_3)_3]$, also called Wilkinson's catalyst (Nobel prize in 1973), for the hydrogenation of terminal alkenes (Figure 4A).³¹ Later, diphosphine-rhodium-diolefin complexes of the type $[(\text{PP})\text{Rh}(\text{diene})]^+$ (PP = bidentate phosphine) known as Schrock-Osborn catalyst has been introduced (Figure 4B).³² Among other findings, norbornadiene (NBD) has been shown to be reduced more rapidly than 1,5-cyclooctadiene (COD). Highly substituted olefins could have not been hydrogenated by the two previous catalysts, but Crabtree's catalyst, an Ir(I) complex of the type $[\text{Ir}(\text{pyridine})(\text{diolefin})(\text{PR}_3)]^+$, significantly broadened the scope (Figure 4C).³³ Later, the unique properties of the 2,2'-bis(diphenylphosphino)-1,1'-binaphthyl (BINAP) ligand have been discovered by Noyori and Takaya in 1980 (Figure 4D).³⁴ This C_2 chiral diphosphine is an essential part of the Noyori's catalyst (Nobel prize in 2001), which allows asymmetric hydrogenation of polar bonds.³⁵

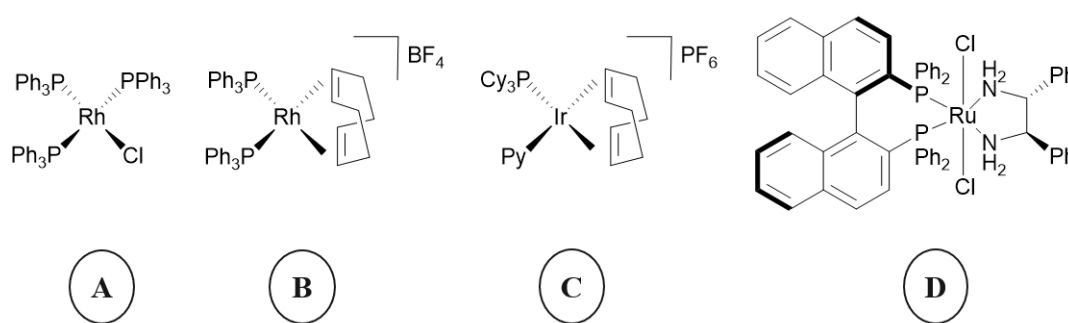


Figure 4. Key catalysts for catalytic hydrogenation: Wilkinson's catalyst (A); Schrock-Osborn catalyst (B); Crabtree's catalyst (C); Noyori's catalyst (D). Only one isomer is shown for simplicity.

Abbreviations contained in the depicted structures: phenyl (Ph); cyclohexyl (Cy); pyridine (Py).

1.3.2. NMR analysis of phosphine complexes

Phosphine complexes are typically air- and/or moisture-sensitive and therefore anaerobic conditions for reaction monitoring must be guaranteed. Standard analytical devices (*e.g.*, mass spectrometers)^{36,37} have been modified to meet the requirements of organometallic compounds.

^{31}P NMR spectroscopy can clearly analyse ligands containing ^{31}P nuclei. Therefore, it is possible to follow transformations such as ligand displacement and ligand oxidation, observing catalyst activation and deactivation processes. Once the complex degradation is understood, the reaction conditions can be adjusted in order to prevent it. As an example, HF ^{31}P NMR spectroscopy is considered a routine method for hydrogenation and hydroformylation reactions catalysed by metal-phosphine complexes and there are various examples in reaction monitoring.³⁸

1.3.3. NMR analysis of rhodium diphosphines complexes

Rhodium diphosphine complexes can be investigated *via* NMR spectroscopy analysing different nuclei.

Proton is a 99.98% abundant, spin half and the most sensitive nucleus in NMR spectroscopy (Figure 5). Immense research has been devoted to this nucleus. However, without using sophisticated pulse sequences, signal overlap remains a major challenge, especially for complex organic structures and biomolecules.

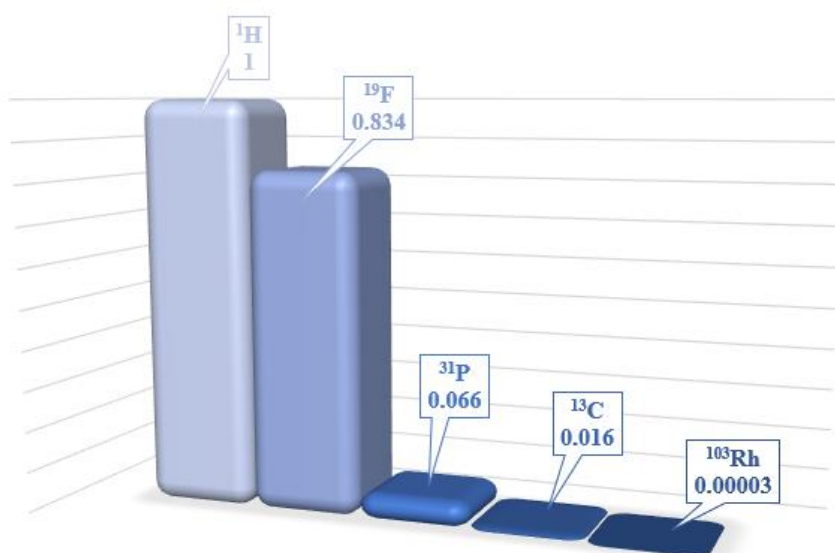


Figure 5. Relative sensitivity of selected nuclei at constant field. The sensitivity of the ^1H nucleus is set with the value of 1 to compare it with the sensitivity of the other nuclei.

Phosphorous-31 is a 100% abundant, spin half nucleus, with relatively high NMR sensitivity for an heteronucleus (^{31}P gyromagnetic ratio is 17.2 MHz T^{-1} , while ^1H gyromagnetic ratio is 42.6 MHz T^{-1}). ^{31}P NMR spectra can be very well-resolved but also highly complicated by both scalar homo- and heterocoupling. In the last case, high concentration and low-temperature studies might help in the interpretation of the multiplet structure.

Rhodium-103 is 100% abundant, spin half nucleus, which has a rather low gyromagnetic ratio. For this reason, the acquisition of ^{103}Rh NMR spectra typically involves polarization transfer and indirect observation *via* more sensitive nuclei like ^1H or ^{31}P .

^{103}Rh NMR spectroscopy is not available on benchtop spectrometers because of the low frequency required. For the investigations of the present thesis, I have mainly explored the ^{31}P nucleus in my reaction monitoring. Phosphorous is superior to proton NMR in terms of precise assignment of the rhodium diphosphine species present in solution.

A challenging choice for rhodium diphosphine complexes is the selection of the correct internal standard (ISTD). Many requirements need to be considered: good solubility, low viscosity, absence of aromatic groups or chloride functionalities that would coordinate to the rhodium center, absence of other phosphorous atoms that would compete with the diphosphine for the coordination to the metal center, stability under reaction conditions, as well as no overlapping peaks in ^1H NMR and ^{31}P NMR. To name an example, trioctyl phosphate should be preferred over the more common tris(2-chloroethyl) phosphate because of the chlorides which would potentially coordinate the rhodium center. For our flow system, I have mainly focused on inertness, which must be guaranteed before any quantitative investigations can be carried out (please refer to [Chapter 3.1](#) for inert conditions).

1.4. Signal enhancement

Sensitive Homogeneous And Resolved PEaks in Real time (SHARPER) is an NMR pulse sequence that belongs to the family of pure shift NMR techniques (Chapter 1.4.5).³⁹ The SHARPER sequence has been published for the first time in 2017 by the Uhrín research group. It allows to remove homo- and heteronuclear scalar couplings to collapse multiplets into singlets. Moreover, the apparent T_2 (*i.e.*, T_2^*) becomes longer, contributing to the enhancement in SNR.

The SHARPER sequence has improved SNR by a factor of 10–30 on a benchtop spectrometer for the ^{19}F nucleus.⁴⁰ Here, there is not only the benefit of collapsing multiples but also the improved decoupling. Indeed, ^1H and ^{19}F share the same coil on a benchtop spectrometer and for this reason the classic decoupling is more problematic. In the case of ^1H and ^{31}P , which have separated channels, the classic decoupling is more efficient and therefore it could be expected a lower enhancement using SHARPER sequence on ^{31}P nuclei.

For the ^{19}F nucleus, there are two applications of the SHARPER sequence reported for reaction monitoring and both are protodeboronation of fluorinated aryl boronic acids *via* HF spectrometers.^{39,41} For the ^{31}P nucleus, there is only one application reported in literature for reaction monitoring. There, a diphenylphosphine has been oxidized by bubbling air into the solution inside an NMR tube in an HF spectrometer.³⁹

1.4.1. SHARPER sequence

Figure 6 illustrates the SHARPER sequence. The first hard 90° pulse (A) brings the magnetization into the transversal plane.^g Then, a first free induction decay (FID) chunk is acquired (B).^h Please note that this is called “half chunk” because it is acquired for half of the time of the following FID chunks. The refocusing loop follows and it consists of a chain of 180° pulses (C) alternated by FID chunks acquisitions (D). The final FID, obtained after processing, stitches together all the FID chunks reordered. Since each FID chunk is very short, there is no time for J -coupling evolution and therefore for the formation of the multiplet. Moreover, the refocusing loop eliminates the effects of field inhomogeneity.

^g Hard pulses are non-selective pulses, characterised by high power and short duration. Soft pulses are instead selective, characterised by low power and long duration.

^h The FID is the time signal induced in the receiver coil, which decreases over time due to relaxation. The FID chunk is a selected portion of an FID.

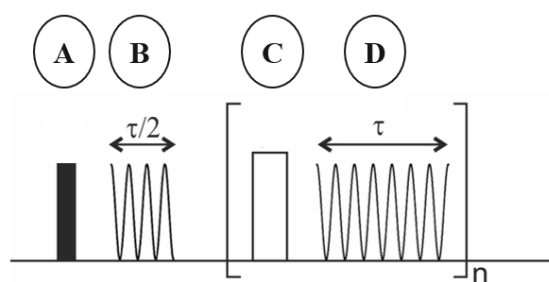


Figure 6. Schematic view of a SHARPER pulse sequence.⁴² The hard 90° (A) and 180° pulse (C) are depicted. The first FID chunk (B) is acquired for half acquisition time ($\tau/2$) while the FID chunks (D) in the refocussing loop are acquired for full acquisition time (τ).

As mentioned, the first FID chunk is half as long as the subsequent ones. This is because the J -coupling is refocused at the center of the echo that is generated after a 180° pulse, and therefore the FID chunk can be doubled without changing the J -evolution. The same is not true for the FID that follows a 90° pulse because this FID is not an echo. The benefit of increasing the chunk duration is that it allows to acquire more data points per chunk and therefore it decreases the experiment time.

The chunking of the FID produces artifacts, also called sidebands, which are recognizable in the NMR spectrum. In particular, they will be surrounding the original peak, at a frequency proportional to the time of the chunk (please refer to [Chapter 3.6](#) for a spectrum illustrating this phenomenon).

The SHARPER sequence should be used if only one multiplet is present in the entire NMR spectrum. In case more multiplets are present, the selective version should be applied ([Chapter 1.4.2](#)). The alternative would be the multi resonance version, where specific resonance conditions need to be met ([Chapter 1.4.4](#)).

1.4.2. Selective SHARPER (sel-SHARPER)

As previously stated, the SHARPER sequence is applied to the full NMR spectrum while selective SHARPER (sel-SHARPER) is band-selective ([Figure 7](#)). The selection is achieved by Pulsed Field Gradients (PFG, [A](#)), which refocus only the wanted spins, so called “active spins”, and dephases the unwanted spins, or “passive spins”. I used a simplified version of the sel-SHARPER sequence developed for HF NMR spectroscopy,³⁹ in which gradient coils are not required.ⁱ This is beneficial as these are not always present on benchtop spectrometers. Instead, shim coils have been used for the generation of PFGs.^j

ⁱ Gradient coils produce a linear dependence of the effective magnetic field on spatial position.

^j Shim coils correct, as much as possible, the inhomogeneities of the magnetic field throughout the sample.

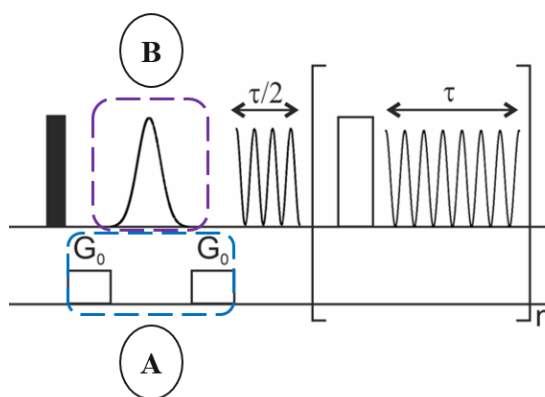


Figure 7. Schematic view of a sel-SHARPER pulse sequence.⁴² The main structure of the SHARPER sequence (Figure 6) is here recognizable. Of note, the hard 180° pulse is here replaced by the Gaussian shaped selective 180° pulse (B), surrounded by gradients (A).

I specifically used a Gaussian shaped selective 180° pulse (B) because of its simple design but more complicated shaped pulses can be found in literature.^k Ideally, the best pulse shape would be the one that generates a perfectly rectangular excitation profile, so there would be no residual sinc-like oscillation capable of exciting unwanted spins.^l

Typically, the higher the separation (in terms of chemical shift) between the multiplets, the higher the boost in SNR because the selective pulse does not need to be highly selective (Chapter 1.4.3). Also, the higher the multiplicity, the higher will be the overall gain from collapsing the multiplet into a singlet.

1.4.3. Calibration of selective pulses

According to the energy-time uncertainty relationship, time and energy are inversely proportional. In terms of NMR, those two variables are better interpreted as the energy bandwidth and the duration of the radio frequency (RF) pulse. Thus, short RF pulses give wide energy bandwidth and are therefore poorly frequency selective (Chapter 3.6.2).

The Single Pulsed Field Gradient (SPFG) spin echo has been used to calibrate Gaussian shaped 180° pulses (Figure 8). This sequence is similar to a classic spin echo sequence.^m Here, the rectangular 180° pulse has been replaced by a selective Gaussian 180° pulse and surrounded by two homospoil gradient pulses of equal gradient strength and phase. The term homospoil derives from the act of spoiling the magnetization, which means spreading out the spins and therefore be able to differentiate them. The first gradient pulse causes a loss in coherence of the spins along the transversal plane. Then the selective 180° pulse inverts only the active spins. Finally,

^k Shaped pulses are amplitude modulated pulses, with a customized bandwidth and behavior.

^l The name “sinc” derives from the sinc function ($\sin x/x$). The Gaussian function is used in this thesis as simple approximation of the sinc function.

^m The classic spin echo sequence starts with a 90° pulse which rotates the Z magnetisation down into the XY plane. A delay follows, in which the magnetisation dephases. A 180° pulse rotates the magnetisation around the X axis. A delay follows, in which the magnetisation rephases, generating an echo.

the second gradient reverts the effect of the first gradient, thus refocusing the transverse magnetization but only of the active spins that experienced the selective 180° pulse. The passive spins are therefore not refocused and cannot be detected.

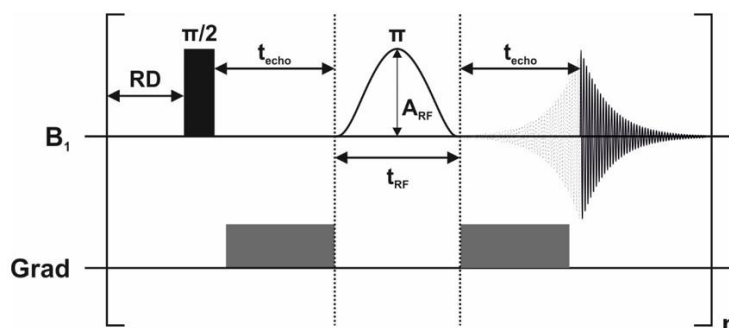


Figure 8. Schematic view of a SPFG spin echo sequence.

Amplitude and offset sweep experiments will bring to a calibrated selective 180° pulse. The principle behind is that the transversal magnetization is best refocused when the selective 180° pulse has the best parameters. Therefore, I performed sequential sweeps changing only one parameter (*e.g.*, the amplitude) and assigned the spectra with the highest intensity to the best parameters (Chapter 3.6.1).

1.4.4. Multi resonance SHARPER (MR-SHARPER)

If a single multiplet is present in the entire spectrum, SHARPER will give better SNR than sel-SHARPER. However, if more than one multiplet is present, it is recommended to switch to a band selective sequence (*e.g.*, sel-SHARPER) to avoid unwanted artifacts in the spectrum.

The alternative is to use multi resonance SHARPER (MR-SHARPER), a version of SHARPER in which one key parameter is defined according to the properties of the multiplets.⁴¹ The chunk length, which is the acquisition time of the FID chunk in the refocussing loop, needs to meet resonance conditions. Indeed, it needs to be inversely proportional to a multiple of the distance, in hertz, between the two multiplets.⁴¹

In practice, if two or more resonancesⁿ are present in the traditional $^{31}\text{P}\{^1\text{H}\}$ NMR spectrum, MR-SHARPER will allow to see them as singlets with enhanced SNR. This is a great advantage over SHARPER. Indeed, SHARPER would mainly enhance one of the resonances and produce artifacts in the spectrum. However, the disadvantage of MR-SHARPER is that more limitations are introduced in order to meet resonance conditions. This could be directly reflected into a lower gain in SNR compared to SHARPER.

ⁿ The two or more resonances may belong to the same species or to a mixture of species.

1.4.5. Pure shift methods

A note should be made regarding the emerging pure shift methods. Applied to both ^1H ³⁹ and ^{13}C ^{40,43} spectrometers, these techniques remove all homonuclear couplings. They have the great advantage of simplifying the spectrum and therefore providing a better understanding of the system. Nevertheless, they generally suffer from a prominent loss in SNR. For example, the Zangger-Sterk method can recover 0.5–10% of the signal.⁴⁴ Pure Shift Yielded by Chirp Excitation (PSYCHE), which is considered one of the most powerful pure shift methods and the one that outstands the others in respect to SNR, can recover 3–20% of the signal.⁴⁵ More than 80% of the signal is fully destroyed and will not appear in the final spectrum. SHARPER also belong to the family of pure shift NMR techniques, but it increases the SNR of the signals.

In summary, a pure-shift sequence such as PSYCHE is simplifying the full spectrum sacrificing SNR, while SHARPER is sacrificing the full spectrum simplification (if many resonances are present) enhancing the SNR.

1.4.6. Transverse encoding

The moment selective pulses are used, it is recommended to switch from continuous flow to stopped-flow conditions.⁴⁶ The reason behind this is that the spins, spatially separated by the gradients, need to refocus and therefore there should not be any movement of the reaction solution during the sequence. Nevertheless, flow conditions could be kept in case of transverse encoding.²²

Standard ^1H NMR probes are equipped with only a Z gradient. This means that only longitudinal (along the Z axis) spatial encoding is available while transverse (along the XY plane) encoding is not.²² Instead, a triple-axis probe allows transverse encoding, so there is no gradient along the Z axis (same as the direction of the flow) and therefore the flow has a much lower impact on the measurement.

Transverse encoding is not a standard technique, but it is possible to implement it to our setup. For this purpose, it is necessary to use only the gradients along the X and Y axis, avoiding the Z axis. This might require the use of stronger gradients, to compensate the missing longitudinal contribution.

2. Objectives

The focus of this PhD thesis is the implementation, development, optimization, and application of LF flow benchtop NMR spectroscopy as a new analytical method in homogeneous catalysis. For this, well-established rhodium species will be used as model complexes in selected transformations.

As an important first part of this PhD project, a dedicated flow setup will be built at LIKAT (Leibniz-Institut für Katalyse, Rostock, Germany) and made suitable for application in organometallic chemistry and homogeneous catalysis. Initially, the commercially available benchtop NMR spectrometer may need to be adapted to meet the experimental requirements of air- and moisture-sensitive organometallic complexes. Finally, potentials as well as limitations of the LF flow ^{31}P NMR reaction monitoring system will be investigated.

As a second important aspect, a great extension will be learning how to program and optimize advanced NMR pulse sequences and applying the acquired knowledge to the flow setup. After understanding how to manipulate an existing sequence and being able to identify the key parameters, a demonstration will be made to show the potential of these pulse sequences on the *on-line* LF NMR spectrometer.

3. Results and Discussion

Commercially available benchtop NMR instruments can typically be used for ^1H and ^{19}F analysis. Our 80 MHz spectrometer (Magritek) has an additional channel probe for the ^{31}P nucleus. Initially, I equipped our flow system with the commercially available flow kit (Magritek) and subsequently customized the entire setup ([Chapter 3.1](#)).

The acronym “SMILE” summarises the main features of our flow setup⁴⁷:

- ✓ **Speciation:** precise assignment of the complexes in solution, focussing on the phosphorous nuclei
- ✓ **Monitoring:** reaction monitoring in static and flow conditions
- ✓ **Inertness:** inert conditions for oxygen-sensitive organometallic complexes
- ✓ **Low-field:** low-cost benchtop spectrometer next to the fume hood
- ✓ **Enhancement:** boost in SNR *via* designed pulse sequences

“Spinsolve” has been the first software used to operate the spectrometer, with additional reaction monitoring and solvent suppression (presaturation sequence) packages. Later, I moved to the advanced version of the software, the so called “Spinsolve Expert”, to create and manipulate the SHARPER sequence ([Chapter 3.6](#)). This sequence has been the focus of my three-months traineeship at the University of York (York, UK), focussed on pulse sequence programming.

To develop the analytical method, known reactions with neutral and cationic Rh(I) diphosphine complexes have been chosen.^{48,49} Chiral and achiral diphosphines have been tested, *i.e.*, (*R,R*)-DIPAMP (1,2-bis[(*o*-methoxyphenyl)(phenyl)phosphino]ethane), (*R*)-BINAP and DPPB (1,4-bis(diphenylphosphino)butane). The corresponding rhodium complexes chosen in this thesis, show moderate to high-sensitivity towards traces of oxygen and are therefore ideally suitable for exploring the inertness of our system. All the hydrogenation reactions reported in this thesis have been performed using molecular hydrogen.

Please note that during reaction monitoring, the term “loop” has often been used. One loop is defined in this thesis as the group of experiments that are repeated multiple times. At the beginning of my PhD studies, for example, I have performed a shim, followed by one ^1H sequence and then one ^{31}P sequence. This is counted as one loop. For every reaction monitoring experiment, several loops have been recoded (varying from a total of 9 to 124). In most cases the interest was mainly on the ^{31}P spectra, but also shimming procedures have been performed to correct for eventual drifts and ^1H spectra to help explain eventually unpredicted results obtained from the ^{31}P spectra.

3.1. Pathway to inertness – Setup evolution

3.1.1. First generation setup

I assembled our first generation setup using only commercially available components (Figure 9). The flow NMR cell (Spinsolve glass centering tube) is inserted into the benchtop spectrometer (80 MHz, with phosphorous as second channel). Highly flexible and chemical resistant HPLC-type polytetrafluoroethylene (PTFE) tubing connects the entire system.^{50,51} The peristaltic pump is responsible to circulate the reaction mixture from the reaction vessel (*i.e.*, a Schlenk flask) into the spectrometer, and back. At this point, the connection between the flow system and the Schlenk flask consist in a pierced rubber septum, an approach that is often used for transferring solutions in organometallic chemistry.⁵² While the volume of the flow NMR cell is 0.5 mL, the one of entire system is approximately 4 mL.

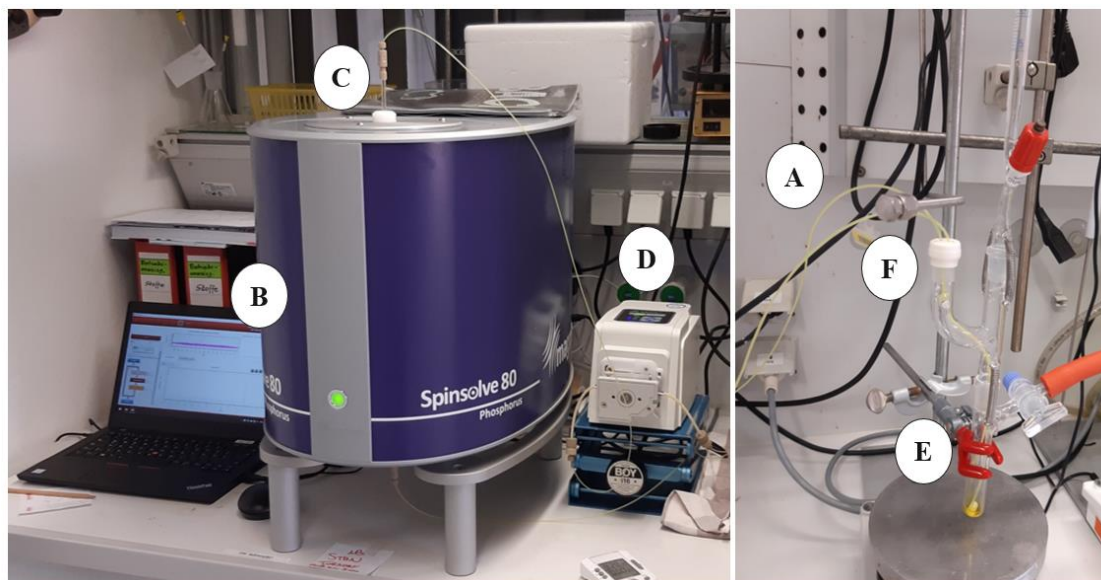
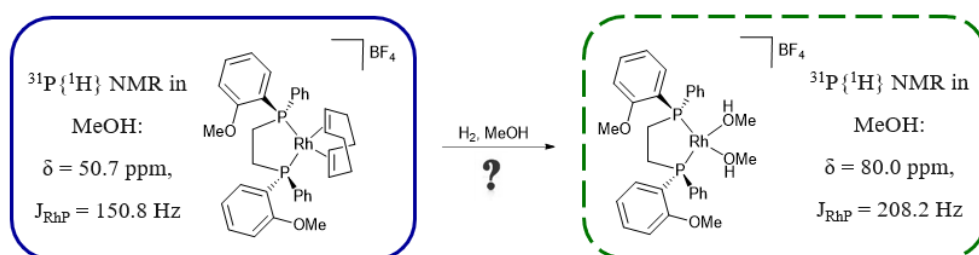


Figure 9. First generation of our setup with PTFE tubing (A). Outside the fume hood (left): benchtop spectrometer (B); flow NMR cell (C); peristaltic pump (BT100-2J, Longer, D). Inside the fume hood (right): Schlenk flask (E); rubber septum (F).

3.1.2. Oxidation

I aimed to monitor the hydrogenation of the Rh(I) COD complex $[\text{Rh}((R,R)\text{-DIPAMP})(\text{COD})]\text{BF}_4$ ($^{31}\text{P}\{^1\text{H}\}$ NMR in MeOH: δ 50.7 ppm, $J_{\text{RhP}} = 150.8$ Hz)⁵³ to yield the highly oxygen-sensitive Rh(I) solvent complex $[\text{Rh}((R,R)\text{-DIPAMP})(\text{MeOH})_2]\text{BF}_4$ (Scheme 1). These reactions are well-studied in the field of organometallic Rh chemistry and have been key to activating Rh diene complexes in homogeneous catalysis.⁵³



Scheme 1. Hydrogenation of $[\text{Rh}((R,R)\text{-DIPAMP})(\text{COD})]\text{BF}_4$ in MeOH. The question mark on the reaction arrow highlights that the expected product could not be observed.

Unfortunately, the desired product expected at 80 ppm could not be detected (Figure 10). Instead, only the oxidized phosphine ligand, appearing as a singlet at 36.7 ppm, was formed over time.

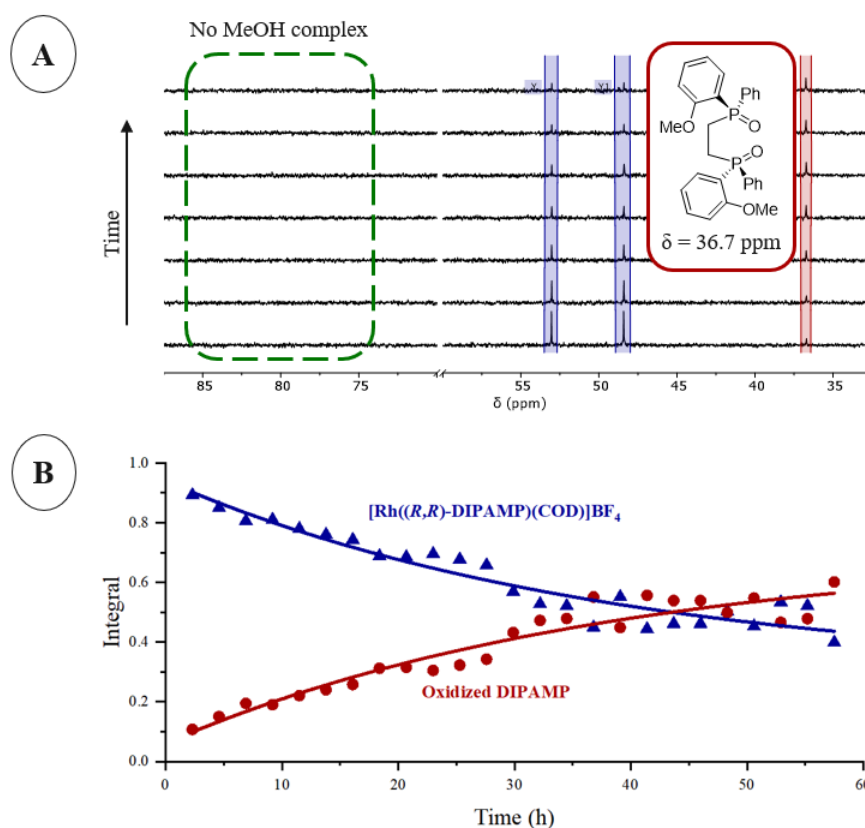


Figure 10. Low-Field Flow $^{31}\text{P}\{^1\text{H}\}$ NMR monitoring (A, MeOH, 32.6 MHz, $[\text{Rh}] = 11.0$ mM) and kinetic profile (B) of the hydrogenation of $[\text{Rh}((R,R)\text{-DIPAMP})(\text{COD})]\text{BF}_4$ (Scheme 1). The MeOH complex could not be detected, instead, oxidized DIPAMP is formed.

Details. Reaction monitoring with 25 loops, characterised by: shim (X, Y, Z, Z2); ^1H NMR (32 scans; 6.4 s acquisition time; 15 s repetition time); $^{31}\text{P}\{^1\text{H}\}$ NMR (256 scans; 1.6 s acquisition time; 30 s repetition time). Each loop lasted 138 min. For clarity, only one spectrum every 4th is shown.

Processing: zero filling to 16k points and exponential line broadening of 0.3 Hz.

The ligand oxidation nicely shows the necessity to optimize the commercially available flow setup. Furthermore, this supports the high sensitivity of the Rh species, making this class of compounds ideal candidates for my investigation.

Cyclooctane (COA) is forming during the reaction, as confirmed by the ^1H NMR spectra (Figure 11). This suggest that the desired highly sensitive solvent complex is generated, but it rapidly decomposes upon exposure to oxygen in the flow system.

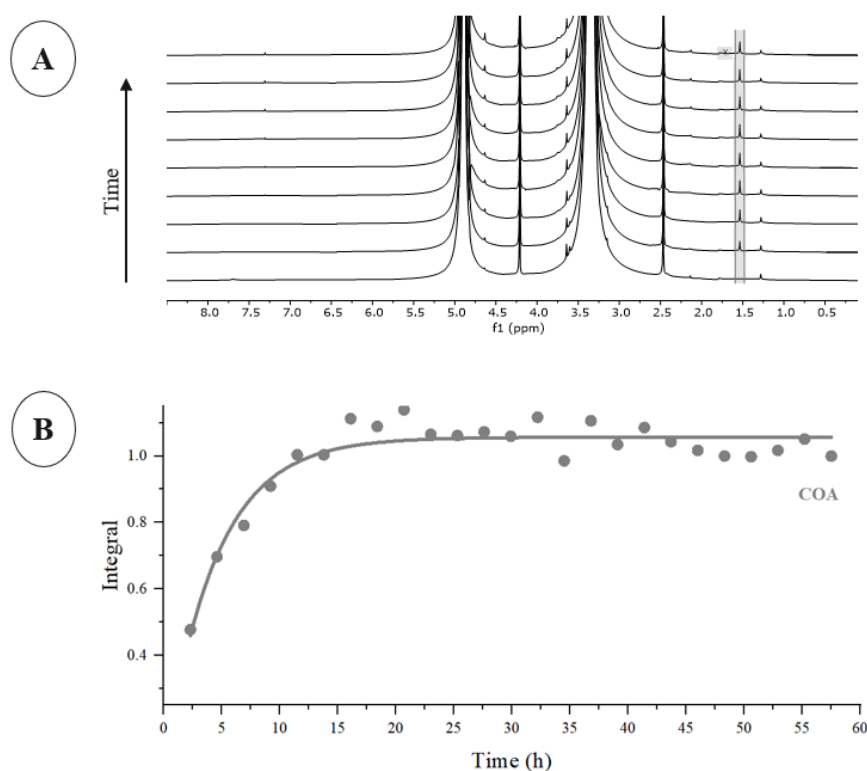


Figure 11. Low-Field Flow ^1H NMR monitoring (A, MeOH, 80 MHz, $[\text{Rh}] = 11.0$ mM) and kinetic profile (B) of the hydrogenation of $[\text{Rh}((R,R)\text{-DIPAMP})(\text{COD})]\text{BF}_4$ (Scheme 1). The CH_2 group of the cyclooctane is highlighted at 1.6 ppm.

Details. Reaction monitoring with 25 loops, characterised by: shim (X, Y, Z, Z2); ^1H NMR (32 scans; 6.4 s acquisition time; 15 s repetition time); $^{31}\text{P}\{^1\text{H}\}$ NMR (256 scans; 1.6 s acquisition time; 30 s repetition time). Each loop lasted 138 min. For clarity, only one spectrum every 4th is shown.

Processing: zero filling to 16k points and exponential line broadening of 0.3 Hz.

3.1.3. Second generation setup

To obtain inert conditions, the pierced rubber septum has been replaced with glass stoppers (Figure 12). The first glass stopper was characterised by two short stainless steel (SS) capillaries glued at the top and the bottom parts (Figure 12A). However, the chosen glue could not tolerate standard organic solvents used in my reaction monitoring experiments. Therefore, I introduced a modified second glass stopper, in which the capillaries are attached by molten glass (Figure 12B).

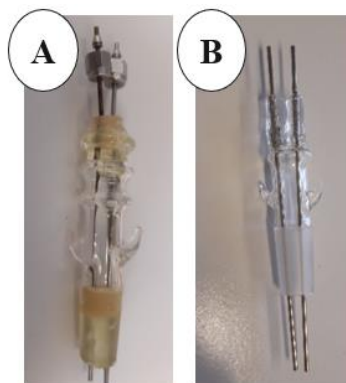


Figure 12. Second generation setup accessories: glass stopper with SS capillaries, connected *via* glue (A); glass stopper with SS capillaries, connected *via* molten glass (B).

PTFE tubing has then been connected to the ends of the SS capillaries inside the adaptor (Figure 13A). The chosen stopper is mounted on a glass adaptor (Figure 13B) and later fitted on a Schlenk flask (Figure 13C). One PTFE tube is long enough to allow sampling of the solution in the Schlenk flask while the other is shorter, to deliver the solution from the flow system back into the Schlenk flask.

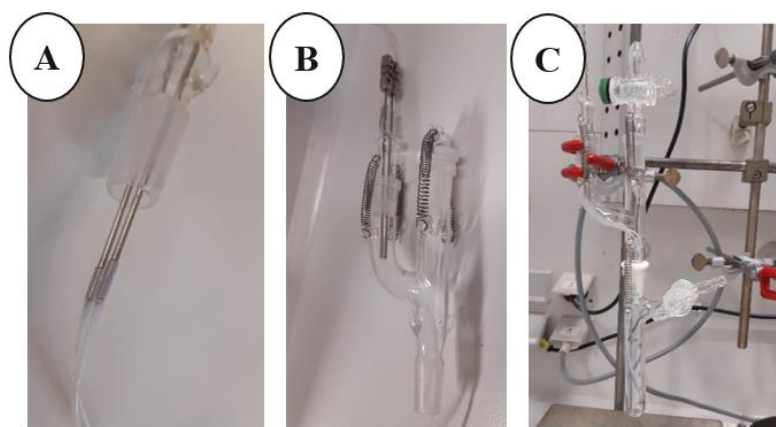
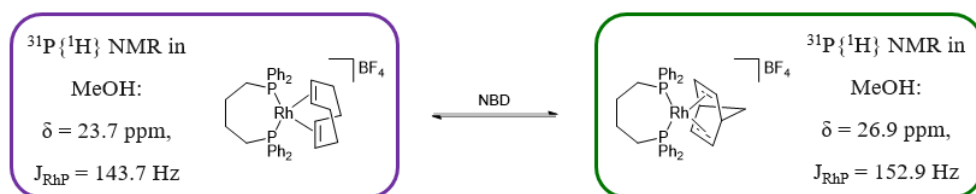


Figure 13. Second generation setup connections: PTFE connection from the stopper to the reaction mixture (A); glass stopper mounted on the glass adaptor (B); glass adaptor mounted on the Schlenk flask (C).

3.1.4. First step to inertness

I investigated a diolefin exchange reaction with DPPB, an achiral ligand cheaper than (*R,R*)-DIPAMP. The corresponding COD complex $[\text{Rh}(\text{DPPB})(\text{COD})]\text{BF}_4$ ($^{31}\text{P}\{^1\text{H}\}$ NMR in MeOH: δ 23.7 ppm, $J_{\text{RhP}} = 143.7$ Hz)^{o,54}, in the presence of excess of norbornadiene (NBD), interconverts into $[\text{Rh}(\text{DPPB})(\text{NBD})]\text{BF}_4$ ($^{31}\text{P}\{^1\text{H}\}$ NMR in MeOH: δ 26.9 ppm, $J_{\text{RhP}} = 152.9$ Hz)^o (Scheme 2, Figure 14).



Scheme 2. Diolefin exchange of $[\text{Rh}(\text{DPPB})(\text{COD})]\text{BF}_4$ into $[\text{Rh}(\text{DPPB})(\text{NBD})]\text{BF}_4$ in MeOH.

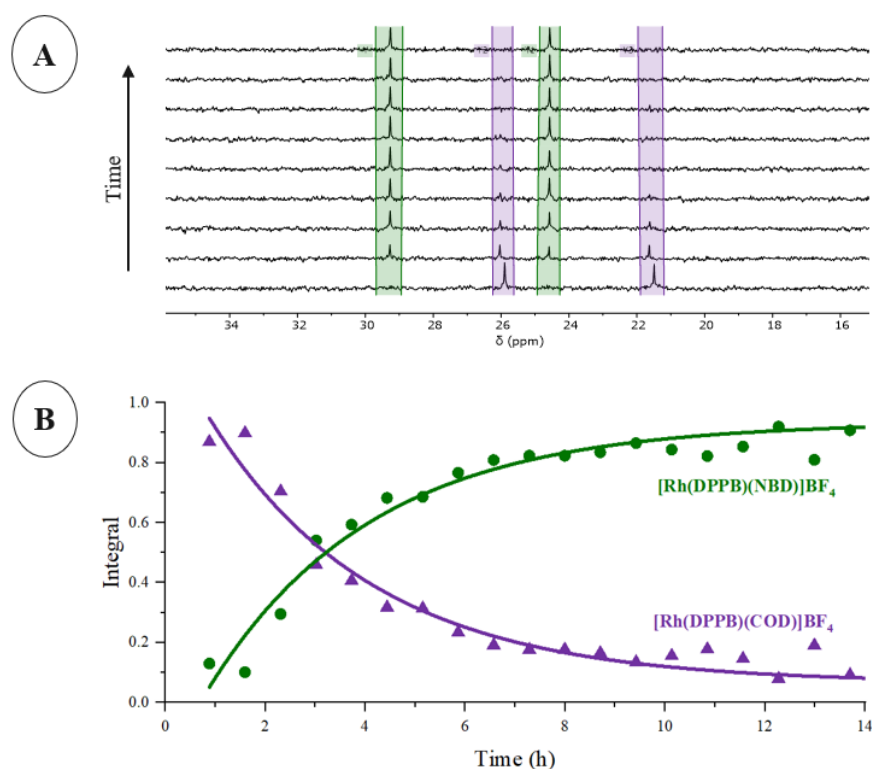


Figure 14. Low-Field Flow $^{31}\text{P}\{^1\text{H}\}$ NMR monitoring (A, MeOH, 32.6 MHz, $[\text{Rh}] = 9.7$ mM) and kinetic profile (B) of the diolefin exchange of $[\text{Rh}(\text{DPPB})(\text{COD})]\text{BF}_4$ into $[\text{Rh}(\text{DPPB})(\text{NBD})]\text{BF}_4$ (Scheme 2).

Details. Reaction monitoring with 25 loops, characterised by: shim (X, Y, Z, Z2); ^1H NMR (32 scans; 6.4 s acquisition time; 15 s repetition time); $^{31}\text{P}\{^1\text{H}\}$ NMR (128 scans; 1.6 s acquisition time; 15 s repetition time). Each loop lasted 43 min. For clarity, only one spectrum every 3rd is shown. Processing: zero filling to 16k points and exponential line broadening of 0.5 Hz.

^o The molecular structure of the complex $[\text{Rh}(\text{DPPB})(\text{COD})]\text{BF}_4$, obtained from single crystals that were grown from MeOH at r.t., is shown in Figure A1.

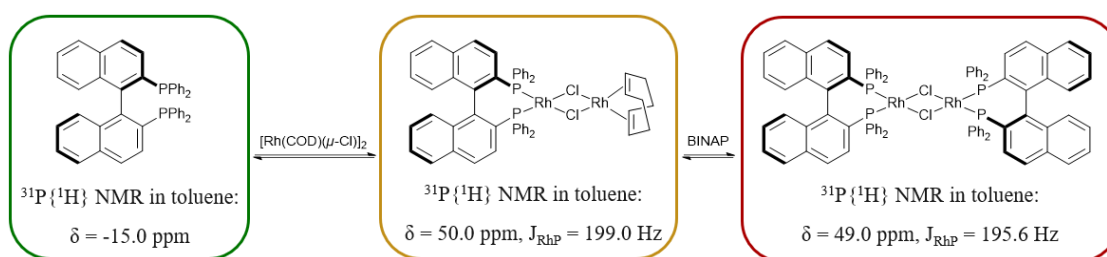
To my delight, the oxidized DPPB ligand ($^3\text{P}\{^1\text{H}\}$ NMR in MeOH: δ 36.7 ppm)⁵⁵ has not been detected with the second generation setup. The kinetic profile shows a clean reaction and formation of the desired NBD complex within a reaction time of approximately 12 hours.

As expected, the supposed intermediate MeOH solvent complex that should be present after release of the hydrogenated COD ligand in MeOH could not be observed *via* NMR reaction monitoring. Indeed, this species could not be detected *via* the faster UV-Vis reaction monitoring, where spectra can be recorded in milliseconds to seconds rather than minutes.⁵⁶ In the NMR monitoring, with higher concentration ($[\text{Rh}] = 9.7$ mM, which is 20-fold higher compared to the concentration in the UV-Vis experiment) and therefore higher rates, the MeOH complex is not expected to be detectable.

3.1.5. Stepwise addition

Switching to another rhodium complex, stepwise additions could be tested on our setup. This is particularly interesting for example for a two-step reaction, where both the intermediate and the final product can be observed.

After recording the first spectrum in the presence of the BINAP ligand alone ($^{31}\text{P}\{^1\text{H}\}$ NMR in toluene: δ -15.0 ppm)⁵⁷, I added one equivalent of the Rh precursor $[\text{Rh}(\text{COD})(\mu\text{-Cl})]_2$, generating the dinuclear monosubstituted species $[(\text{COD})\text{Rh}(\mu\text{-Cl})_2\text{Rh}((R)\text{-BINAP})]$ ($^{31}\text{P}\{^1\text{H}\}$ NMR in toluene: δ 50.0 ppm, $J_{\text{RhP}} = 199.0$ Hz)^{53,58} (Scheme 3, Figure 15). In the following loop, I added the second equivalent of BINAP to yield the dinuclear disubstituted species $[\text{Rh}((R)\text{-BINAP})(\mu\text{-Cl})]_2$ ($^{31}\text{P}\{^1\text{H}\}$ NMR in toluene: δ 49.0 ppm, $J_{\text{RhP}} = 195.6$ Hz).^{53,59} Both complexes disappeared rapidly over time due to the undesired oxidation, forming the mono- and di-oxidized BINAP ligands ($^{31}\text{P}\{^1\text{H}\}$ NMR in toluene: δ 26.3, -14.7 ppm for mono-oxidized BINAP; δ 27.6 ppm for di-oxidized BINAP)⁵⁹.



Scheme 3. Stepwise ligand exchange of $[\text{Rh}(\text{COD})(\mu\text{-Cl})]_2$ in the presence of (*R*)-BINAP in toluene.

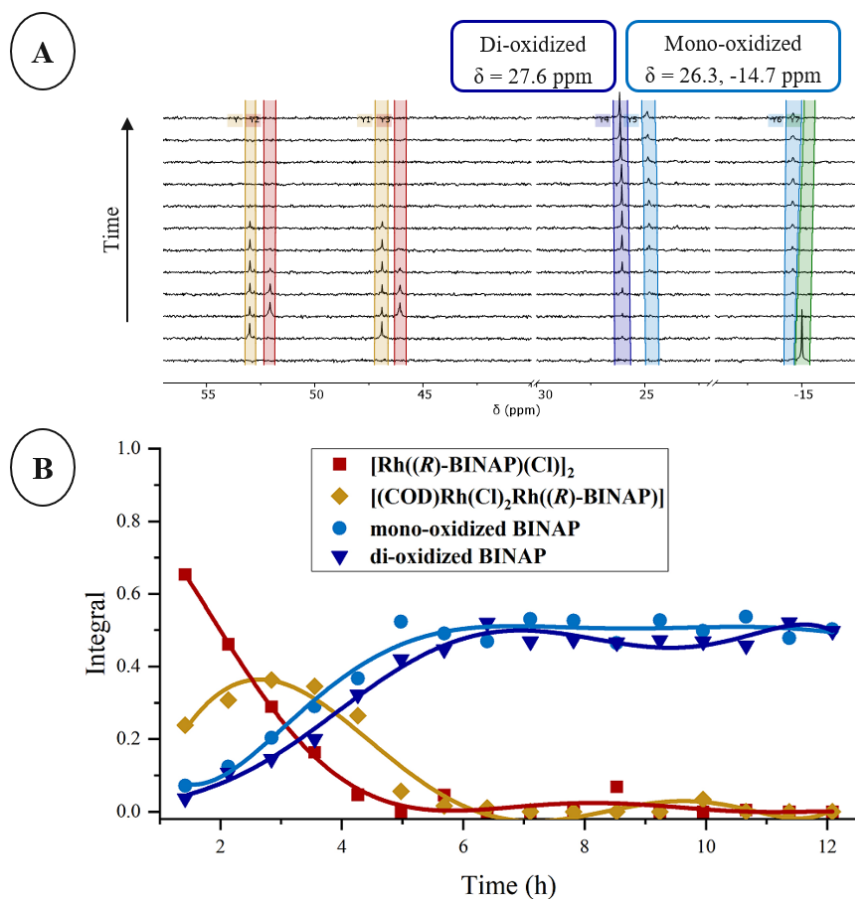


Figure 15. Low-Field Flow $^{31}\text{P}\{^1\text{H}\}$ NMR monitoring (A, toluene, 32.6 MHz, $[\text{Rh}] = 10.8$ mM) and kinetic profile (B) of the stepwise ligand exchange of $[\text{Rh}(\text{COD})(\mu\text{-Cl})_2]$ in the presence of (R)-BINAP (Scheme 3). The first spectrum has been recorded with only the first equivalent of BINAP. The second spectrum has been recorded after the addition of $[\text{Rh}(\text{COD})(\mu\text{-Cl})_2]$. The third and the following spectra have been recorded after the addition of the second equivalent of BINAP. Oxidation does not allow the complete formation of the desired product.

Details. Reaction monitoring with 15 loops, characterised by: shim (X, Y, Z, Z2); ^1H NMR (32 scans; 6.4 s acquisition time; 15 s repetition time); $^{31}\text{P}\{^1\text{H}\}$ NMR (128 scans; 1.6 s acquisition time; 15 s repetition time). Each loop lasted 43 min. Processing: zero filling to 16k points and exponential line broadening of 0.5 Hz.

3.1.6. Third generation setup

The flow generated by the peristaltic pump (**Pump1**, [Figure 16A](#)), which was part of the commercially available Magritek reaction monitoring kit, was not regular. Moreover, after various reaction monitoring experiments, the capillary inside the pump got deteriorated. Deformation and swelling could be observed ([Figure 16B](#)). Especially the latter issue could be responsible for the oxidation observed in some of the above reactions. An evaluation of different pumps and filters followed ([Figure 16](#), [Figure 17](#)). **Pump2** generated a regular flow but has been excluded because of the relatively large internal volume of the coupled filter ([Figure 16C](#)). **Pump3** seemed to provide inert conditions at the beginning, but I soon observed leaking of the reaction solution into the sealing liquid contained in the syringe ([Figure 16D](#)). Inertness has been guaranteed with **Pump4**, which does not require any additional sealing liquid ([Figure 16E](#)).

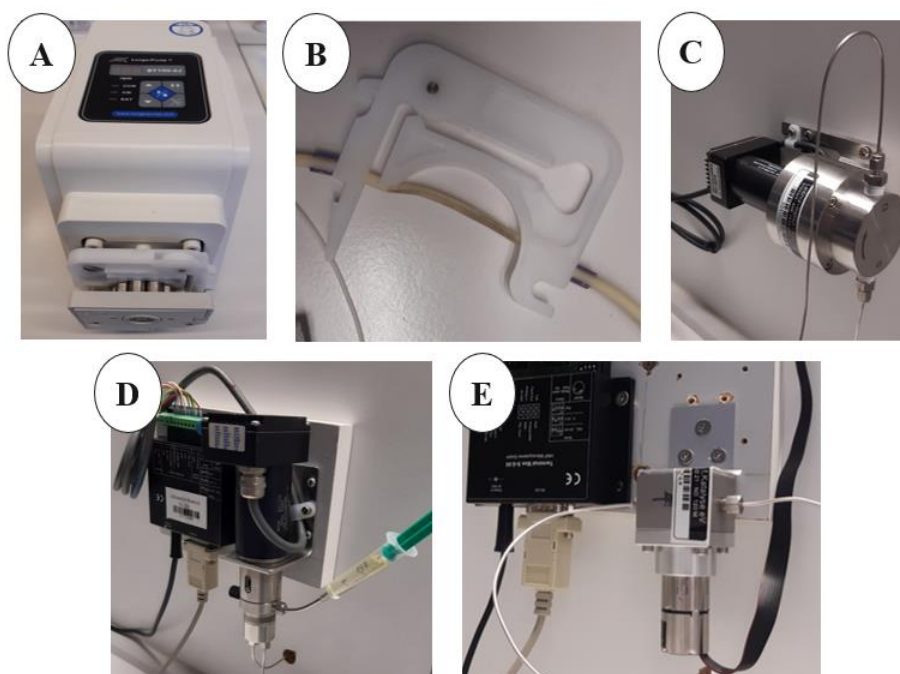


Figure 16. Pumps screening: **Pump1**: BT100-2J, peristaltic Longer pump ([A](#)); inset of **Pump1** after extensive use of solvents ([B](#)); **Pump2**: mzr-6355-cy-f, hermetic inert pump series ([C](#)); **Pump3**: mzr-2905, high performance pump series ([D](#)); **Pump4**: mzr-2965-hs-f, magnetic hermetic pump series ([E](#)).

Please refer to the [Chapter 5.1](#) for additional information.

Filters have been introduced to prevent the pump from clogging due to solid particles, eventually formed during reaction. After quickly discarding **Filter1** because of the large dead volume ([Figure 17A](#)), I equipped the inlet **Filter2** ([Figure 17B](#)). Unfortunately, a minimum amount of solution is required to keep the filter fully immersed, otherwise formation of gas bubbles occurs, disrupting a good acquisition of NMR spectra ([Figure 17C](#)). Furthermore, the filter could easily get damaged by stirring the reaction solution. To overcome those disadvantages and become much more flexible and independent from a specific geometry of the reaction vessel, I adopted the inline **Filter3** ([Figure 17D](#)).

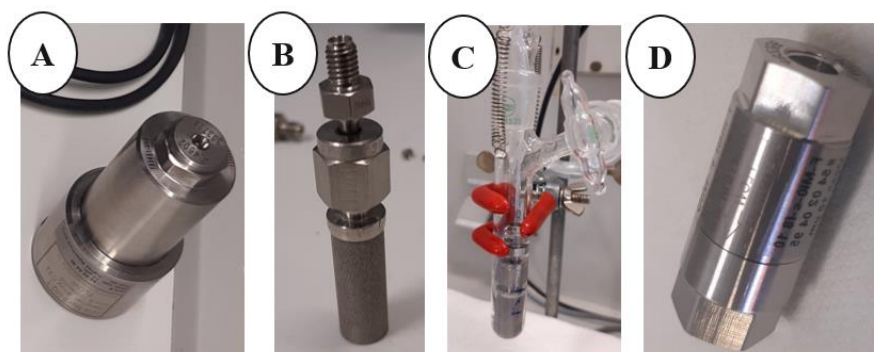


Figure 17. Filters screening: **Filter1**: inline filter F-MI2-T (A); **Filter2**: CPI inlet filter F-MI0 (B); **Filter2** inserted into solution in a Schlenk flask (C); **Filter3**: inline filter F-MI0-s-f8 (D). Please refer to the [Chapter 5.1](#) for additional information.

Figure 18 shows the final customized setup. All the PTFE tubing has been replaced with SS capillaries (outer diameter of 1/16'') except for the short capillaries inside the glass adaptor located on top of the Schlenk flask. The volume of the flow system – excluding the reaction vessel – is now of ca. 3.5 mL, allowing a full exchange of the reaction solution in less than 1 min (with our typical flow rate of 4 mL min⁻¹). The evaluation of the long-term inertness of the flow system under realistic conditions^p follows in the next chapter.

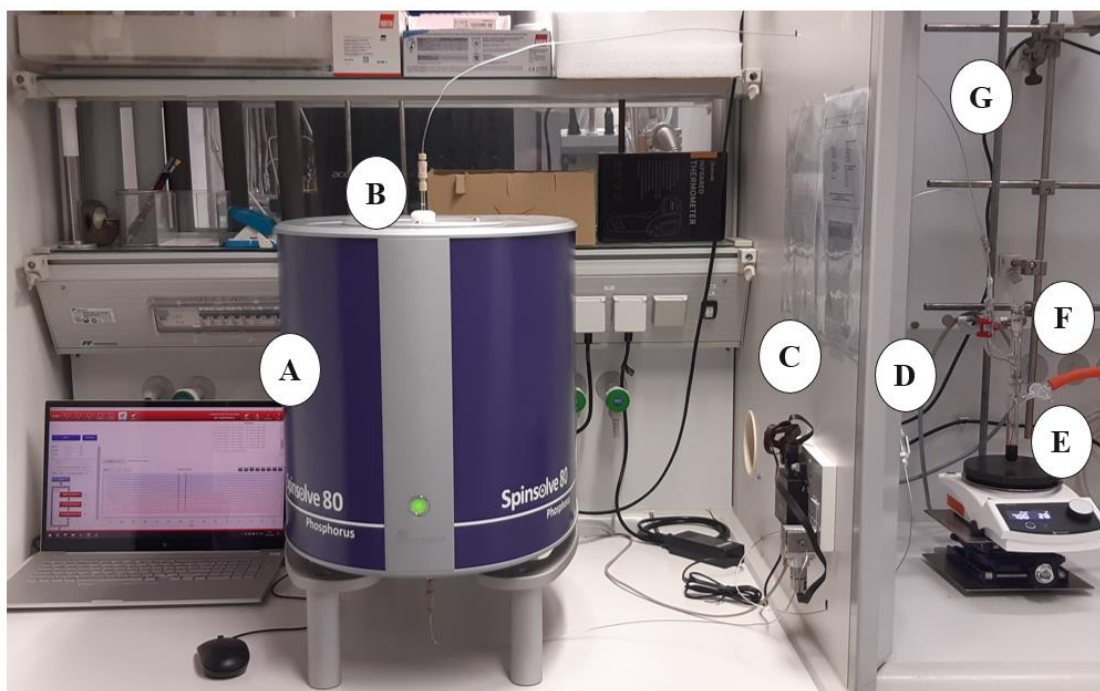
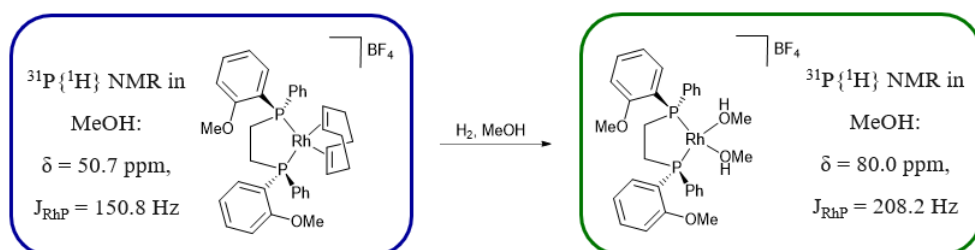


Figure 18. Third generation of our setup: benchtop spectrometer (A); flow NMR cell (B); micro annular gear pump (**Pump4**, C); inline filter (**Filter3**, D); Schlenk flask (E); glass adaptor (F); SS capillaries (G).

^p By realistic condition I mean classic anaerobic organometallics conditions obtained *via* Schlenk techniques.

3.1.7. Inertness

To evaluate the inertness of our customized setup, the hydrogenation of $[\text{Rh}((R,R)\text{-DIPAMP})(\text{COD})]\text{BF}_4$ in MeOH has been repeated (shown before, in Figure 10). To my delight, I could now observe the formation of the highly oxygen-sensitive solvent complex $[\text{Rh}((R,R)\text{-DIPAMP})(\text{MeOH})_2]\text{BF}_4$ ($^{31}\text{P}\{^1\text{H}\}$ NMR in MeOH: δ 80.0 ppm, $J_{\text{RhP}} = 208.2$ Hz)⁶⁰ (Scheme 4, Figure 19). Moreover, formation of the oxidized ligand has not been detected for 18 hours during reaction monitoring, as confirmed later by HF NMR (Figure A3).



Scheme 4. Hydrogenation of $[\text{Rh}((R,R)\text{-DIPAMP})(\text{COD})]\text{BF}_4$ to $[\text{Rh}((R,R)\text{-DIPAMP})(\text{MeOH})_2]\text{BF}_4$ in MeOH.

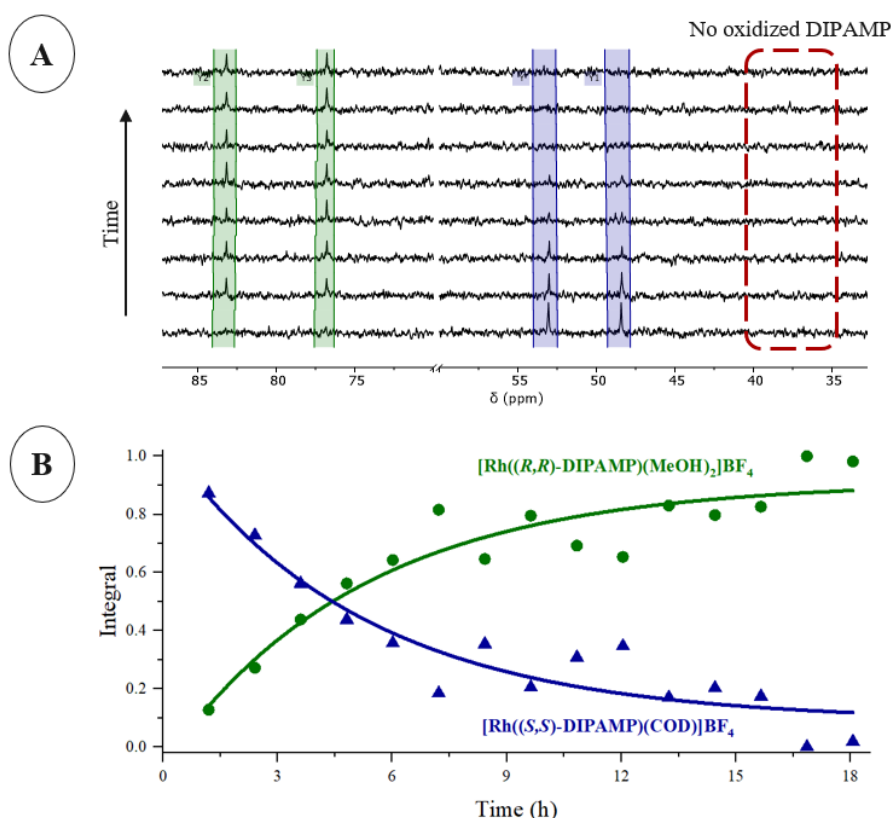
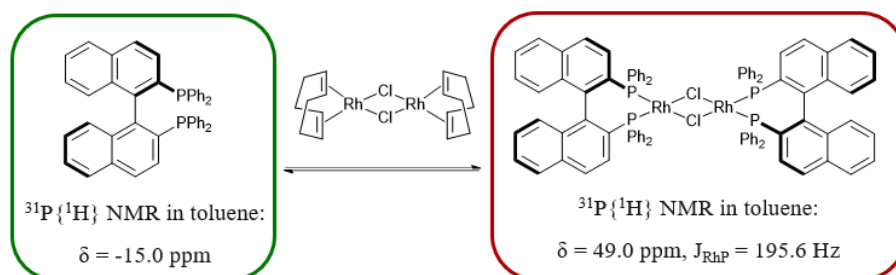


Figure 19. Low-Field Flow $^{31}\text{P}\{^1\text{H}\}$ NMR monitoring (A, MeOH, 32.6 MHz, $[\text{Rh}] = 11.1$ mM) and kinetic profile (B) of the hydrogenation of $[\text{Rh}((R,R)\text{-DIPAMP})(\text{COD})]\text{BF}_4$ to $[\text{Rh}((R,R)\text{-DIPAMP})(\text{MeOH})_2]\text{BF}_4$ (Scheme 4).

Details. Reaction monitoring with 16 loops, characterised by: shim (X, Y, Z, Z2); ^1H NMR with presaturation (32 scans; 6.4 s acquisition time; 10 s repetition time); $^{31}\text{P}\{^1\text{H}\}$ NMR (256 scans; 3.2 s acquisition time; 15 s repetition time). Each loop lasted 72 min. For clarity, only one spectrum every 2nd is shown. Processing: zero filling to 64k points and exponential line broadening of 1.0 Hz.

Similarly, the diolefin-BINAP ligand exchange reaction using $[\text{Rh}(\text{COD})(\mu\text{-Cl})]_2$ (Scheme 5) to produce the dimeric species $[\text{Rh}(\text{R-BINAP})(\mu\text{-Cl})]_2$, which has already proved to allow stepwise addition of the components, has been repeated (Figure 15).



Scheme 5. Ligand exchange of $[\text{Rh}(\text{COD})(\mu\text{-Cl})]_2$ in the presence of excess of (*R*)-BINAP in toluene.

Aiming to verify the inert conditions, the experiment in the excess of ligand has been carried out (Figure 20). The ligand exchange is too fast to be monitored under the given experimental conditions, so the reaction could not be followed. However, I could confirm the stability of the BINAP product complex with our third generation setup. Negligible amount of oxidized ligand could be found in the HF spectrum recorded afterwards (Figure A4).

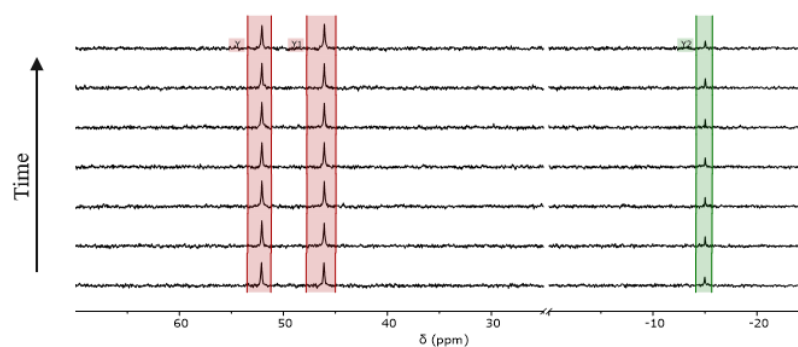


Figure 20. Low-Field Flow $^{31}\text{P}\{^1\text{H}\}$ NMR monitoring (toluene, 32.6 MHz, $[\text{Rh}] = 9.3 \text{ mM}$) of the stability of $[\text{Rh}((\text{R})\text{-BINAP})(\mu\text{-Cl})]_2$ (Scheme 5).

Details. Reaction monitoring with 14 loops, characterised by: shim (X, Y, Z, Z2); ^1H NMR with presaturation (4 scans; 6.4 s acquisition time; 10 s repetition time); $^{31}\text{P}\{^1\text{H}\}$ NMR (128 scans; 3.2 s acquisition time; 15 s repetition time). Each loop lasted 35 min. For clarity, only one spectrum every 2nd is shown. Processing: zero filling to 32k points and exponential line broadening of 1 Hz.

3.2. Reproducibility – Setup details

I would like to include some comments on the setup used for reaction monitoring, to assure reproducibility in future studies. A metal gasket is typically the best choice for a metal junction, *e.g.*, between SS capillary and the filter or the pump (Figure 21A). In case of a plastic junction, like the ones at the extremes of the flow cell, a plastic gasket (here shown in blue) is preferable (Figure 21B). In this way, the gasket bridges between the metal junction on the SS capillary and the plastic junction on the flow NMR cell, avoiding problems of leakage.

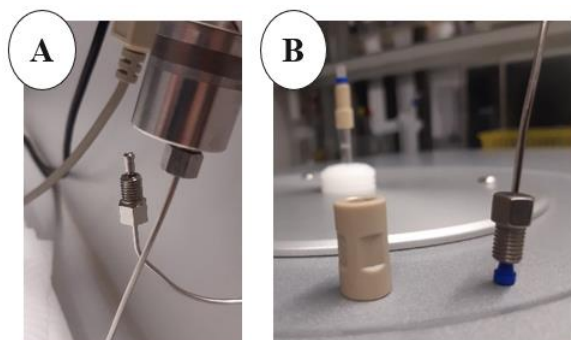


Figure 21. Junctions and gaskets in metal (A) and in plastic (B).

I preferred to install the micro annular gear pump before the spectrometer to have a “push behavior” under argon pressure instead of a “pull behavior” with the pump located after the spectrometer. It has been assumed this could help to prevent air from entering the system. As suggested by the pump manufacturer (HNP), I flipped the pump orientation upside down to favour elimination of gas (Figure 22).^q

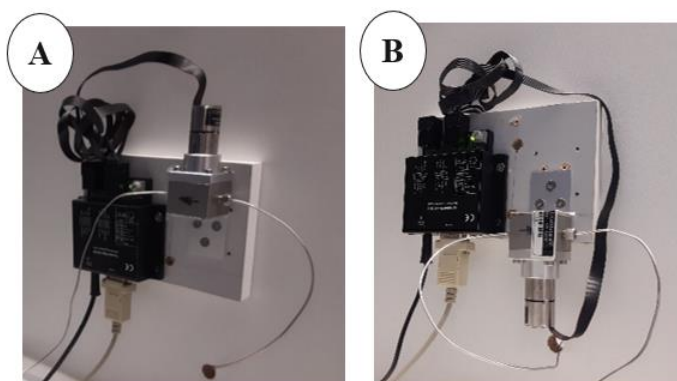


Figure 22. Pump in the incorrect (A) and correct orientation (B).

Calibration of the pumps has been done with ethanol in triplicate. Herein are reported the data for the first generation setup (Figure 23A) and the third generation setup (Figure 23B). In the final setup, to have a flow rate of 4 mL min^{-1} , a pump speed of v1400 has been set.

^q As gas, I mean the argon present in the flow system before the reaction solution is pumped through it.

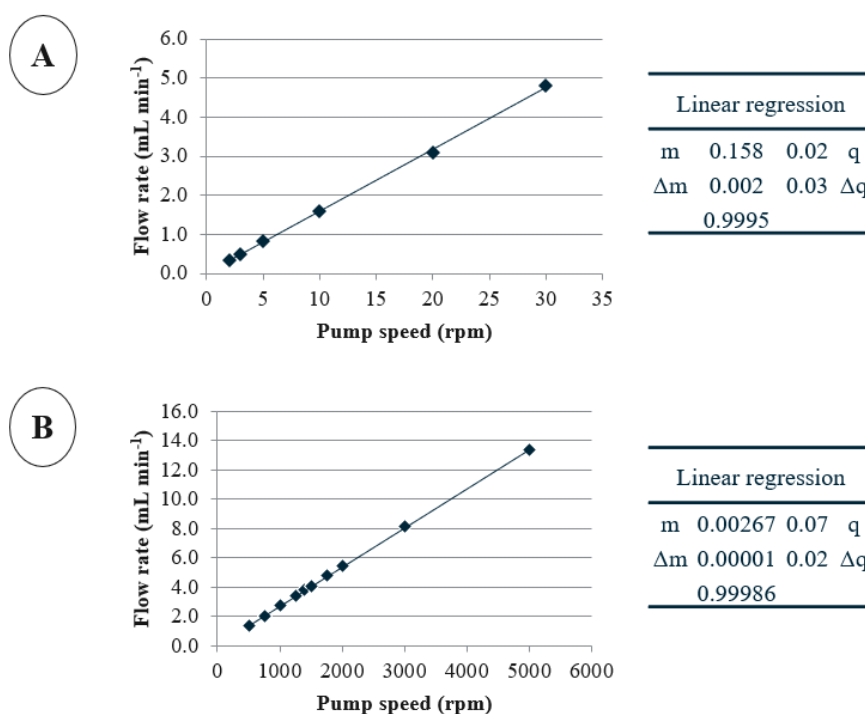


Figure 23. Flow calibration of the flow setup with **Pump1** (A) and with **Pump4** (B).

If ligand oxidation occurs, it is likely to have metallic rhodium accumulation in the flow system (Figure 24A,B).[†] To clean the system, appropriate solvents have been pumped forward and backward at atmospheric pressure. For the more challenging situation (*i.e.*, with metal particles trapped in the system), I excluded the flow cell from the flow setup and pumped solvents against positive pressure of argon, applied in an additional receiver Schlenk flask (Figure 24C).



Figure 24. Accumulation of metal after ligand oxidation and system cleaning: accumulation of metal in rings along the wall of the flow cell (A); accumulation of metal, visible after opening the filter (B); setup configuration for pump cleaning (C).

Regarding the type of addition of reagents, I typically preferred adding the reagent in solid form in the Schlenk flask and add solvent *via* a burette (Figure 25A). When this option was not

[†] The black accumulation is believed to be metallic rhodium. Indeed, this accumulation only formed when the ligand oxidation was observed by $^{31}\text{P}\{^1\text{H}\}$ NMR monitoring. Moreover, the black accumulation was not soluble in hydrochloric acid and slightly soluble in aqua regia (a mixture of concentrated nitric and hydrochloric acids, in a ratio 1:3).

available, the pre-dissolved reaction mixture has been added from a second Schlenk flask *via* canula (Figure 25B) or *via* syringe (Figure 25C).



Figure 25. Different type of additions: *via* burette (A); *via* canula (B); *via* syringe (C).

The stopped-flow mode could be used on Spinsolve to eliminate flow effects. At the beginning, with the setup equipped with **Pump1** (Figure 16), I preferred the continuous flow, especially for long experiment times. In this way, continuous stirring of the reaction mixture and no precipitation of the rhodium complexes could be assured. Moving to the second and then third generation setup, only continuous flow could be chosen. **Pump2**, **Pump3** and **Pump4** (Figure 16), provided by HNP, are not compatible with the Spinsolve software, offered from Magritek. The pump is indeed controlled from the pump software (Motion Manager, version number 5). No direct communication between the two software was available at the time of writing.

3.2.1. Temperature remarks

In this thesis, only reactions at room temperature (r.t.) have been reported and monitored. This is due to the magnet temperature limits (temperature range of 18–27 °C, as provided by the supplier). For a wider application of this benchtop NMR approach in homogeneous catalysis it would however be desirable to also monitor reactions at elevated temperatures (higher than r.t.) as it is possible in HF NMR spectroscopy. I have tried to overcome this limitation by cooling down the reaction solution coming from the Schlenk flask, which is warmed up by the heating plate. For this purpose, I installed a cooling bath, filled with water at r.t., to cool down the SS capillaries and therefore the solution contained inside (Figure 26).

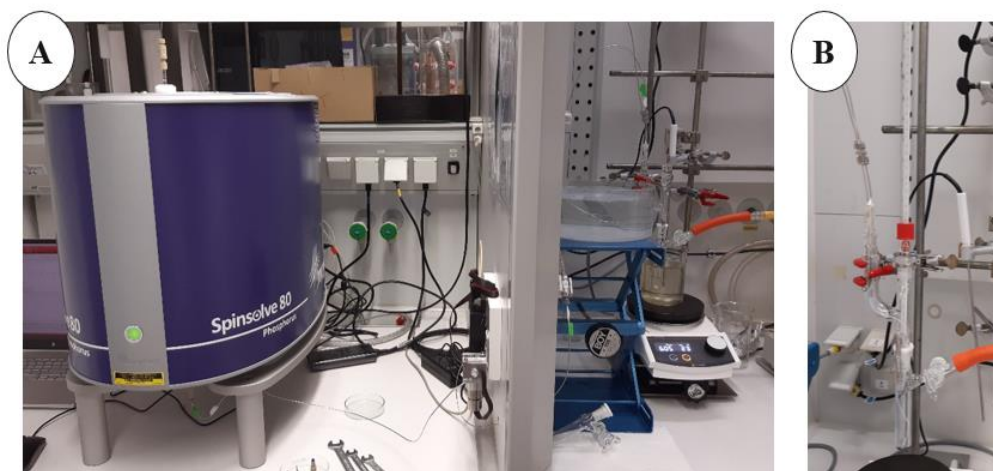


Figure 26. Setup configuration for high temperature reaction (higher than r.t., **A**); adaptor with the thermometer mounted on the Schlenk flask (**B**).

The temperature controller of the instrument might not give the correct temperature of the solution inside the spectrometer because it necessarily needs to be placed below the tube (or close to the flow cell, if in flow conditions). A calibration of an NMR sample that has a known temperature-dependent chemical shift has been performed. Methanol^{61,62} is typically used but, because of its boiling point of 65 °C, I choose a mixture of 1,2-ethanediol and dimethyl sulfoxide (1,2-ethanediol/DMSO 80:20). Following the calibration curve available in literature,⁶³ it is possible to precisely assign the temperature inside the flow cell.

With a constant flow rate of 4 mL min⁻¹ and the calibration mixture in the flow system, I increased stepwise the temperature. In my first attempt, I put the cooling bath between the pump and the spectrometer, and I increased the temperature from 35 °C to 80 °C (this refers to the temperature measured by the thermometer, not the temperature set on the heating plate). This led to broadening of the peaks as well as to error messages from the spectrometer because of the instable temperature of the magnet. As expected, a chemical shift change has been observed in the ¹H NMR spectrum (**Figure 27A**). The lower the chemical shift difference of the 1,2-ethanediol, the higher is the temperature measured by the spectrometer. Afterwards, the bath has been moved between the reaction vessel and the filter. In this way, the capillaries are exposed for longer time at air at r.t., and so a better equilibration of the temperature is achieved. Starting from 35 °C, I increased the bath temperature up to 150 °C. Now, no change in chemical shift could be observed (**Figure 27B**).

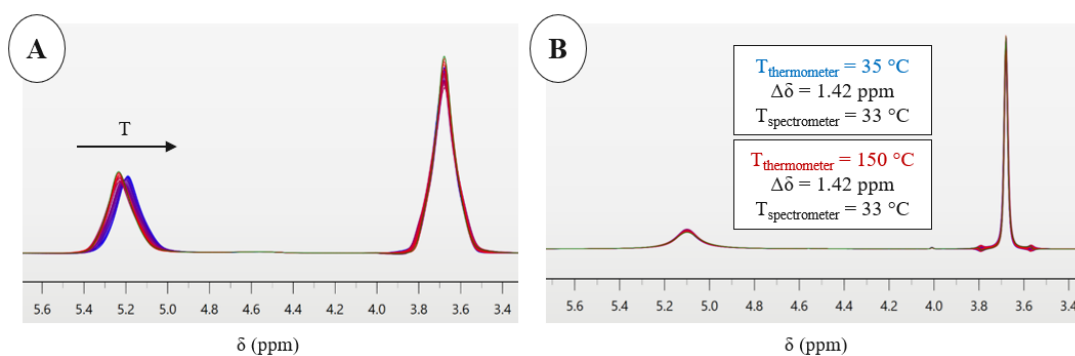


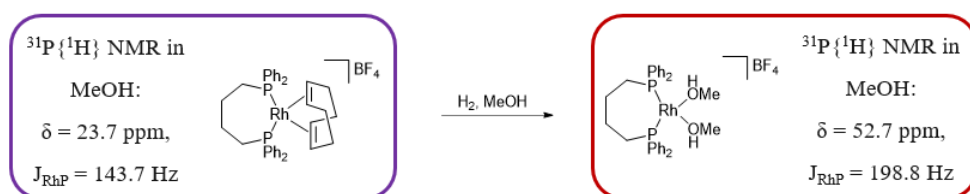
Figure 27. ^1H NMR monitoring while the temperature of the solution inside the spectrometer changes (A); ^1H NMR monitoring while the temperature is constant (B).

I verified that the temperature inside the spectrometer remains at constant r.t. for more than two days, while the thermometer inside the oil bath is at $150\text{ }^{\circ}\text{C}$. The next step would have been to monitor a reaction but after a couple of trials I decided to focus my efforts on other projects. Here, two main challenges remain for following a reaction running at high temperature, cooling it down to r.t. and bringing it back to high temperature in the reaction vessel. First, no side reactions can take place while the solution is cooled down, or at least these reactions need to be much slower than the one under study. Second, good solubility must be maintained while the solution has been cooled down, otherwise precipitation might occur. In this case, not only the filter will get blocked, but it would not be possible to follow the species of interest *via* the NMR spectrometer.

3.3. Mass transfer – Flow vs static conditions

Reaction monitoring in NMR tubes suffers from mass transfer issues as the reaction mixture is not stirred and therefore the reaction is slower due to poor diffusion. This effect is even more pronounced considering a reaction where one reagent in the gas phase and the other in the liquid phase, *e.g.*, a hydrogenation reaction. Use of our flow setup would mitigate these phenomena and allow a reaction monitoring under more realistic reaction conditions. Thus, our LF NMR setup in static *versus* flow conditions has been compared. For static conditions I used a J Young tube, classically inserted into the spectrometer, while for flow conditions I refer to our previously described third generation setup (Figure 18).

In static conditions, the hydrogenation of $[\text{Rh}(\text{DPPB})(\text{COD})]\text{BF}_4$ to $[\text{Rh}(\text{DPPB})(\text{MeOH})_2]\text{BF}_4$ ($^{31}\text{P}\{^1\text{H}\}$ NMR in MeOH: δ 52.7 ppm, $J_{\text{RhP}} = 198.8$ Hz)⁶⁴ has been followed (Scheme 6). The *in situ* reaction monitoring shows that approximately one day is required for full conversion and formation of the MeOH complex (Figure 28).



Scheme 6. Hydrogenation of $[\text{Rh}(\text{DPPB})(\text{COD})]\text{BF}_4$ to $[\text{Rh}(\text{DPPB})(\text{MeOH})_2]\text{BF}_4$ in MeOH.

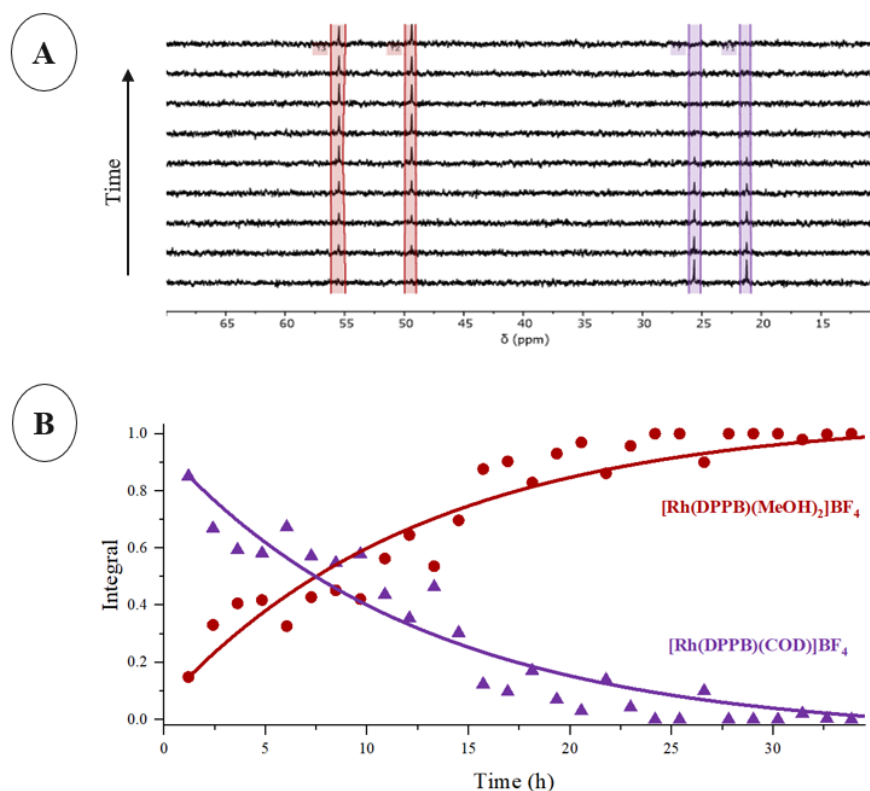


Figure 28. Low-Field static $^{31}\text{P}\{^1\text{H}\}$ NMR monitoring (A, methanol- d_4 , 32.6 MHz, $[\text{Rh}] = 4.1$ mM) and kinetic profile (B) of the hydrogenation of $[\text{Rh}(\text{DPPB})(\text{COD})]\text{BF}_4$ to $[\text{Rh}(\text{DPPB})(\text{MeOH})_2]\text{BF}_4$ (Scheme 6).

Details. Reaction monitoring with 25 loops, characterised by: shim (X, Y, Z, Z2); ^1H NMR (32 scans; 6.4 s acquisition time; 15 s repetition time); $^{31}\text{P}\{^1\text{H}\}$ NMR (256 scans; 3.2 s acquisition time; 15 s repetition time). Each loop lasted 72 min. For clarity, only one spectrum every 3rd is shown. Processing: zero filling to 32k points and exponential line broadening of 0.5 Hz.

In flow conditions, I followed the reaction *via* ^1H NMR spectroscopy with solvent suppression, specifically opting for the presaturation method (Figure 29, please refer to Figure A8 for an example of presaturation parameter screening). I could not rely on ^{31}P NMR data due to the short reaction time, but I could at least delete the shim from the reaction monitoring loop to record more data points.

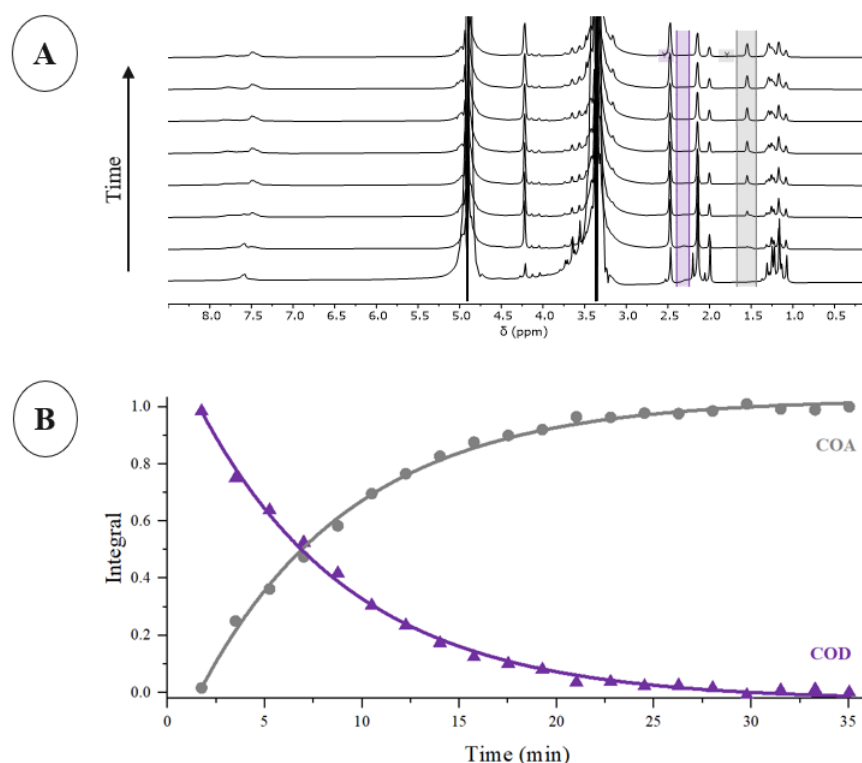


Figure 29. Low-Field Flow ¹H NMR monitoring with presaturation (**A**, MeOH, 80 MHz, [Rh] = 10.8 mM) and kinetic profile (**B**) of the hydrogenation of [Rh(DPPB)(COD)]BF₄ to [Rh(DPPB)(MeOH)₂]BF₄ (**Scheme 6**). The CH₂ group of the cyclooctane is highlighted at 1.6 ppm. **Details.** Reaction monitoring with 15 loops, characterised by ¹H NMR with presaturation (8 scans; 6.4 s acquisition time; 10 s repetition time). Each loop lasted 1.75 min. For clarity, only one spectrum every 2nd is shown. Processing: zero filling to 64k points and exponential line broadening of 0.2 Hz.

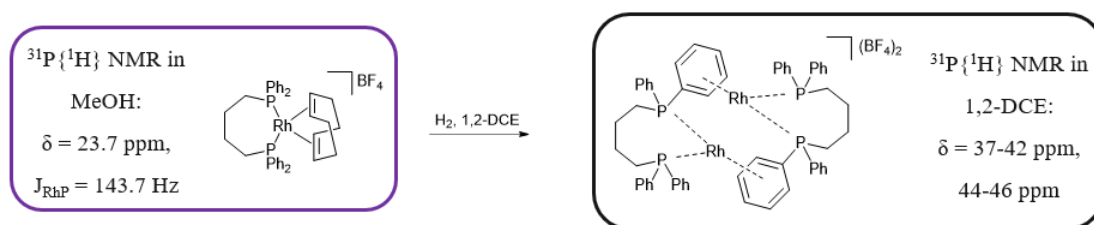
As reported in literature,⁵⁴ the reaction is completed after approximately 30 minutes. Moreover, no oxidation has been detected in LF flow ³¹P NMR reaction monitoring over a period of 60 hours and in the static sample analysed by HF NMR spectroscopy afterwards (**Figure A5**).

The difference in reaction time between static and flow conditions is evident. Kinetic profiles obtained *via on-line* reaction monitoring are thus much more reliable than the one from *in situ* experiments.

3.4. Limitations – High multiplicity signals

The hydrogenation of rhodium diolefin complexes is sensitive to the chosen solvent. As shown before, the solvent complex is formed in coordinating solvents (*e.g.*, MeOH, [Scheme 6](#)). In cases where arene groups are part of the diphosphine ligand, η^6 -arene species are formed in non-coordinating solvents (*e.g.*, 1,2-dichloroethane).^{60,65,66} Such complexes can also be obtained in arene solvents, which is commonly the reason for lower catalytic activity of Rh(I) complexes under these conditions.

To evaluate the potential of our setup for the identification of dinuclear η^6 -arene rhodium complexes, which typically show higher multiplicity signals, I followed the hydrogenation of $[\text{Rh}(\text{DPPB})(\text{COD})]\text{BF}_4$ in 1,2-dichloroethane (1,2-DCE) to the isomers of $[\text{Rh}(\text{DPPB})]_2(\text{BF}_4)_2$ ($^{31}\text{P}\{^1\text{H}\}$ NMR in 1,2-DCE: signals between 37–42 ppm, 44–46 ppm)⁶⁷ ([Scheme 7](#), [Figure 30](#)). LF ^1H NMR reaction monitoring shows the progress of the reaction, *i.e.*, the hydrogenation of the COD ligand to COA.



[Scheme 7](#). Hydrogenation of $[\text{Rh}(\text{DPPB})(\text{COD})]\text{BF}_4$ to isomers of $[\text{Rh}(\text{DPPB})]_2(\text{BF}_4)_2$ in 1,2-DCE.

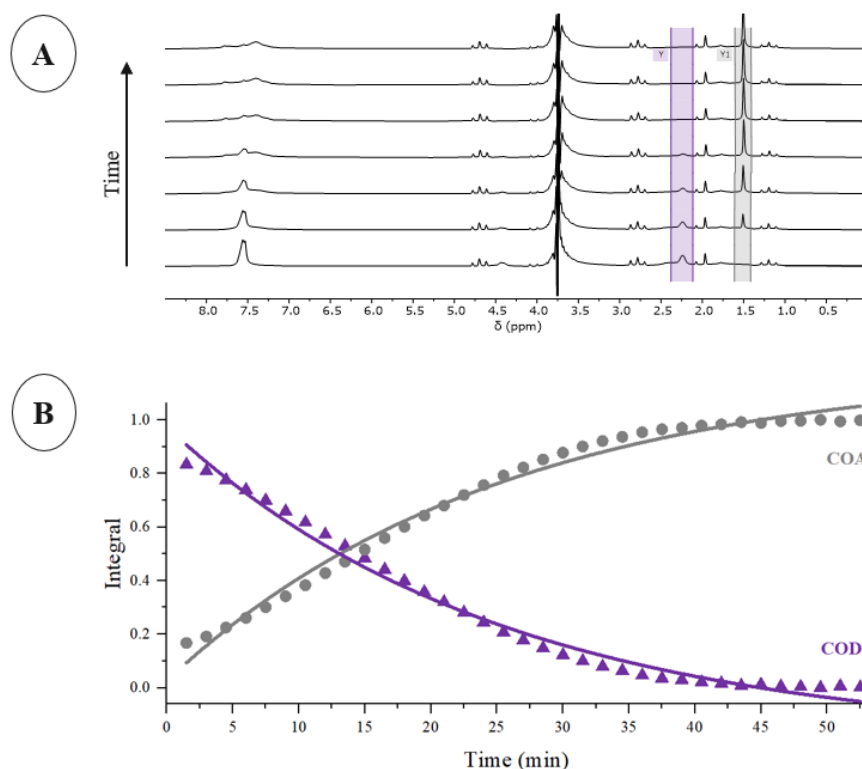


Figure 30. Low-Field Flow ^1H NMR monitoring with presaturation (**A**, 1,2-DCE, 80 MHz, $[\text{Rh}] = 41 \text{ mM}$) and kinetic profile (**B**) of the hydrogenation of $[\text{Rh}(\text{DPPB})(\text{COD})]\text{BF}_4$ to isomers of $[\text{Rh}(\text{DPPB})]_2(\text{BF}_4)_2$ (**Scheme 7**). The CH_2 group of the cyclooctane is highlighted at 1.6 ppm. **Details.** Reaction monitoring with 35 loops, characterised by ^1H NMR with presaturation (8 scans; 6.4 s acquisition time; 10 s repetition time). Each loop lasted 1.5 min. For clarity, only one spectrum every 5th is shown. Processing: zero filling to 64k points and exponential line broadening of 0.1 Hz.

Unclear resonances appear in LF ^{31}P NMR reaction monitoring (**Figure 31A**). At the end of the reaction (as confirmed by ^1H NMR reaction monitoring), I acquired the LF ^{31}P NMR spectrum in static conditions, but I still could not properly attribute the signals obtained (**Figure 31B**). The comparison with HF ^{31}P NMR spectra shows the limitation of our LF NMR spectrometer for high multiplicity signals (**Figure 31C,D**). Signal patterns of similar complexity have been observed for other related η^6 -arene dinuclear Rh complexes.⁶⁵

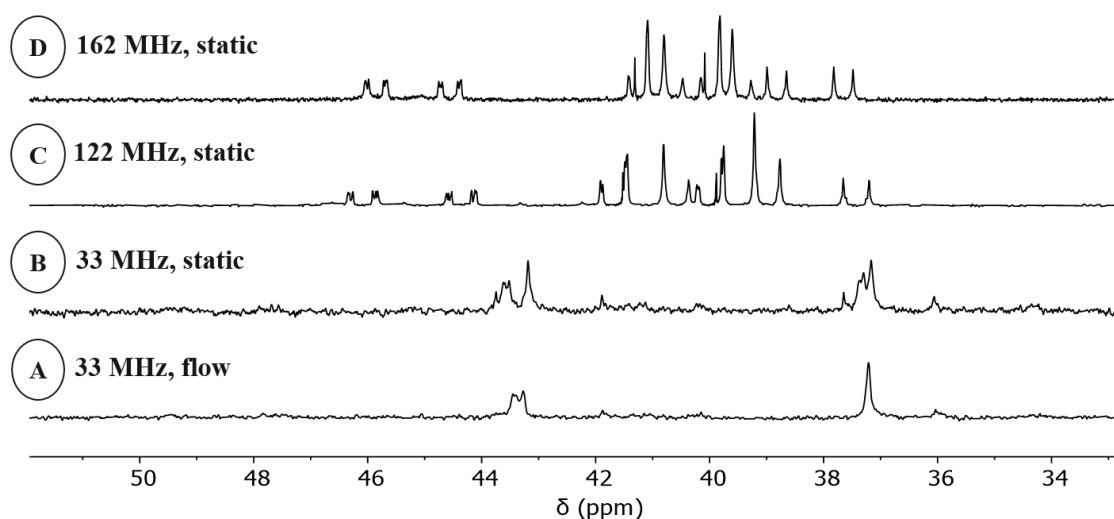


Figure 31. Comparison between LF and HF $^{31}\text{P}\{^1\text{H}\}$ NMR spectrum of the isomers of $[\text{Rh}(\text{DPPB})_2](\text{BF}_4)_2$ ($[\text{Rh}] = 41 \text{ mM}$, [Scheme 7](#)): LF flow (33 MHz, 1,2-DCE) $^{31}\text{P}\{^1\text{H}\}$ NMR spectrum (**A**); LF static (33 MHz, 1,2-DCE) $^{31}\text{P}\{^1\text{H}\}$ NMR spectrum (**B**); HF static (122 MHz, $\text{DCM}-d_2$) $^{31}\text{P}\{^1\text{H}\}$ NMR spectrum (**C**); HF static (162 MHz, 1,2-DCE- d_4) $^{31}\text{P}\{^1\text{H}\}$ NMR spectrum (**D**). All spectra are characterised by 256 number of scans.

If the rearrangement in the space for chemically equivalent phosphorous atoms is different, the magnetic field experienced is different. The signals could be attributed to a major and minor isomers of the dimer $[\text{Rh}(\text{DPPB})_2](\text{BF}_4)_2$, calculated to be in a ratio of 6:4 ([Figure 32](#)).

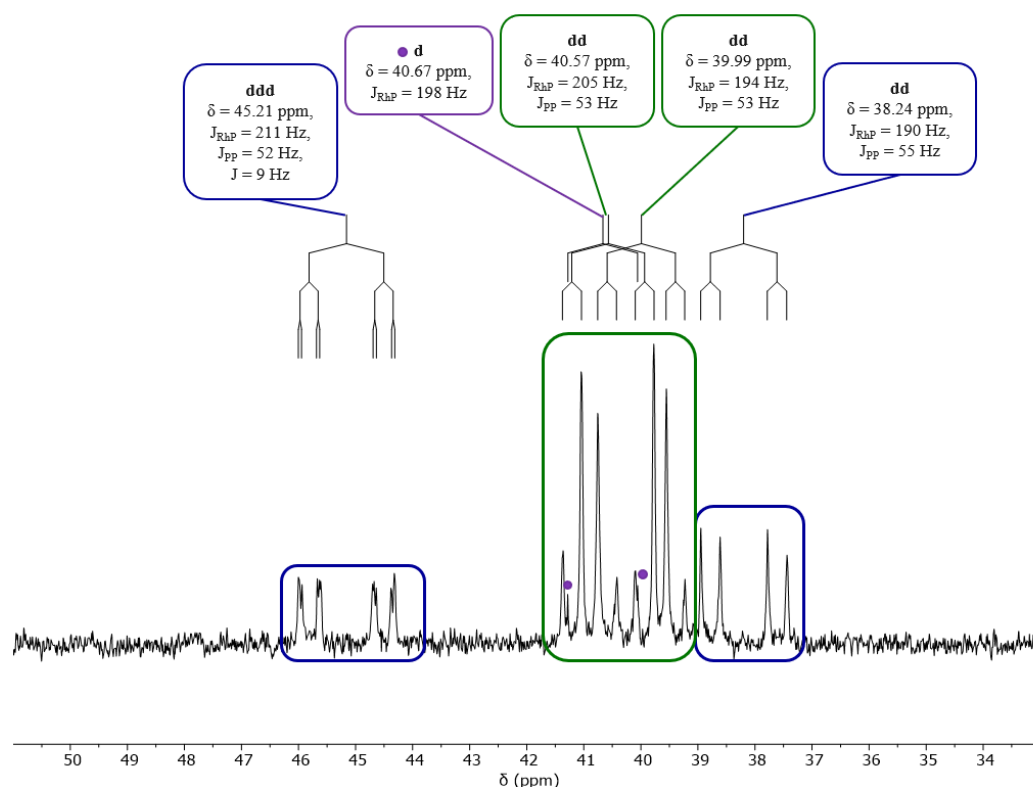


Figure 32. HF $^{31}\text{P}\{^1\text{H}\}$ NMR spectrum of the isomers of $[\text{Rh}(\text{DPPB})]_2(\text{BF}_4)_2$ (1,2-DCE- d_4 162 MHz, $[\text{Rh}] = 41$ mM, [Scheme 7](#)). The major isomer is highlighted in green while the minor isomer in blue (the attribution is derived from [Figure 33](#) and [Figure 34](#)). Detectable J_{RhP} and J_{PP} coupling constant are indicated. The species highlighted in purple remains unknown.

The attribution of major and minor isomers in the $^{31}\text{P}\{^1\text{H}\}$ NMR spectrum has been derived from $^{31}\text{P}\{^1\text{H}\}$ COSY analysis ([Figure 33](#)).

The $^{31}\text{P}\{^1\text{H}\}$ - ^{103}Rh HMQC NMR spectrum further confirms the previous shown attribution ([Figure 34](#)). Of note, the ^{103}Rh NMR signals of -547.7 ppm and -555.5 ppm are in the expected range for η^6 -arene rhodium complexes. For example, $[\text{Rh}(\text{BINAP})]_2(\text{BF}_4)_2$ in DCM, appear at -394 ppm in ^{103}Rh NMR spectrum.⁶⁵

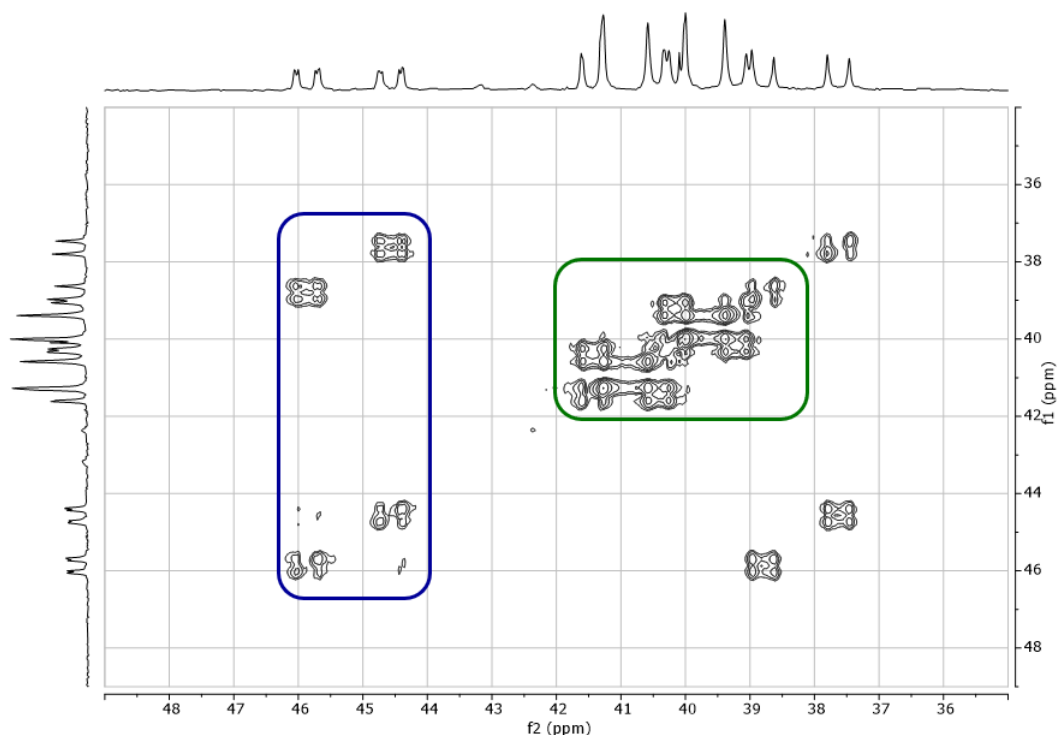


Figure 33. HF $^{31}\text{P}\{^1\text{H}\}$ COSY of the isomers of $[\text{Rh}(\text{DPPB})_2(\text{BF}_4)_2]$ ($\text{DCM}-d_2$, 162 MHz, $[\text{Rh}] = 41 \text{ mM}$, Scheme 7). The different isomers are highlighted in different colors, as before.

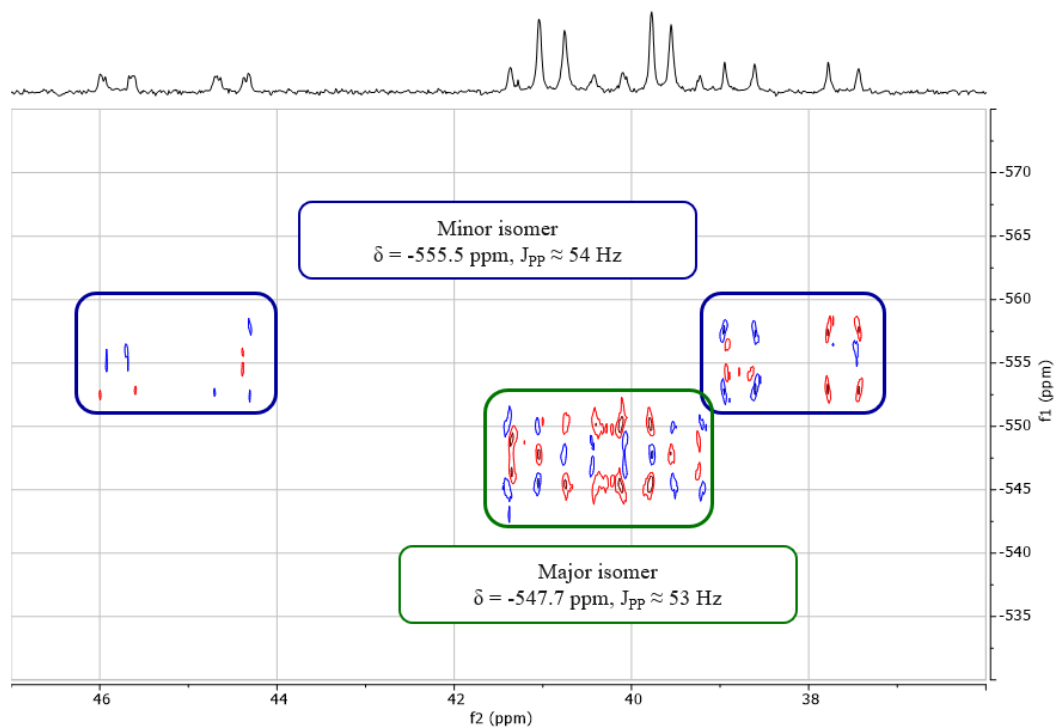


Figure 34. HF $^{31}\text{P}\{^1\text{H}\}-^{103}\text{Rh}$ HMQC NMR spectrum of isomers of $[\text{Rh}(\text{DPPB})_2(\text{BF}_4)_2]$ (1,2-DCE + 1,2-DCE- d_4 , 162 MHz, $[\text{Rh}] = 23 \text{ mM}$, 297 K, Scheme 7). The minor isomer (in blue) appears at -555.5 ppm while the major isomer (in green) appears at -547.7 ppm.

Complex $[\text{Rh}(\text{DPPB})]_2(\text{BF}_4)_2$ could be crystallised in 1,2-DCE at 8 °C. Single crystal X-ray diffraction (SC-XRD) analysis confirms that each DPPB ligand acts as a bridging ligand between two rhodium centers (**Rh1**). Rhodium (**Rh1**) is coordinated by the two phosphorus atoms (**P1**, **P2**) and one phenyl group of a second DPPB ligand in a η^6 -coordination. Half of the molecule had been calculated with a symmetry operation. Similar structures have been obtained before, *e.g.*, for the dimer of $[\text{Rh}(\text{DIPAMP})_2](\text{BF}_4)_2$ ⁶⁵ and bond metrics are in accordance with previously reported data.

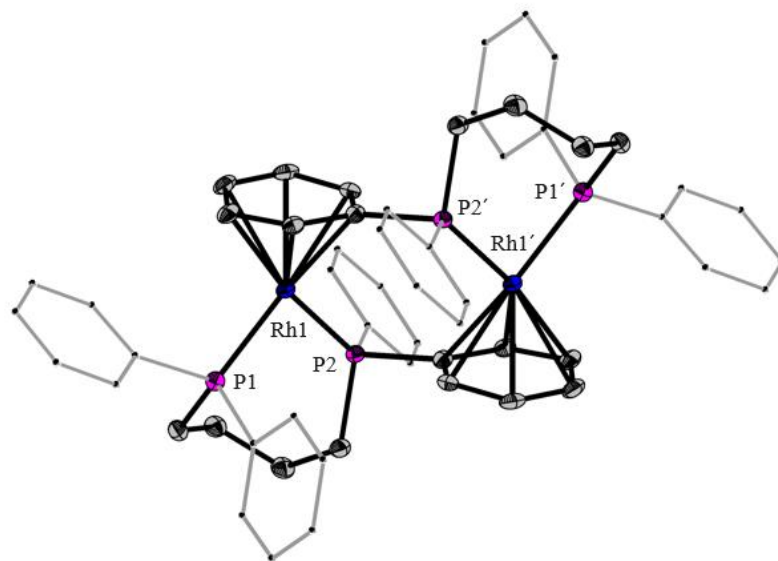
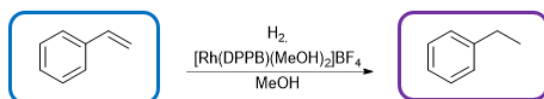


Figure 35. Molecular structure of the dication of one isomer of $[\text{Rh}(\text{DPPB})]_2(\text{BF}_4)_2$ (**Scheme 7**). Thermal ellipsoids are set at 30% probability. For clarity, hydrogen atoms are omitted. Phenyl groups not involved in the coordination to the rhodium centers are represented as wireframes.

3.5. Catalysis – Styrene hydrogenation

A catalytic hydrogenation reaction has been followed with our third generation setup using molecular hydrogen. The model substrate styrene has been hydrogenated in the presence of $[\text{Rh}(\text{DPPB})(\text{MeOH})_2]\text{BF}_4$ to yield ethylbenzene (ratio $[\text{Rh}]/\text{styrene}$ 1:100, [Scheme 8](#), [Figure 36](#)).



[Scheme 8](#). Hydrogenation of styrene, in the presence of $[\text{Rh}(\text{DPPB})(\text{MeOH})_2]\text{BF}_4$ in MeOH, to produce ethylbenzene.

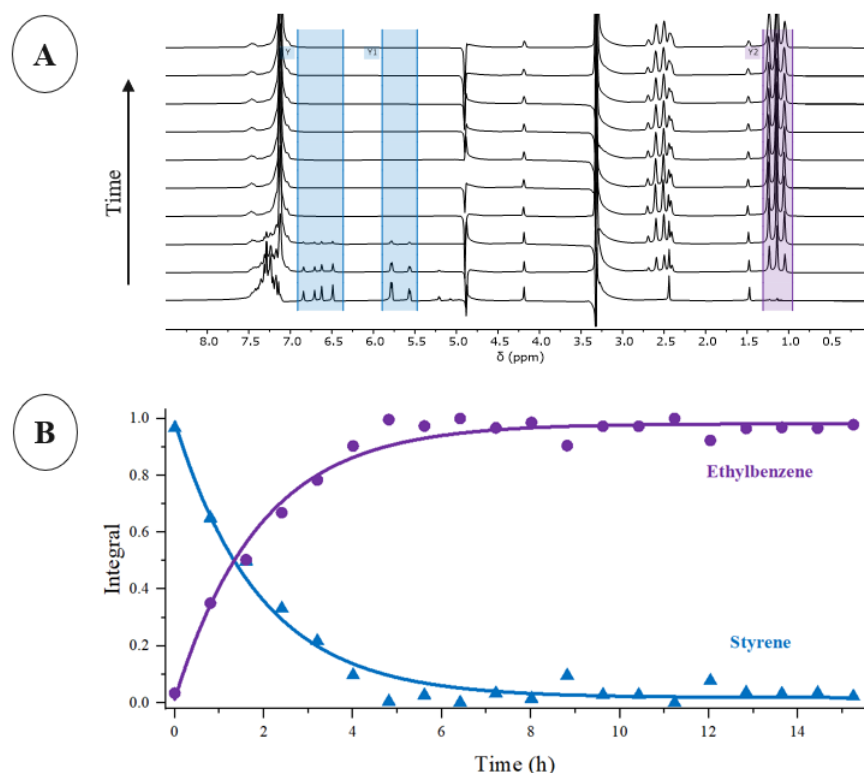


[Figure 36](#). Low-Field Flow ^1H NMR monitoring with presaturation ([A](#), MeOH, 80 MHz, $[\text{Rh}] = 12.2 \text{ mM}$) and kinetic profile ([B](#)) of the hydrogenation of styrene in the presence of $[\text{Rh}(\text{DPPB})(\text{MeOH})_2]\text{BF}_4$ ([Scheme 8](#)).

Details. Reaction monitoring with 20 loops, characterised by: shim (X, Y, Z, Z2); ^1H NMR with presaturation (16 scans; 6.4 s acquisition time; 10 s repetition time); $^{31}\text{P}\{^1\text{H}\}$ NMR (256 scans; 2 s acquisition time; 10 s repetition time). Each loop lasted 48 min. For clarity, only one spectrum every 2nd is shown. Processing: zero filling to 64k points and exponential line broadening of 0.2 Hz.

^{31}P NMR monitoring shows that the solvent complex immediately coordinates the substrate, forming the η^6 -styrene complex $[\text{Rh}(\text{DPPB})(\eta^6\text{-styrene})]\text{BF}_4$ ($^{31}\text{P}\{^1\text{H}\}$ NMR in 1,2-DCE: δ 40.6 ppm, $J_{\text{RhP}} = 198.1 \text{ Hz}$)^{47,68} ([Figure 37](#), [Figure 38](#), [Figure A6](#)). The latter is slowly converted into the η^6 -ethylbenzene complex $[\text{Rh}(\text{DPPB})(\eta^6\text{-ethylbenzene})]\text{BF}_4$ ($^{31}\text{P}\{^1\text{H}\}$ NMR

in 1,2-DCE: δ 41.0 ppm, $J_{\text{RhP}} = 198.7$ Hz)^{47,68} (Figure A7) under hydrogen atmosphere.^s Our setup allowed the distinction of the two rhodium species involved, despite the challenging proximity of the doublets. Indeed, the only structural difference between the two complexes, *i.e.*, the vinyl vs the ethyl group, is remote from the phosphorous atoms. Once again oxidation of the diphosphine ligand has not been observed, as confirmed afterwards by HF NMR spectroscopy.

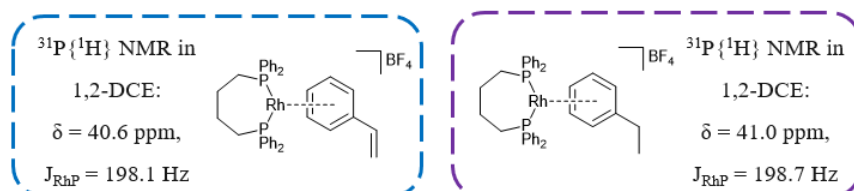


Figure 37. Involved η^6 -arene rhodium complexes in the hydrogenation of styrene in the presence of $[\text{Rh}(\text{DPPB})(\text{MeOH})_2]\text{BF}_4$ in MeOH (Scheme 8).

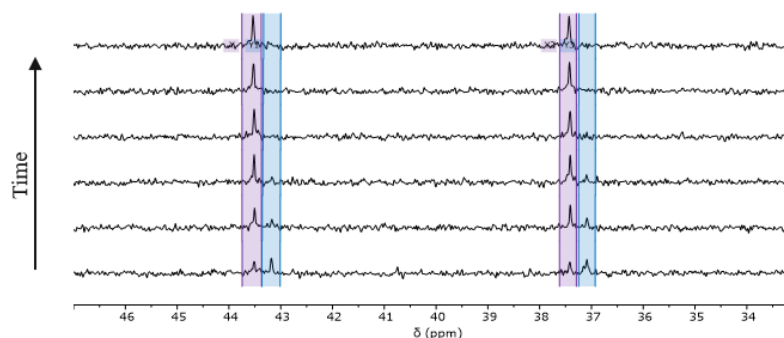


Figure 38. Low-Field Flow $^{31}\text{P}\{^1\text{H}\}$ NMR monitoring (MeOH, 32.6 MHz, $[\text{Rh}] = 12.2$ mM) of the hydrogenation of styrene in the presence of $[\text{Rh}(\text{DPPB})(\text{MeOH})_2]\text{BF}_4$ (Scheme 8).

Details. Reaction monitoring with 20 loops, characterised by: shim (X, Y, Z, Z2); ^1H NMR with presaturation (16 scans; 6.4 s acquisition time; 10 s repetition time); $^{31}\text{P}\{^1\text{H}\}$ NMR (256 scans; 2 s acquisition time; 10 s repetition time). Each loop lasted 48 min. For clarity, only one spectrum every 2nd is shown. Processing: zero filling to 64k points and exponential line broadening of 0.2 Hz.

Different trials have been made to obtain single crystals of $[\text{Rh}(\text{DPPB})(\eta^6\text{-ethylbenzene})]\text{BF}_4$, suitable for SC-XRD analysis from the solvent complex in MeOH, but failed. The molecular structure shown here has eventually been obtained from the dimer $[\text{Rh}(\text{DPPB})]_2(\text{BF}_4)_2$ in 1,2-DCE at r.t. (Figure 39, Table A1). SC-XRD analysis confirmed the nature of the hydrogenation product. The complex $[\text{Rh}(\text{DPPB})(\eta^6\text{-ethylbenzene})]\text{BF}_4$ shows the same coordination pattern as in dimer $[\text{Rh}(\text{DPPB})]_2(\text{BF}_4)_2$ (Figure 35) with intermolecular η^6 -coordination of the arene. The Rh-P bonds (Rh1-P1 2.2420(8), Rh1-P2 2.2464(9) Å) are slightly shorter than in the dimer (2.2470, 2.2566(11) Å) and the η^6 coordination of ethylbenzene (Rh-C 2.272 – 2.370(4) Å) is in the same range of $[\text{Rh}(\text{DPPB})]_2(\text{BF}_4)_2$ (Rh-C 2.279 – 2.365(4) Å).

^s The same hydrogenation reaction has been followed *via* a setup that allows to measure the hydrogen uptake (Table A2, Figure A2).

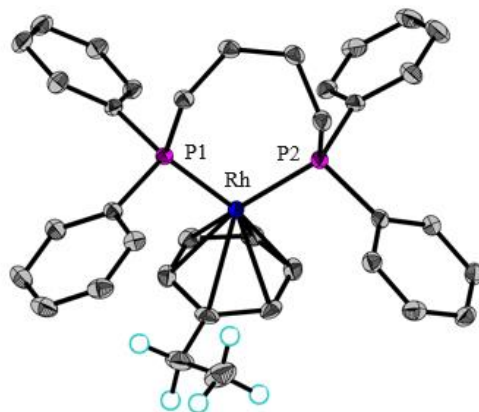


Figure 39. Molecular structure of the cation of $[\text{Rh}(\text{DPPB})(\eta^6\text{-ethylbenzene})]\text{BF}_4$ (Scheme 8). Thermal ellipsoids are set at 30% probability. For clarity, hydrogen atoms (except for the ethyl group of ethylbenzene) are omitted.

Further NMR spectroscopic characterisation of the two rhodium η^6 -arene complexes has been done in the presence of excess of the respective substrate to avoid its decoordination (Figure 40). Of note, the antiphase characteristic is due to the missed refocussing, otherwise the two signals of the doublet would appear with the same phase.

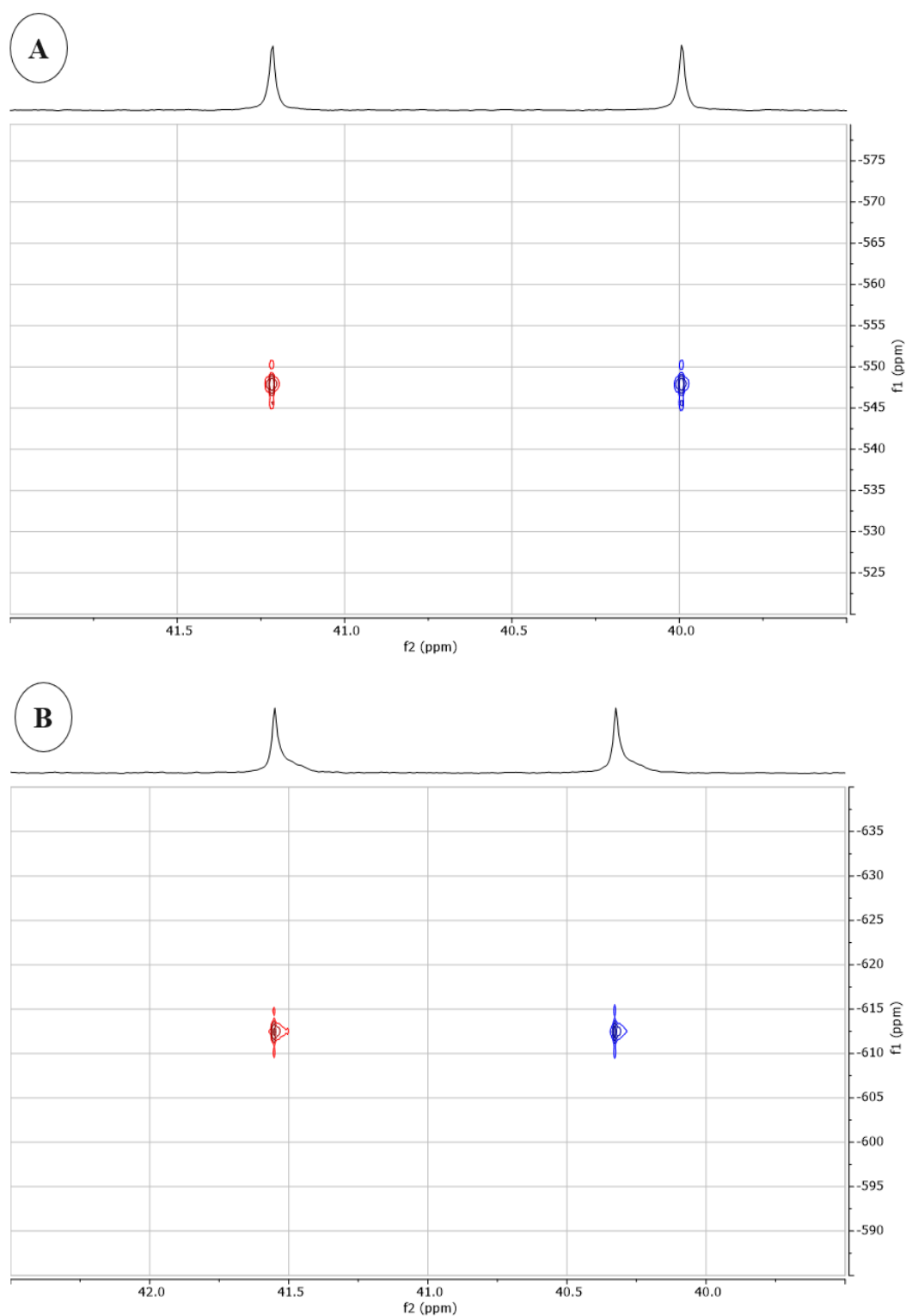


Figure 40. $\text{HF } ^{31}\text{P}\{^1\text{H}\}\text{-}^{103}\text{Rh}$ HMQC NMR spectrum of $[\text{Rh}(\text{DPPB})(\eta^6\text{-styrene})]\text{BF}_4$ (1,2-DCE + 1,2-DCE- d_4 , 162 MHz, $[\text{Rh}] = 23$ mM, 297 K, **A**, [Figure 37](#)) and of $[\text{Rh}(\text{DPPB})(\eta^6\text{-ethylbenzene})]\text{BF}_4$ (1,2-DCE + 1,2-DCE- d_4 , 162 MHz, $[\text{Rh}] = 27$ mM, 297 K, **B**, [Figure 37](#)). The styrene complex appears at -548 ppm while the ethylbenzene complex appears at -613 ppm.

3.6. Signal enhancement – SHARPER ^{31}P NMR sequence

All $^{31}\text{P}\{^1\text{H}\}$ NMR experiments reported up to this point show rather low SNR. In the last section of this thesis, I used different SHARPER pulse sequences. The aim is to increase SNR and ultimately allow faster acquisition of ^{31}P NMR spectra. This is relevant, not only for monitoring fast catalytic reactions involving organophosphorus species, but also for developing new methods for NMR spectroscopy.

I report the SHARPER sequence as visualised by the Spinsolve Expert software (Figure 41, please refer to the Chapter 5.5 for the SHARPER macro). After technical settings relevant for the spectrometer, the Waltz sequence is applied on the proton channel to produce the nuclear Overhauser effect (NOE, A). After a delay, the hard 90° pulse (B) is applied to bring the magnetization into the XY plane. After a delay, the FID half chunk is acquired (C). The refocusing loop follows, characterised by the hard 180° pulse (E) surrounded by delays (D, F) and the FID chunk (G). The pulse gated overhear (pgo) and receiver latency (rxLat) values are delays due to the electronics in the spectrometer. The first corresponds to a delay before a pulse while the second refers to a delay before the acquisition of the FID. Echo time (ET) is defined in this thesis as the delay that precedes and follows the 180° pulse (corrected accordingly with the pgo or rxLat parameter). The chunk length (CL) corresponds to the acquisition time of the various FID chunks inside the refocussing loop.

Another technical issue led to the creation of the last separated repetition. Spinsolve requires the number of acquisition points to always be a power of 2. For this reason, the last repetition has been moved outside of the refocussing loop to allow a separated calculation of its number of points (H). Basically, there is no physical meaning behind it. This procedure is just a practical trick to overcome technical limitations, which could be ignored on a spectrometer which has no such limitation.

The sel-SHARPER sequence is also reported (Figure 42, please refer to the Chapter 5.6 for the sel-SHARPER macro). The new aspects, compared to SHARPER, are the following: the hard 180° pulse is now replaced by a Gaussian 180° pulse (J) and is now surrounded by gradients (I, K). Three selective pulses, all shaped as Gaussian but with different selectivity, have been screened (Chapter 3.6.1). As explicitly indicated in the figure, the gradients are applied along the three dimensions (X , Y and Z). The first gradient (I) and the second one (K) have the same phase. In this way, the magnetization that is inverted by the selective Gaussian pulse is refocussed while the one that is outside of the range gets even more dephased.

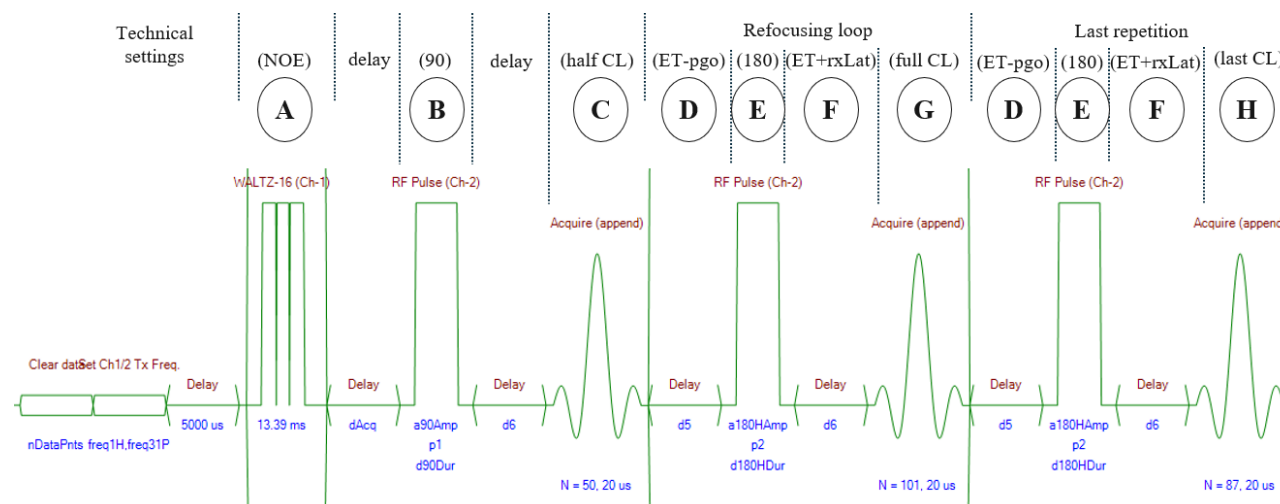


Figure 41. SHARPER sequence as visualised in Spinsolve Expert. Additional comments to guide the reader are shown in black.

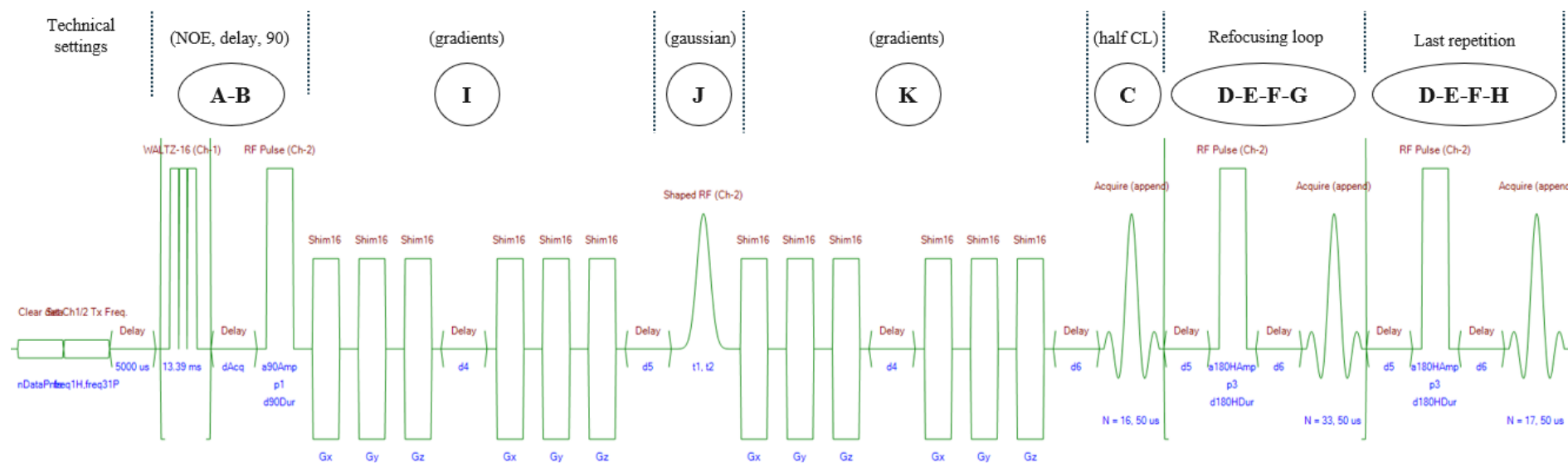


Figure 42. Sel-SHARPER sequence as visualised in Spinsolve Expert. Additional comments to guide the reader are shown in black.

As shown in the detailed parameters table (Table A7), the imaginary part has never been removed because no additional improvement in SNR could be observed. I typically removed one point from each chunk for getting a cleaner FID. This is necessary because the chunking of the FID in the SHARPER sequence creates a reconstructed FID with artifacts, which could be slightly improved removing the first point of acquisition in each chunk.

Sidebands often appear in the final processed spectrum, but they are recognizable and usually very small. The following example explicitly shows this phenomenon with a $[\text{Rh}((R,R)\text{-DIPAMP})(\text{NBD})]\text{BF}_4$ sample ($^{31}\text{P}\{^1\text{H}\}$ NMR in MeOH: δ 49.7 ppm, $J_{\text{RhP}} = 158.4$ Hz, Figure 43). There are two low intensity peaks on both sides of the main peak, at the same distance of 19.17 ppm. Which is predictable, knowing that the chunk length is 1.6 ms (set acquisition parameters: 32 number of points of the chunk; 50 μs dwell time). Its reciprocal is a frequency of 625 Hz, which correspond to 19.17 ppm on our spectrometer (32.6 MHz for the ^{31}P nucleus).

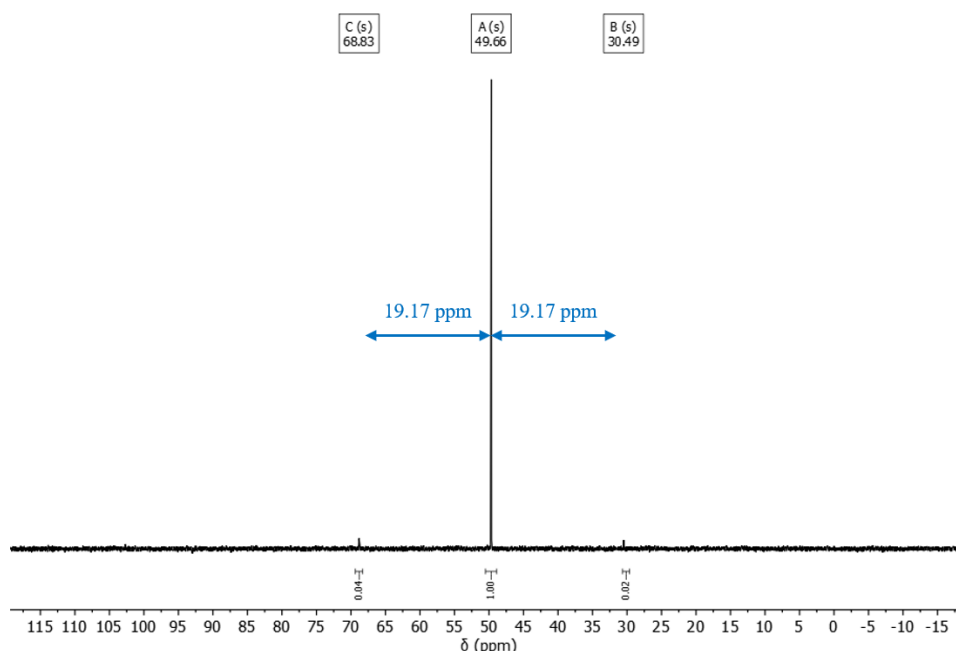


Figure 43. SHARPER ^{31}P NMR spectrum of $[\text{Rh}((R,R)\text{-DIPAMP})(\text{NBD})]\text{BF}_4$ (112 mM in $\text{DCM-}d_2$, 32.6 MHz). Sidebands are visible around the main peak.

Please note that, in the following spectra, the stacked plots for reaction monitoring have been cut for a better visualisation of the peaks in a chemical shift range that does not contain those sidebands. They might be present but not visible in the depicted spectra. Anytime that strong sidebands appeared during my experiments, the analysis has been discarded and the parameters have been optimized to minimise these sidebands.

I have added the NOE part to the SHARPER sequence for ^{31}P nucleus, gaining increase in the SNR (please refer to Chapter 3.6.2 for a stacked plot illustrating this phenomenon). A key point consisted in merging the phase cycle of traditional ^{31}P sequence with NOE and the phase of the

SHARPER sequence (please refer to the [Chapter 5.3](#) for the full phase cycling lists). The SHARPER sequence boosts different peaks in a different way.

3.6.1. Pulse calibration

Before applying any pulse like sel-SHARPER, it is recommended to first calibrate the spectrometer. First of all, the basic 90° and 180° hard pulses should be checked, for both ^1H and ^{31}P nuclei. It is recommended to find the duration required for a 180° pulse and then derive from it the duration for a 90° pulse. Indeed, the change in duration is more prominent for a 180° than a 90° pulse.

On our 80 MHz spectrometer, the calibrated values for the hard 90° pulse turned out to be 13 μs and 67 μs , respectively for ^1H and ^{31}P nuclei (water and KH_2PO_4 have been used as samples).

Afterwards, it is important to check if the RF amplifier gives a linear response and otherwise calibrate it. The amplifier of our spectrometer proved to have a linear response, while a response correction has been necessary in an older generation spectrometer (this was the case in one of the spectrometers available at the University of York, *i.e.*, a 40 MHz spectrometer from Magritek, with an additional channel probe for the ^{13}C nucleus).

Finally, the selective pulses need to be calibrated. I performed an amplitude sweep and plotted the intensity of the integral of the peak obtained in function of the power set for the Gaussian pulse (Figure 44A). As expected, the Gaussian pulse with the longest duration (duration of 10 ms) requires the lowest power (power of -37.5 dB). With the same three chosen durations of the pulse (*i.e.*, 10 ms, 5 ms and 3 ms), I performed an offset sweep (Figure 44B). In this experiment, the same pulse (with the same power and duration) is applied to a changing chemical shift offset. The corresponding plot of integrals vs chemical shift determines the selectivity. The Gaussian pulse with the longest duration (duration of 10 ms) is the one with the smallest FWHM (FWHM of 4.79 ppm) which corresponds to the most selective pulse.

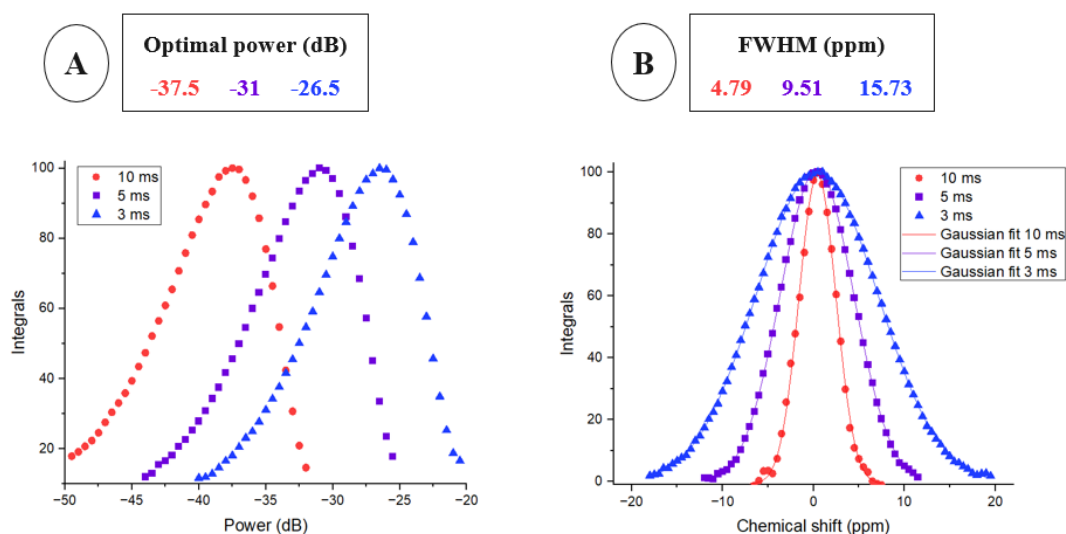


Figure 44. ^{31}P SPFG spin echo of KH_2PO_4 in water. The amplitude sweep allows the determination of the optimal power (A) while the offset sweep allows the determination of the selectivity (B).

Please note that the chemical shift on the horizontal axis is set to zero at the center of the peak.

Please note that the ^{31}P SPFG sequence did not require any ^1H decoupling in my calibration because of the nature of the sample. However, in case of a samples where ^{31}P is coupling with ^1H nuclei, the decoupling should be integrated. Indeed, the J evolution is initially refocused by the spin echo sequence, but it later evolves during acquisition.

It is recommended to check that the duration of the gradients is long enough to guarantee the differentiation of the spins but not too long to allow diffusion effects (if the spins have time to move in solution they will not be refocussed properly). To check the first condition, it is possible to repeat the sequence eliminating the selective 180° pulse: if the gradients are long enough there should be no signal appearing in the acquired spectrum. Also, it should be mentioned that care should be taken while changing to higher power since it could cause overheating that could damage the electronics of the spectrometer.

Regarding the hard 180° pulse, I have decided to avoid the use of composite pulses.[†] I have been satisfied with the classic hard 180° pulse but in case more precise pulses are required, it is suggested to switch to composite pulses.

The receiver gain has been set to obtain a high intensity peak without any saturation. Higher receiver gain would not lead to an improvement in terms of SNR since both the signal of the analyte and the noise would get enhanced.

[†] Composite pulses improve the quality of the RF excitation in NMR experiment. For example, a 180_x pulse could be replaced with a composite pulse like $90_y - 180_x - 90_y$. One disadvantage to keep in mind is that, replacing one pulse with a composite one, the experiment duration is increasing.

3.6.2. Single-component solution *via* SHARPER

I compared the NMR spectra of a single-component solution containing the above described Rh complex $[\text{Rh}((R,R)\text{-DIPAMP})(\text{NBD})]\text{BF}_4$ obtained from traditional ^{31}P NMR and different SHARPER sequences (Figure 45).

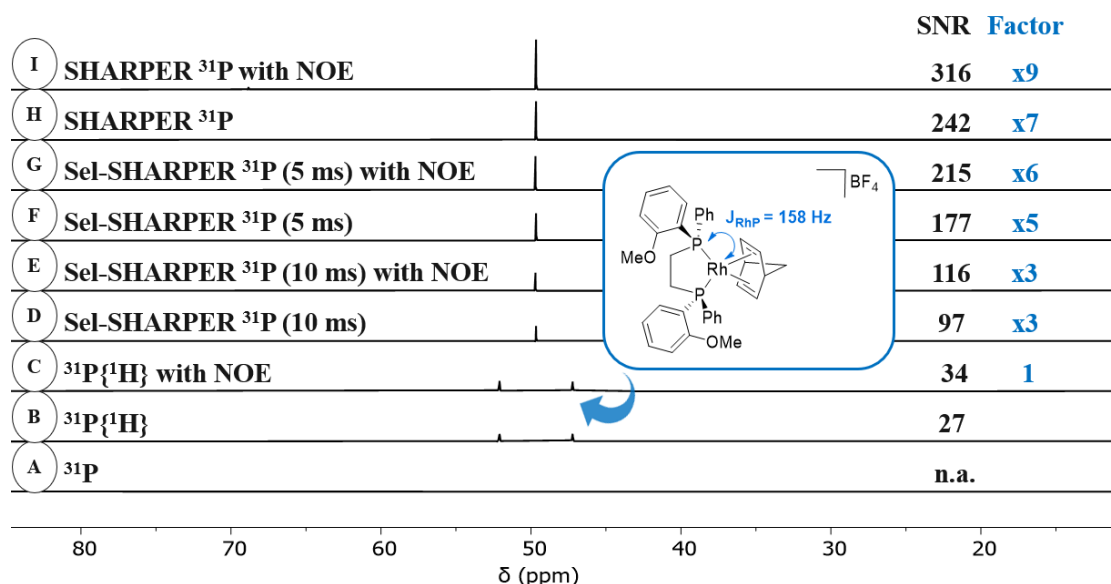


Figure 45. Comparison between ^{31}P NMR and SHARPER experiments of $[\text{Rh}((R,R)\text{-DIPAMP})(\text{NBD})]\text{BF}_4$ (112 mM in $\text{DCM-}d_2$, 32.6 MHz): ^{31}P NMR spectrum without decoupling from ^1H and without NOE (A); $^{31}\text{P}\{^1\text{H}\}$ NMR spectra, with or without NOE (B,C); sel-SHARPER ^{31}P NMR spectra with a Gaussian-shaped selective pulse of the duration of 10 ms, with or without NOE (D,E); sel-SHARPER ^{31}P NMR spectra with a Gaussian-shaped selective pulse of the duration of 5 ms, with or without NOE (F,G); SHARPER ^{31}P NMR spectra, with or without NOE (H,I).

Details. Processing: zero filling to 128k points and exponential line broadening of 0.2 Hz. Please refer to Table A7 for additional information.

The complex $[\text{Rh}((R,R)\text{-DIPAMP})(\text{NBD})]\text{BF}_4$ in $\text{DCM-}d_2$ gives rise to a doublet in the ^{31}P NMR spectrum. Decoupling is indispensable to be able to detect the desired signal (Figure 45A,B). Addition of the NOE positively impacts the SNR, both in the case of ^{31}P NMR and SHARPER spectra (Figure 45B,C). Consequently, all SHARPER spectra shown from now on are carried out with NOE (even if not explicitly stated). The shorter selective Gaussian (5 ms vs 10 ms), the higher is the SNR enhancement (Figure 45E,G). Following this trend, SHARPER sequences give a higher SNR compared to sel-SHARPER analogs (Figure 45G,I).

3.6.3. Simulated two-components solution via MR-SHARPER

Having identified the optimal parameters for SHARPER, the next step involved simulating a two-component solution. As two-component solution, I specifically consider a mixture of two species which gives two resonances in the $^{31}\text{P}\{^1\text{H}\}$ NMR spectrum. As simulated two-component solution, an NMR sample containing only one complex, $[\text{Rh}((R,R)\text{-DIPAMP})(\text{NBD})]\text{BF}_4$, has been prepared. As explained in the introduction (Chapter 1.4.4), I moved from SHARPER to MR-SHARPER sequence. For the simulation, the relevant parameter for hitting resonance condition (*i.e.*, the chunk length), has been optimized considering a hypothetical second peak at higher field at 25 ppm difference (Figure 46).

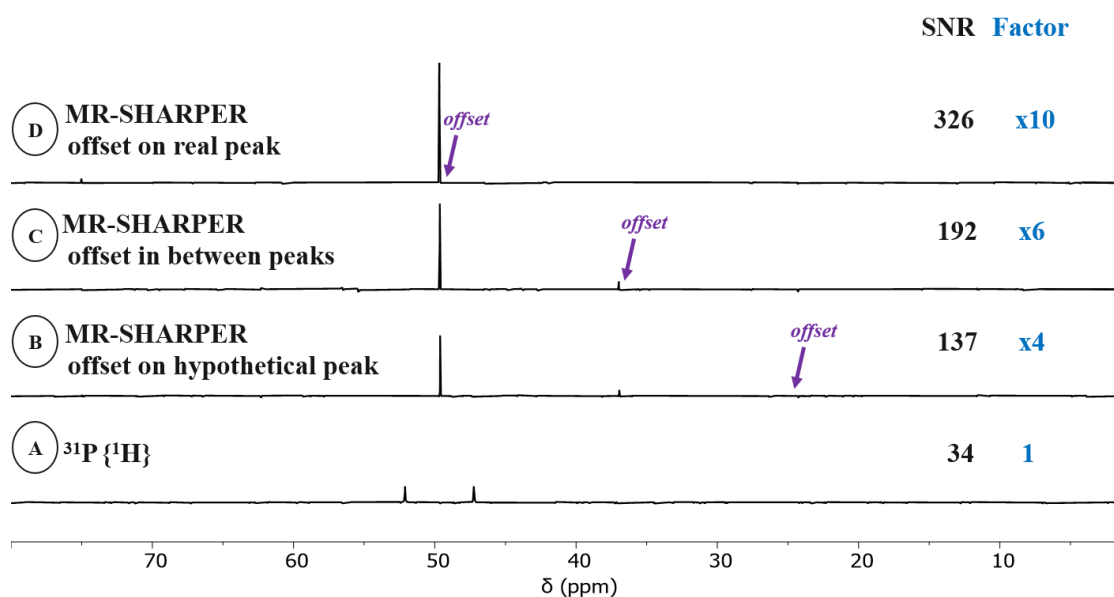


Figure 46. Comparison between $^{31}\text{P}\{^1\text{H}\}$ NMR and MR-SHARPER experiments of $[\text{Rh}((R,R)\text{-DIPAMP})(\text{NBD})]\text{BF}_4$ (112 mM in $\text{DCM-}d_2$, 32.6 MHz): $^{31}\text{P}\{^1\text{H}\}$ NMR spectrum with NOE (A); MR-SHARPER ^{31}P NMR spectrum with NOE and offset on hypothetical peak at 24.27 ppm (B); MR-SHARPER ^{31}P NMR spectrum with NOE and offset in between hypothetical and real peak at 35.97 ppm (C); MR-SHARPER ^{31}P NMR spectrum with NOE and offset on real peak at 49.67 ppm (D).

Details. Processing: zero filling to 128k points and exponential line broadening of 0.2 Hz. Please refer to Table A7 for additional information.

Centring the offset on the hypothetical peak gives better SNR with respect to the traditional $^{31}\text{P}\{^1\text{H}\}$ NMR spectrum (Figure 46A,B). Centring the offset in the middle between the real and the hypothetical peaks shows further improvement (Figure 46C). The best result, an improvement by a factor of 10 compared to the standard $^{31}\text{P}\{^1\text{H}\}$ NMR sequence, is achieved by centring the offset on the real peak of the analyte (Figure 46D).

3.6.4. Two-components solution *via* MR-SHARPER

Next, I moved to a real two-component solution, in which each of the two diolefin complexes $[\text{Rh}((R,R)\text{-DIPAMP})(\text{NBD})]\text{BF}_4$ and $[\text{Rh}(\text{DPPB})(\text{COD})]\text{BF}_4$ (ratio $\approx 1:1$) gives rise to a doublet resonance in the $^{31}\text{P}\{^1\text{H}\}$ NMR spectrum (Figure 47). Both complexes show no interconversion under the chosen conditions, *i.e.*, in the absence of excess free diolefin.

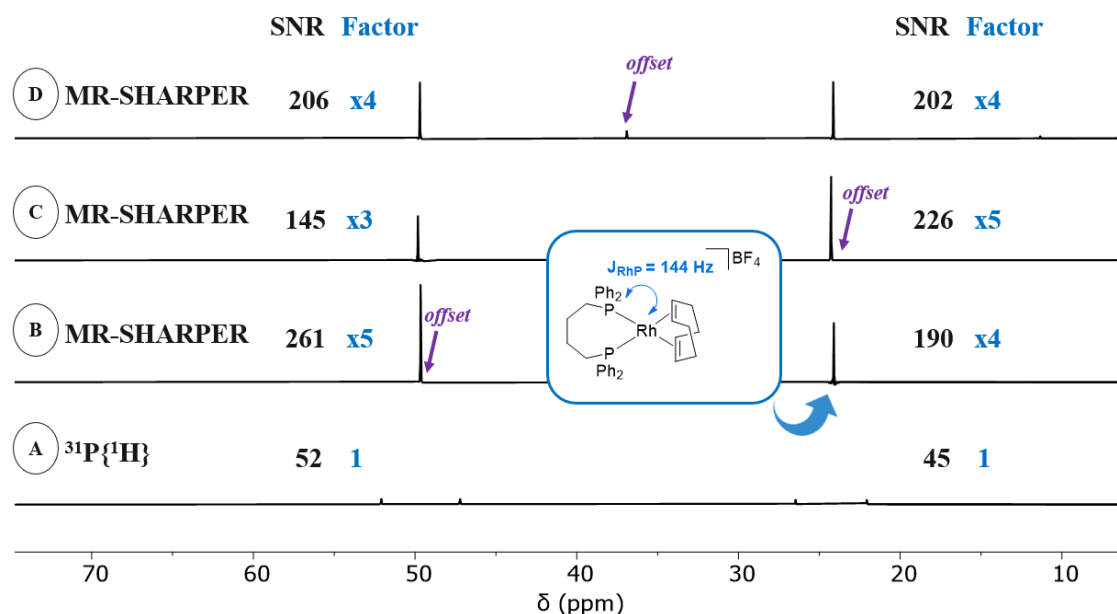


Figure 47. Comparison between $^{31}\text{P}\{^1\text{H}\}$ NMR and MR-SHARPER experiments of a mixture of $[\text{Rh}((R,R)\text{-DIPAMP})(\text{NBD})]\text{BF}_4$ (107 mM in DCM-d_2 , 32.6 MHz) and $[\text{Rh}(\text{DPPB})(\text{COD})]\text{BF}_4$ (106 mM in DCM-d_2 , 32.6 MHz): $^{31}\text{P}\{^1\text{H}\}$ NMR spectrum with NOE (A); MR-SHARPER ^{31}P NMR spectrum with NOE and offset on peak at 49.66 ppm (B); MR-SHARPER ^{31}P NMR spectrum with NOE and offset on peak at 24.27 ppm (C); MR-SHARPER ^{31}P NMR spectrum with NOE and offset between peaks at 36.92 ppm (D).

Details. Processing: zero filling to 256k points and exponential line broadening of 0.3 Hz. Please refer to Table A7 for additional information.

I found that having the offset on one peak gives the best results for that peak at the expense of intensity of the other one (Figure 47B,C). To have a balanced enhancement, with reliable integrals for both species, I preferred to put the offset in the middle between the two peaks (Figure 47D). The SNR boost of each peak is therefore reduced but still better compared to the traditional $^{31}\text{P}\{^1\text{H}\}$ NMR spectrum (Figure 47A).

In the previous single-component solution I achieved a 9-fold SNR enhancement (Chapter 3.6.2) and in the simulated two-components experiment I could go up to 10-fold SNR boost (Chapter 3.6.3). Now, with the two-components solution, a 5-fold enhancement has been obtained. The lower enhancement factor is due to the different processing required.

As previously described (Chapter 1.4.4), the chunk length needs to be inversely proportional to a multiple of the distance between the two multiplets. In case of strong J_{RhP} coupling of about

140–210 Hz, like in my case, only relatively short chunk lengths are allowed. To deal with this limitation, it is recommended to screen the acquisition time of the FID chunk. A relative too short acquisition time will give low SNR because of the relaxation process. A relative too long one will let the scalar coupling constant evolve and therefore the multiplet will not fully collapse into a singlet anymore. Indeed, dominating artifacts will appear in the spectrum (Figure A16).

As reported in the appendix (Figure A10, Figure A11), the echo time has been screened. For our complexes, the best results in SNR have been obtained with very short echo times (*e.g.*, 20 μ s).

I have chosen those two Rh diolefin complexes [Rh((*R,R*)-DIPAMP)(NBD)]BF₄ and [Rh(DPPB)(COD)]BF₄ as model components, showing well-separated peaks at 25 ppm distance, as a good simulation for my desired reaction, with peaks at 30 ppm difference (Chapter 3.6.5).

3.6.5. Reaction monitoring *via* MR-SHARPER

The repetition time of the $^{31}\text{P}\{^1\text{H}\}$ NMR sequence used as a reference in these considerations is 15 s while the one for SHARPER is 25 s. Until now, the sequences have been compared having equal number of scans. To allow for a more meaningful comparison between these two different techniques, I also compared the sequences having equal experiment time. Here, a single-component solution containing $[\text{Rh}((R,R)\text{-DIPAMP})(\text{NBD})]\text{BF}_4$ in MeOH has been tested (Figure 48).

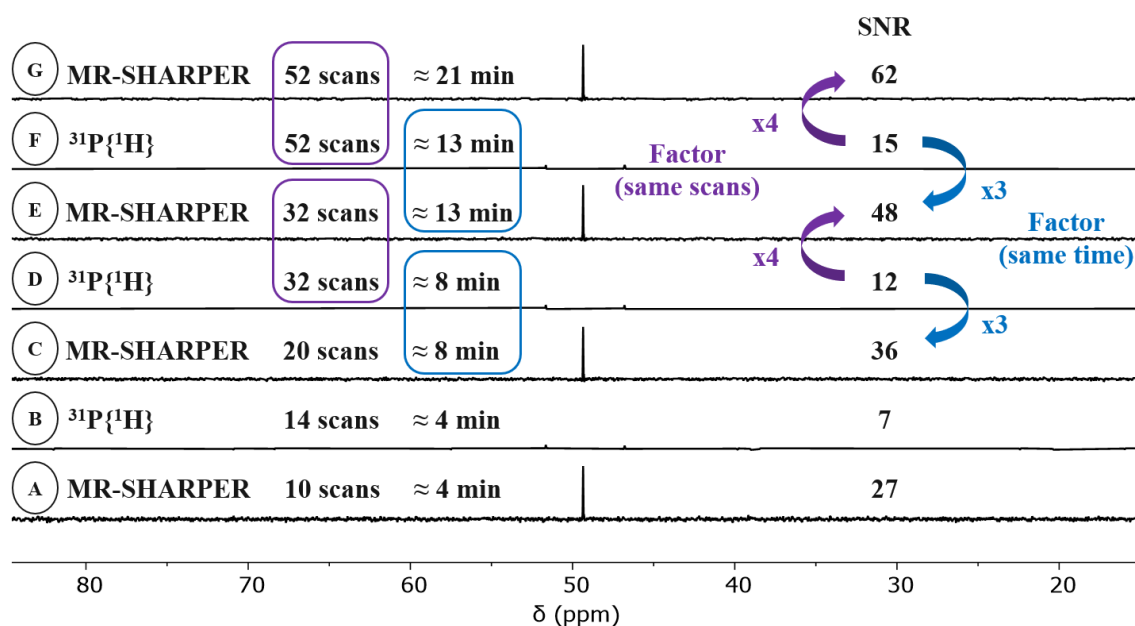
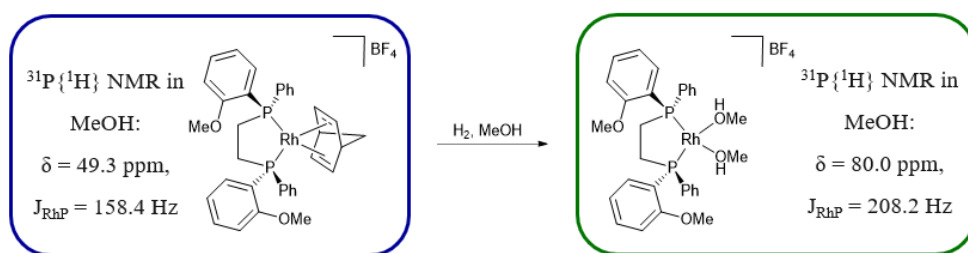


Figure 48. Comparison between $^{31}\text{P}\{^1\text{H}\}$ NMR and MR-SHARPER experiments of $[\text{Rh}((R,R)\text{-DIPAMP})(\text{NBD})]\text{BF}_4$ (9 mM in MeOH, 32.6 MHz): $^{31}\text{P}\{^1\text{H}\}$ NMR spectra with NOE (B,D,F); MR-SHARPER ^{31}P NMR spectra with NOE (A,C,E,G).

Details. Processing: zero filling to 128k points and exponential line broadening of 0.3 Hz. Please refer to Table A7 for additional information.

As a result, the enhancement factor decreases from 4, having the same number of scans (Figure 48F,G), to 3, considering the same period of time (Figure 48E,F).

To evaluate the potential of the SHARPER ^{31}P NMR method, I have then followed the hydrogenation of $[\text{Rh}((R,R)\text{-DIPAMP})(\text{NBD})]\text{BF}_4$ in MeOH (Scheme 9), a similar reaction to the one used before for the implementation and evaluation of our customized setup in flow conditions (Scheme 4, Figure 19).



Scheme 9. Hydrogenation of $[\text{Rh}((R,R)\text{-DIPAMP})(\text{NBD})]\text{BF}_4$ to produce $[\text{Rh}((R,R)\text{-DIPAMP})(\text{MeOH}_2)]\text{BF}_4$ in MeOH.

The SHARPER sequence proved to be superior to the traditional ^{31}P NMR one (Figure 49). Obtaining each spectrum in approximately 8 minutes, better SNR could be obtained *via* SHARPER ^{31}P NMR monitoring. Moreover, much less scattering of the data points is observed in the kinetic profile, giving a very good R^2 value of 0.96. Scattering of data points at high conversion is however a problem that should be taken into account when interpreting these kinetic data quantitatively.

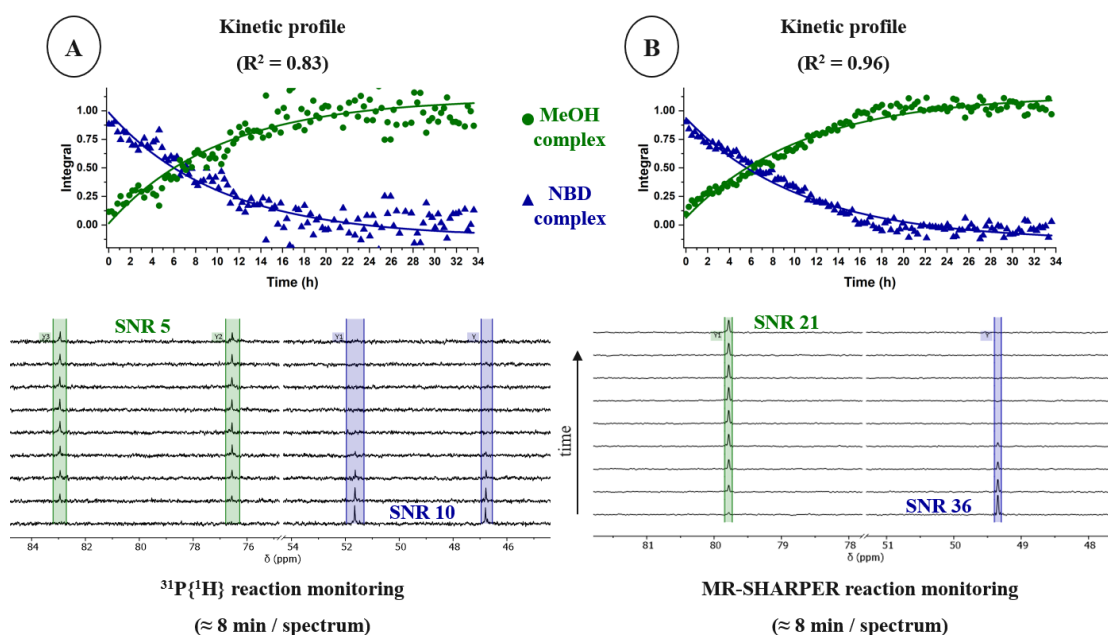


Figure 49. Comparison between $^{31}\text{P}\{^1\text{H}\}$ NMR (A) and MR-SHARPER (B) reaction monitoring (9 mM in MeOH, 32.6 MHz) of the hydrogenation of $[\text{Rh}((R,R)\text{-DIPAMP})(\text{NBD})]\text{BF}_4$ to produce $[\text{Rh}((R,R)\text{-DIPAMP})(\text{MeOH}_2)]\text{BF}_4$ (Scheme 9).

Details. Reaction monitoring with 124 loops, characterised by: $^{31}\text{P}\{^1\text{H}\}$ NMR (32 scans; 3.3 s acquisition time; 15 s repetition time; 7 min 50 s experiment time); MR-SHARPER ^{31}P NMR (20 scans; 2.02 ms chunk length; 25 s repetition time; 7 min 59 s experiment time). Each loop lasted 17 min 1 s.

For clarity, only one spectrum every 15th is shown. Processing: zero filling to 256k points and exponential line broadening of 0.3 Hz. Please refer to Table A7 for additional information.

Repeating the same comparison but now obtaining each spectrum in approximately 1 minute, the difference between the $^{31}\text{P}\{^1\text{H}\}$ and SHARPER data is even more pronounced (Figure 50).

No fitting could be performed on the data derived from the traditional $^{31}\text{P}\{^1\text{H}\}$ NMR spectra. With SHARPER, the kinetic profile is meaningful, showing a reasonable R^2 value of 0.89.

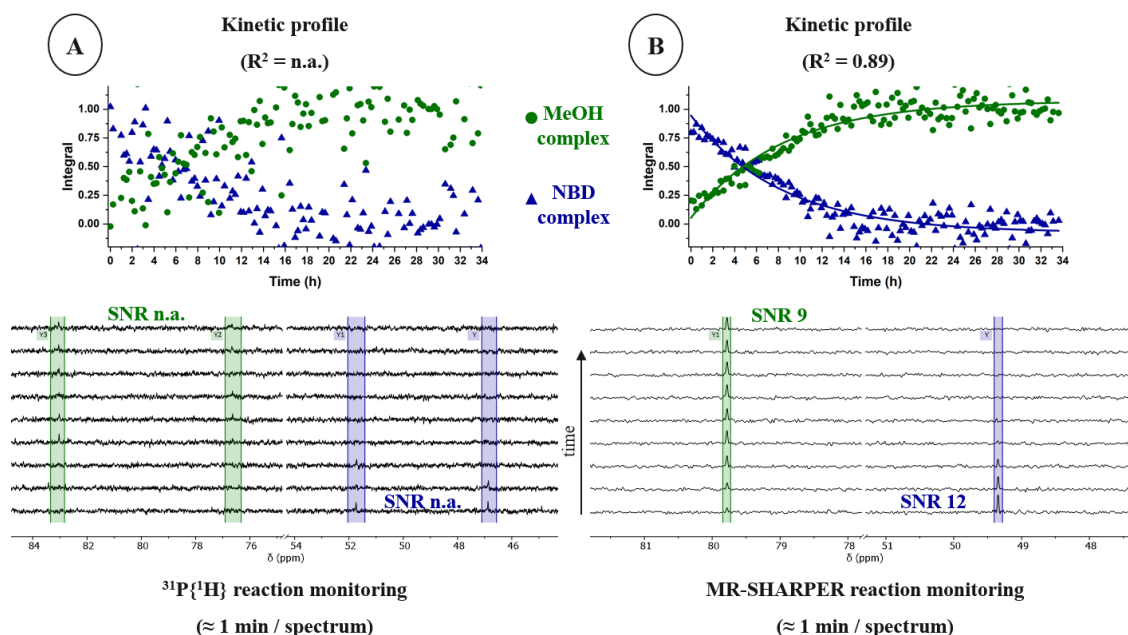


Figure 50. Comparison between $^{31}\text{P}\{^1\text{H}\}$ NMR (A) and MR-SHARPER (B) reaction monitoring (9 mM in MeOH, 32.6 MHz) of the hydrogenation of $[\text{Rh}((R,R)\text{-DIPAMP})(\text{NBD})]\text{BF}_4$ to produce $[\text{Rh}((R,R)\text{-DIPAMP})(\text{MeOH}_2)]\text{BF}_4$ (Scheme 9).

Details. Reaction monitoring with 124 loops, characterised by: $^{31}\text{P}\{^1\text{H}\}$ NMR (4 scans; 3.3 s acquisition time; 15 s repetition time; 51 s experiment time); MR-SHARPER ^{31}P NMR (3 scans; 2.02 ms chunk length; 25 s repetition time; 54 s experiment time). Each loop lasted 16 min 58 s (additional delay has been added to compare with the reaction monitoring in Figure 49). For clarity, only one spectrum every 15th is shown. Processing: zero filling to 256k points and exponential line broadening of 0.3 Hz. Please refer to Table A7 for additional information.

A cross comparison between the two experiments could be derived, considering the results from the reaction monitoring by $^{31}\text{P}\{^1\text{H}\}$ NMR where each spectrum is obtained in approximately 8 minutes (Figure 49A) and the SHARPER sequence where each spectrum is obtained in *ca.* 1 minute (Figure 50B). Remarkably, similar results (in terms of SNR and dispersion of data points) could be obtained reducing the experiment time by a factor of 8. Despite this, the SHARPER sequence still gives a slightly better SNR and lower dispersion error.

I expected that this reaction monitoring sequence could be applied for faster reactions or for reactions at lower concentration. I therefore moved from static to flow conditions (Chapter 3.6.7), where the reaction time is shorter (please refer to Chapter 3.3 for reaction time comparison between static and flow conditions).

3.6.6. Simulated two-component solution in flow conditions *via* MR-SHARPER

As explained in the introduction (Chapter 1.2.1), the values of T_1 and T_2 decrease going from static to flow conditions and they become T_1^* and T_2^* . As consequence, the repetition time also decreases. This is valid for both $^{31}\text{P}\{^1\text{H}\}$ NMR (Figure A12, Figure A13) as well as for SHARPER sequence (Figure A14, Figure A15). For example, the repetition time of 25 s required for a static experiment is now optimized to 9 s for SHARPER in flow conditions. After screening different chunk lengths on an NMR sample containing $[\text{Rh}((R,R)\text{-DIPAMP})(\text{NBD})]\text{BF}_4$, a value of 2 ms resulted to give the higher SNR without introducing undesired artifact in the spectrum (Table A5).

Once the desired chunk length is known, it is possible to tune the two directly related parameters, *i.e.*, the number of points and the dwell time.^u In particular, I obtained two best couples of parameters as candidates (number of points of 59 and dwell time of 17 μs , as in Figure 51A, vs number of points of 50 and dwell time of 20 μs , as in Figure 51B). The first one yielded a better SNR of the desired signal when the offset was set on the peak (at 49.5 ppm). When the offset was set in the middle (at 64.75 ppm), between the real peak and one hypothetical peak as simulation of the new appearing peak of the product of the reaction, the acquired resonance appeared to be shifted in the NMR spectrum (Figure 51C). For this reason, the second couple of parameters (Figure 51D) has been used for the following reaction monitoring (Chapter 3.6.7).

^u The value of the chunk length is equal to the double of the number of points multiplied for the dwell time.

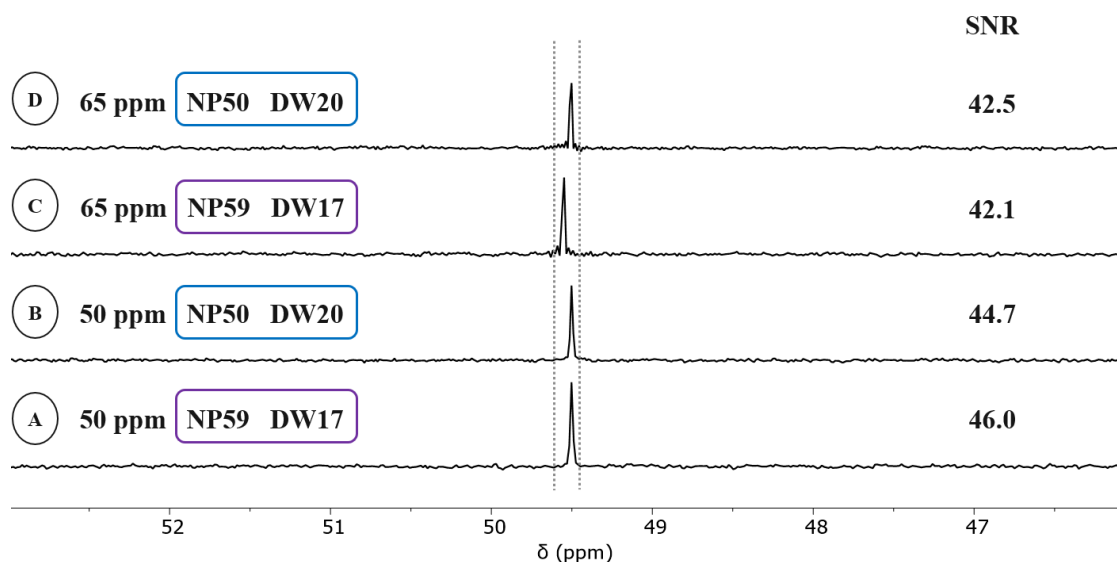


Figure 51. MR-SHARPER ^{31}P NMR spectra of $[\text{Rh}((R,R)\text{-DIPAMP})(\text{NBD})]\text{BF}_4$ (23 mM in MeOH, 32.6 MHz): MR-SHARPER ^{31}P NMR spectrum with offset on real peak at 49.5 ppm, 59 number of points (NP) and 17 μs dwell time (DW, **A**); MR-SHARPER ^{31}P NMR spectrum with offset on real peak at 49.5 ppm, 50 number of points and 20 μs dwell time (**B**); MR-SHARPER ^{31}P NMR spectrum with offset in between hypothetical and real peaks at 64.75 ppm, 59 number of points and 17 μs dwell time (**C**); MR-SHARPER ^{31}P NMR spectrum with offset in between hypothetical and real peaks at 64.75 ppm, 50 number of points and 20 μs dwell time (**D**).

Details. Processing: zero filling to 128k points and exponential line broadening of 0.2 Hz. Please refer to [Table A7](#) for additional information.

3.6.7. Reaction monitoring in flow conditions *via* MR-SHARPER

In the last section, I demonstrate the application of the SHARPER sequence with *on-line* monitoring. The above-described hydrogenation of the diolefin complex $[\text{Rh}((R,R)\text{-DIPAMP})(\text{NBD})]\text{BF}_4$ has been followed by traditional $^{31}\text{P}\{^1\text{H}\}$ NMR and by MR-SHARPER techniques (Scheme 9, Figure 52).

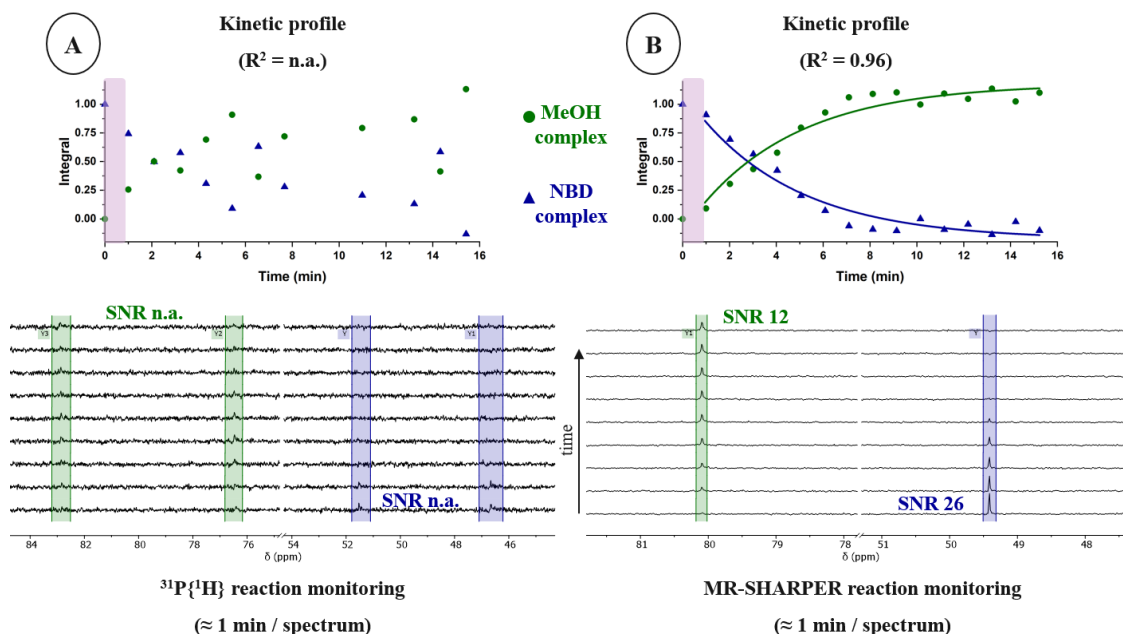


Figure 52. Comparison between $^{31}\text{P}\{^1\text{H}\}$ NMR (A) and MR-SHARPER (B) reaction monitoring (30 mM in MeOH, 32.6 MHz) of the hydrogenation of $[\text{Rh}((R,R)\text{-DIPAMP})(\text{NBD})]\text{BF}_4$ to produce $[\text{Rh}((R,R)\text{-DIPAMP})(\text{MeOH}_2)]\text{BF}_4$ (Scheme 9). In purple is highlighted the preparation time. The two points in each kinetic profile appearing at time zero has been taken from the spectra ($^{31}\text{P}\{^1\text{H}\}$ NMR and MR-SHARPER ^{31}P NMR) in flow conditions of the starting material.

Details. The first reaction monitoring with 9 loops, characterised by: $^{31}\text{P}\{^1\text{H}\}$ NMR (10 scans; 1.6 s acquisition time; 6 s repetition time; 59 s experiment time). The second reaction monitoring with 9 loops, characterised by: MR-SHARPER ^{31}P NMR (7 scans; 2.0 ms chunk length; 9 s repetition time; 58 s experiment time). Each loop lasted 59 s for $^{31}\text{P}\{^1\text{H}\}$ NMR and 58 s for MR-SHARPER ^{31}P NMR reaction monitoring. Processing for both reaction monitoring: zero filling to 128k points and exponential line broadening of 0.2 Hz. Please refer to Table A7 for additional information.

To collect a reasonable number of data points for a good comparison and evaluation, both reactions have been monitored independently because the reaction time is in the order of minutes.⁶⁰ A delay in both measurements of *ca.* 1 min, herein called preparation time, could not be avoided. It consists of the time required to stir the reaction mixture after the addition of hydrogen and to pump the reaction mixture into the spectrometer. $^{31}\text{P}\{^1\text{H}\}$ NMR monitoring (Figure 52A) does not allow for fitting of the data points. In contrast, SHARPER monitoring could nicely produce the profile shown (Figure 52B). As in static conditions, significantly better SNR has been obtained with the SHARPER sequence.

With this improved protocol in hand, I could conveniently monitor a hydrogenation reaction of an organometallic rhodium species that requires less than 15 minutes for full conversion. Compared to the standard experiments available on commercial benchtop NMR spectrometers, SHARPER gives an impressive enhancement in sensitivity for a ^{31}P spectrum.

4. Summary and Outlook

This PhD thesis describes the evolution of a commercially available low-field NMR spectrometer with limited applicability to the field of organometallic chemistry into a customized flow setup that can be used for monitoring highly oxygen-sensitive organometallic species in catalytic reactions.

As the first key result, I realised inert conditions in our customized flow setup despite the intrinsic challenge of air- and/or moisture-sensitive complexes, *e.g.*, $[\text{Rh}((R,R)\text{-DIPAMP})(\text{MeOH})_2]\text{BF}_4$. All components of the setup (*e.g.*, pump, capillaries, junctions) have been appropriately selected to allow inert conditions. Our customized system allows real-time and non-invasive reaction monitoring, despite flow effects and relatively low concentration of the rhodium species.

Afterwards, advantages as well as limitations of our benchtop NMR system have been explored, following selected stoichiometric and catalytic reactions. The flow conditions are superior to the static ones in terms of mass transfer, as confirmed by the faster reaction time obtained *via* the *on-line* system. Stepwise additions of reactants also proved to be possible, maintaining inert conditions for our sensitive rhodium diphosphine complexes. Different equivalent of reactants can be added separately to monitor the effect on the reaction system.

I challenged the low magnetic field and the low sensitivity of the heteronucleus ^{31}P introducing designed NMR pulse sequences. *Via* the pulse sequence Sensitive Homogeneous And Resolved PEaks in Real time (SHARPER), I could boost the signal-to-noise ratio (SNR) of the desired signals and follow reactions which would have not been possible to monitor with traditional $^{31}\text{P}\{^1\text{H}\}$ NMR sequences.

SHARPER enhances SNR and produces kinetic profiles with lower dispersion, which ultimately leads to either faster analysis or analysis at lower concentration of analyte. I have proved the feasibility of the former and I am confident that the latter could be proved as well in the future. Drawbacks such as pre-knowledge of the species involved in the reaction and limitation of the signals in the spectrum are however still valid. I hope that, in the next future, new developments will arise to deal with the remaining limitations.

Coupling of other orthogonal analytical techniques, *e.g.*, UV-Vis spectroscopy or volumetric analysis, could cover the next chapter of our customized system. Transverse encoding could also increase the value of our setup, allowing gradients to be applied in flow conditions (*e.g.*, *on-line* sel-SHARPER for reaction monitoring).

5. Appendix

5.1. General remarks

High-field NMR spectroscopy

^1H and ^{31}P NMR spectra have been recorded on Bruker 300 Fourier, Bruker AV300 and AV400 spectrometers at 297 or 298 K. Chemical shifts (δ) are reported in parts per million (ppm), internally referenced to the chosen deuterated solvent and externally referenced, respectively, to tetramethylsilane (TMS) for ^1H NMR or 85% H_3PO_4 solution for ^{31}P NMR. Coupling constants are given in hertz (Hz). All ^{31}P NMR spectra have been recorded with proton decoupling.

Low-field NMR spectroscopy

^1H and ^{31}P NMR spectra have been recorded on a Spinsolve benchtop 80 MHz spectrometer (Magritek), with ^1H , ^{19}F detection and an additional channel for the ^{31}P nucleus. Chemical shifts (δ) are reported in parts per million (ppm), internally referenced to the chosen deuterated or non-deuterated solvent. All ^{31}P NMR spectra have been recorded with proton decoupling unless otherwise stated. Shimming has been periodically performed on 90% deuterated water. The spectrometer has been purchased together with the reaction monitoring software package (RMX) and a kit for reaction monitoring, containing a glass centering tube (flow cell), a peristaltic pump (BT100-2J, Drifton) and PTFE tubing. Afterwards, the Spinsolve software has been updated to the latest version (Spinsolve 2.0.0) and the solvent suppression (presaturation sequence) package has been included. Finally, to create and manipulate the SHARPER sequences, the Spinsolve Expert software has been purchased (version 1.41.22).

According to the supplier, the flow NMR cell can be operated with a pressure of up to 10 bar. Regarding the temperature, the limits are reported to be 20–25 °C, with a tolerable fluctuation of ± 2 °C.

Materials

$[\text{Rh}(\text{DPPB})(\text{COD})]\text{BF}_4$ has been synthesised according to literature procedure from ligand and $[\text{Rh}(\text{COD})(\text{acac})]$ (acac = acetylacetonate) by treatment with HBF_4 .⁶⁹ $[\text{Rh}((R,R)\text{-DIPAMP})(\text{COD})]\text{BF}_4$ and $(R)\text{-BINAP}$ have been received as a donation from Grünenthal and Songlin Zhang (Soochow University, China), respectively. $[\text{Rh}((R,R)\text{-DIPAMP})(\text{NBD})]\text{BF}_4$ (Umicore, 100%) and $[\text{Rh}(\text{COD})(\mu\text{-Cl})_2]$ (Sigma, 98%) have been transferred to a Schlenk flask and kept under inert atmosphere. NBD (Sigma, 100%) and styrene (Acros, 99%) have been distilled prior to use. All non-deuterated solvents used (MeOH, toluene, 1,2-DCE, DCM) have been distilled under argon and stored in burettes under inert atmosphere. All deuterated solvent used (methanol- d_4 , toluene- d_8 , 1,2-DCE- d_4 , DCM- d_2) have been distilled under argon and afterwards the freeze-pump-thaw method was applied.

Pump and filters (additional information)

The pumps and filters described for the third generation setup (Figure 16, Figure 17) are here reported with additional details. **Pump1**: max flow rate 48 mL min⁻¹; **Pump2**: flow rate 0.024–144 mL min⁻¹, internal volume 3.4 µL; **Pump3**: flow rate 0.003–18 mL min⁻¹, internal volume 41.0 µL; **Pump4**: flow rate 0.003–18 mL min⁻¹, internal volume 0.9 µL; **Filter1**: mesh size 10 µm, internal volume 26–30 mL; **Filter2**: mesh size 10 µm; **Filter3**: mesh size 10 µm, internal volume 0.3 mL.

Analysis via MestReNova (for all NMR spectra)

All NMR spectra have been analysed via Mestrenova (Mestrelab Research, version 14.3.2). Manual baseline correction and phase correction have been preferred to the corresponding automatic ones. In the case of ³¹P NMR, apodization has been typically applied, typically with exponential line broadening. Zero filling has also been applied, if considered appropriate.

The data analysis tool of MestReNova has been used for reaction monitoring after applying phase correction, baseline correction, zero filling and apodization in stack mode.

Analysis via MestReNova (specifically for SHARPER spectra)

Most of the SHARPER spectra have required first order phase correction (PH1) in addition to the zero order phase correction (PH0) because of the consequences of the FID truncation.

Analysis via Origin

All kinetic profiles have been analysed via Origin (OriginLab Corporation, version 10.0.5.157). Plots showing the evolution of the normalised integral values over time have been obtained by normalising for the number of nuclei and the total amount of active nuclei. The exponential fits have been calculated for a better visualisation of the data.

5.2. General procedures

Preparation (for static and flow conditions)

All manipulations have been carried out using standard Schlenk techniques under oxygen- and moisture-free conditions. Inert conditions have been achieved performing at least six vacuum/argon cycles. Hydrogenations have been conducted under 1.3–1.5 bar of hydrogen, supplied directly into the fume hood from a central line available at LIKAT.

Preparation (specifically for flow conditions)

For all experiments under flow conditions, the entire setup has been rigorously cleaned, dried as well as evacuated and back-filled with argon multiple times (more time for these cycles is required in flow compared to static conditions). Flow calibration has been performed as soon as a new setup has been established. Before starting the reaction monitoring, the solution has been pumped from the reaction vessel into the flow system at the double of the speed used during reaction monitoring, only for the first minute. This has been required to help the pump to push the solution against the argon present in the flow.

5.3. Phase cycling lists

Phase list for traditional $^{31}\text{P}\{^1\text{H}\}$ with NOE:

[0,2,0,2; # 90 pulse (p1)
0,0,2,2; # NOE and decoupling (p2)
2,2,0,0; # NOE and decoupling (p3)
0,2,0,2] # acquisition (p4)

Phase list for SHARPER ^{31}P without NOE:

[0,0,2,2,1,1,3,3; # 90 pulse (p1)
3,1,3,1,2,0,2,0; # 180 pulse (p2)
0,0,2,2,1,1,3,3] # acquisition (p3)

Phase list for SHARPER ^{31}P with NOE:

[0,2,0,2; # 90 pulse (p1)
3,1,3,1; # 180 pulse (p2)
0,0,2,2; # NOE (p3)
2,2,0,0; # NOE (p4)
0,2,0,2] # acquisition (p5)

Phase list for sel-SHARPER ^{31}P without NOE:

[0,0,2,2,1,1,3,3; # 90 hard pulse (p1)
1,3,1,3,0,2,0,2; # 180 selective pulse (p2)
3,1,3,1,2,0,2,0; # 180 hard pulse (p3)
0,0,2,2,1,1,3,3] # acquisition (p4)

Phase list for sel-SHARPER ^{31}P with NOE:

[0,2,0,2; # 90 hard pulse (p1)
1,3,1,3; # 180 selective pulse (p2)
3,1,3,1; # 180 hard pulse (p3)
0,0,2,2; # NOE (p4)
2,2,0,0; # NOE (p5)
0,2,0,2] # acquisition (p6)

5.4. Macros remarks

To guarantee transparency and reproducibility, the SHARPER and sel-SHARPER sequences are reported in the appendix as they are programmed in Spinsolve Expert. Both are formed by five macros, all interconnected with each other. Four of them are fully disclosed herein while the last macro is only displayed partially for space reasons. This last one, called “Spectrometer ASM file”, is generated by the pulse program compiler and contains information strictly related to the spectrometer.

I report the SHARPER and sel-SHARPER sequences with NOE. The respective ones without NOE could be derived from the first two. Non necessarily, but if desired, the phase cycling can be set with the original parameters ([Chapter 5.3](#)). MR-SHARPER experiments are performed using exactly the SHARPER macro but appropriately setting the chunk length parameter, crucial for meeting the resonance condition ([Chapter 1.4.4](#)).

5.5. Macro of SHARPER sequence with NOE

Macro n°1 – Pulse program

```
#procedure(pulse_program,dir,mode,pars)
```

```
procedure(pulse_program,dir,mode)
```

```
# Interface description (name, label, ctrl, vartype)
```

```
interface = ["nucleus",      "Nucleus",      "tb", "readonly_string";
             "b1Freq31P",    "B1 Frequency (MHz)",    "tbw", "freq";
             "PPMOffset31P", "Offset Frequency (ppm)", "tbw", "float";
             "repTime",      "Repetition time (ms)",    "tbw", "reptime";
             "b1Freq1H",     "1H frequency (MHz)",    "tb", "freq";
             "noeDelay",     "NOE delay time (ms)",    "tb", "reptime";
             "noeAmp",       "NOE power (dB)",    "tb", "pulseamp";
             "pulseLengthH180", "1H 180 pulse length (us)", "tb", "pulselength";
             "acqDelay",     "Pulse acqu. delay (us)", "tb", "sdelay";
             "90Amplitude31P", "90 Pulse amplitude (dB)", "tb", "pulseamp";
             "180HAmplitude31P", "180 Pulse amplitude (dB)", "tb", "pulseamp";
             "180Amplitude31P", "180 sel-Pulse amp (dB)", "tb", "pulseamp";
             "90pulseLength31P", "90 Pulse length (us)", "tb", "pulselength";
             "180HpulseLength31P", "180 Pulse length (us)", "tb", "pulselength";
             "180pulseLength31P", "Sel-Pulse length (us)", "tb", "float,[0.1,10000]";
             "nSteps",       "Num. steps in sel-Pulse", "tb", "integer";
             "cutFac",       "Gaussian truncation (%)", "tb", "float,[0.1,50]";
             "spoilAmp",     "Homospoil amplitude (?)", "tbw", "float,[0,50000]";
             "spoilDur",     "Homospoil duration (us)", "tbw", "sdelay";
             "dAcqDelay",    "Pulse acqu. delay (us)", "tb", "sdelay";
             "acqPoints",    "total number of points", "tm",
             "integer,[128,256,512,1024,2048,4096,8192,16384,32768]";
             "corPoints",    "removed points", "tb", "integer";
             "remImag",     "remove imaginary", "tm", "integer,[1,0]"]
```

```
# Relationships to determine remaining variable values
```

```
relationships = ["b1Freq = b1Freq31P",
                 "nDataPnts = nrPnts",
                 "centerFreqPPM = PPMOffset31P",
                 "waltzDuration = WALTZ16:duration(pulseLengthH180/2,pgo)",
                 "nNOE = trunc(1000*noeDelay/waltzDuration)+1",
                 "aNOE = noeAmp",
                 "d180 = pulseLengthH180",
                 "d90 = pulseLengthH180/2",
                 "d270 = 3*pulseLengthH180/2",
                 "d360 = 2*pulseLengthH180",
                 "offFreq31P = (centerFreqPPM-wvPPMOffset31P)*b1Freq31P",
                 "freq31P = double(b1Freq31P)+double(offFreq31P/1e6d)",
                 "freq1H = double(b1Freq1H)",
                 "w1 = noeDelay*1000",
                 "dAcq = acqDelay",
                 "nSHARPER = trunc(acqPoints/(2*nrPnts)-0.5)",
                 "nchunk = 2*nrPnts+corPoints",
                 "nchunkhalf = nrPnts",
                 "nlastchunk = acqPoints - 2*nrPnts*(nSHARPER) - nrPnts+corPoints",
                 "n2 = xshim",
                 "n3 = yshim",
                 "n4 = zshim",
                 "n5 = xshim-(spoilAmp*xshim/(abs(xshim)+1))",
                 "n6 = yshim-(spoilAmp*yshim/(abs(yshim)+1))",
                 "n7 = zshim-(spoilAmp*zshim/(abs(zshim)+1))",
                 "a90Amp = 90Amplitude31P",
                 "d90Dur = 90pulseLength31P",
                 "a180HAmp = 180HAmplitude31P",
                 "d180HDur = 180HpulseLength31P",
                 "a180Amp = 180Amplitude31P",
                 "d180Dur = 180pulseLength31P/nSteps",
                 "t1 = P_SHARPER_withNOE_LAT01:getAmpTable(nSteps,cutFac,a180Amp)",
                 "t2 = t1*0",
```

```

        "d4 = spoilDur",
        "d5 = dAcqDelay-pgo",
        "d6 = dAcqDelay+rxLat",
        "totPnts = acqPoints",
        "O1 = (PPMOffset31P-wvPPMOffset31P)*b1Freq31P",
        "totTime = dwellTime*acqPoints/1000"]

# Define the tabs and their order
groups = ["Pulse_sequence","Progress","Acquisition",
          "Processing_Std","Display_Std","File_Settings"]

# These parameters may be changed between experiments
variables = [""]

# Pulse sequence
initpp(dir)

cleardata(nDataPnts)
settxfreqs(freq1H,freq31P)
delay(5000)
loop(12,nNOE)
    WALTZ16(1, aNOE, d90, d180, d270, d360, p3, p4, 1, 1)
endloop(12)
delay(dAcq)

pulse(2,a90Amp,p1,d90Dur)
delay(d6)
acquire("append",nchunkhalf)

loop(11,nSHARPER)
    delay(d5)
    pulse(2,a180HAmp,p2,d180HDur)
    delay(d6)
    acquire("append",nchunk)
endloop(11)

delay(d5)
pulse(2,a180HAmp,p2,d180HDur)
delay(d6)
acquire("append",nlastchunk)

parList = endpp(mode)

# Phase cycle list
phaseList = [0,2,0,2;
             3,1,3,1;
             0,0,2,2;
             2,2,0,0;
             0,2,0,2]

endproc(parList,groups,interface,relationships,variables,null,phaseList)

procedure(getFactoryBasedParameters, par)
    specPar = SpinsolveParameterUpdater:readDSPPar(null)
    if(specPar == null)
        return(null)
    endif
    assignlist(specPar)
    modelPar = ucsUtilities:getModelBasedParameters("31P",specPar)
    par = ["rxGain = $modelPar->rxGain$",
          "b1Freq31P = $Frequency_X$"]
endproc(par)

```

Macro n°2 – Experiment control

```

procedure(P_SHARPER_withNOE_LAT01, parameters=null)

```

```

macroLocation = getmacropath()
parentPath = getbasepath(macroLocation)
ppGroup = getbasedir(parentPath)
if(iskeypressed("shift"))
    PulseProgramCompiler(guiwinnr(),null,parentPath,"P_SHARPER_withNOE_LAT01")
elseif(iskeypressed("control"))
    gView->showExperimentHelp("P_SHARPER_withNOE_LAT01")
else
    gExpt->addExperiment(ppGroup,"P_SHARPER_withNOE_LAT01",parameters)
endif
endproc()

procedure(backdoor, guipar)
    seqInfo = :getseqpar()
    r = gSeq->initAndRunPP(getmacropath(), getmacroname(), guipar, seqInfo)
endproc(r)

procedure(getseqpar)
    rel = ["b1Freq      = b1Freq31P",
        "nDataPnts    = nrPnts",
        "centerFreqPPM = PPMOffset31P",
        "waltzDuration = WALTZ16:duration(pulseLengthH180/2,pgo)",
        "nNOE          = trunc(1000*noeDelay/waltzDuration)+1",
        "aNOE          = noeAmp",
        "d180           = pulseLengthH180",
        "d90            = pulseLengthH180/2",
        "d270           = 3*pulseLengthH180/2",
        "d360           = 2*pulseLengthH180",
        "offFreq31P     = (centerFreqPPM-wvPPMOffset31P)*b1Freq31P",
        "freq31P        = double(b1Freq31P)+double(offFreq31P/1e6d)",
        "freq1H         = double(b1Freq1H)",
        "w1             = noeDelay*1000",
        "dAcq           = acqDelay",
        "nSHARPER       = trunc(acqPoints/(2*nrPnts)-0.5)",
        "nchunk         = 2*nrPnts+corPoints",
        "nchunkhalf     = nrPnts",
        "nlastchunk     = acqPoints - 2*nrPnts*(nSHARPER) - nrPnts+corPoints",
        "n2 = xshim",
        "n3 = yshim",
        "n4 = zshim",
        "n5 = xshim-(spoilAmp*xshim/(abs(xshim)+1))",
        "n6 = yshim-(spoilAmp*yshim/(abs(yshim)+1))",
        "n7 = zshim-(spoilAmp*zshim/(abs(zshim)+1))",
        "a90Amp         = 90Amplitude31P",
        "d90Dur         = 90pulseLength31P",
        "a180HAmp        = 180HAmplitude31P",
        "d180HDur        = 180HpulseLength31P",
        "a180Amp         = 180Amplitude31P",
        "d180Dur         = 180pulseLength31P/nSteps",
        "t1 = P_SHARPER_withNOE_LAT01:getAmpTable(nSteps,cutFac,a180Amp)",
        "t2 = t1*0",
        "d4 = spoilDur",
        "d5 = dAcqDelay-pgo",
        "d6 = dAcqDelay+rxLat",
        "totPnts         = acqPoints",
        "O1              = (PPMOffset31P-wvPPMOffset31P)*b1Freq31P",
        "totTime         = dwellTime*acqPoints/1000"]
    var = [""]
    pp_list =
["nDataPnts","freq1H","freq31P","nNOE","l2","aNOE","p4","d270","p3","d360","d180","d90","dAcq","a90Amp",
    "p1","d90Dur","d6","nchunkhalf","nSHARPER","l1","d5","a180HAmp","p2","d180HDur","nchunk","nlastchunk"]
    pp_name = "P_SHARPER_withNOE_LAT01.p"
    phase_list = [0,2,0,2;3,1,3,1;0,0,2,2;2,2,0,0;0,2,0,2]
    seqInfo = struct(rel,var,pp_list,pp_name,phase_list)
endproc(seqInfo)

procedure(execpp,guipar,ppList,pcList,pcIndex,varIndex)

```

```

# Make all gui parameters available
assignlist(guiPar)

# Calculate pulse sequence parameters
nSHARPER = trunc(acqPoints/(2*nrPnts)-0.5)
nchunk = 2*nrPnts
nchunkhalf = nrPnts
nlastchunk = acqPoints - 2*nrPnts*(nSHARPER) - nrPnts
ngetPoints = nchunkhalf + (nchunk+corPoints)*nSHARPER + nlastchunk + corPoints
pr nSHARPER
pr nchunk
pr nchunkhalf
pr nlastchunk
pr ngetPoints

# Allocate space for output data
sumData = cmatrix(totPnts)

# Calculate suitable time and frequency axes
tAxis = ([0:1:totPnts-1]/totPnts)*totTime*1000 # ms
fAxis = [-totPnts*zf/2:totPnts*zf/2-1]/(totTime*zf)*1000 # Hz

# Time domain filter
if(filter == "yes")
    flt = filters:get_filter(filterType,"FTFid",totPnts)
else
    flt = matrix(totPnts)+1
endif

# Get plot regions
(prt,prf) = ucsPlot:getPlotRegions(guiPar,2,wvPP)

# First order phase correction
guiPar = guiPar + ["firstOrderCorr = 2*pi"]

# Handle ppm scale
if(usePPMScale == "yes")
    fAxisDisp = single(double(fAxis)/b1Freq31P)+PPMOffset31P
    prf->axes->xdirection("reversed")
    prf->axes->xppmscale("true")
    fAxisLabel = "Frequency (ppm)"
else
    prf->axes->xdirection("reversed")
    prf->axes->xppmscale("false")
    fAxisDisp = fAxis
    fAxisLabel = "Frequency (Hz)"
endif

# Intialise progress bar
:updateProgress(-1,guiPar)

if nrScans > 1
    allData = cmatrix(totPnts,nrScans)
endif

# Accumulate scans
for(scan = 0 to nrScans-1)

    # Check timing
    t1 = time()

    # Set phases for this scan
    (ppList,pAcq) = ucsRun:setPPPhase(ppList,scan,pcList,pcIndex)

    # Send phase parameters to DSP
    dspwrite("x",0x00,ppList)

    # Run the pulse program and collect the data

```

```

    ucsUtilities:suspendLock()
    (status,data) = ucsRun:getData(ngetPoints,guipar)
    ucsUtilities:resumeLock()

# See if stop button/escape key pressed
if(status != "ok")
    return(0)
endif

# Process chunked data to remove extra point as start of each chunk
procData = cmatrix(totPnts)
procData[0:nchunkhalf-1] = data[0:nchunkhalf-1]
count0 = nchunkhalf # index in output array
count1 = nchunkhalf+corPoints # index in data array
for (sharp = 0 to nSHARPER-1)
    procData[count0:(count0+nchunk-1)] = data[count1:(count1+nchunk-1)]
    count0 = count0+nchunk
    count1 = count1+nchunk+corPoints
next(sharp)
procData[count0:(count0+nlastchunk-1)] = data[count1:(count1+nlastchunk-1)]

# Accumulate the data
if bkgdCorr == 1
    sumData = sumData + procData
    sumDataR = real(sumData) + i*matrix(totPnts)
else
    sumData = ucsRun:accumulate(accumulate,pAcq,sumData,procData)
    sumDataR = real(sumData) + i*matrix(totPnts)
endif
if nrScans > 1
    allData[:,scan] = procData*round(exp(i*pAcq/16384*pi/2))
endif
if remImag == 1

# Process data
(phasedTimeData,spectrum,ph0) =
ucsRun:transformData(zeroFill(sumDataR.*flt,zf*totPnts,"end"),fAxis,guipar,"fid")

# Plot the data
if bkgdCorr == 1
    ucsPlot:graphTimeAndFreq(prt,prf,tAxis,sumDataR,fAxisDisp,spectrum,0,guipar,
        "Time data","Spectral data",
        "Time (ms)","Amplitude (\G(m)V)",
        fAxisLabel,"Amplitude")
else
    ucsPlot:graphTimeAndFreq(prt,prf,tAxis,sumDataR,fAxisDisp,spectrum,scan,guipar,
        "Time data","Spectral data",
        "Time (ms)","Amplitude (\G(m)V)",
        fAxisLabel,"Amplitude")
endif
else
endif

# Process data
(phasedTimeData,spectrum,ph0) =
ucsRun:transformData(zeroFill(sumData.*flt,zf*totPnts,"end"),fAxis,guipar,"fid")

# Plot the data
if bkgdCorr == 1
    ucsPlot:graphTimeAndFreq(prt,prf,tAxis,sumData,fAxisDisp,spectrum,0,guipar,
        "Time data","Spectral data",
        "Time (ms)","Amplitude (\G(m)V)",
        fAxisLabel,"Amplitude")
else
    ucsPlot:graphTimeAndFreq(prt,prf,tAxis,sumData,fAxisDisp,spectrum,scan,guipar,
        "Time data","Spectral data",
        "Time (ms)","Amplitude (\G(m)V)",
        fAxisLabel,"Amplitude")
endif
endif

```

```

endif

# Update progress bar
:updateProgress(scan,guipar)

# Save the data
if(isvar("wvUsingExpertGUI"))
    ucsFiles:savePlot(prt,:getPlotInfo("pt1"),guipar,"noReport")
    ucsFiles:savePlot(prf,:getPlotInfo("pt2"),guipar,"noReport")
    ucsFiles:saveMNOvaData(prt,"",guipar,"noReport",phase0=ph0)
    if bkgdCorr == 1
        ucsFiles:save1DDData(guipar,tAxis,sumData,"dataRaw")
        ucsFiles:save1DDData(guipar,tAxis,sumDataR,"dataProc")
    else
        ucsFiles:save1DDData(guipar,tAxis,sumData/(scan+1),"dataRaw")
        ucsFiles:save1DDData(guipar,tAxis,sumDataR/(scan+1),"dataProc")
    endif
    if nrScans > 1
        ucsFiles:save2DDData(guipar,allData,"allData")
    endif
else
    ucsFiles:save1DDData(guipar,tAxis,sumData/scan,"data")
endif

# Save the processing parameters
:saveProcPar(guipar,ph0)

# Check timing
check = ucsRun:checkTimeAndAbort(guipar,t1,scan,pcList,"ignoreLastScan")
if(check == "abort")
    return(0)
elseif(check == "finish")
    scan = scan+1
    exitfor()
endif

next(scan)

# Save the data
if(isvar("wvUsingExpertGUI"))
    ucsFiles:savePlot(prt,:getPlotInfo("pt1"),guipar,"noReport")
    ucsFiles:savePlot(prf,:getPlotInfo("pt2"),guipar,"noReport")
    ucsFiles:saveMNOvaData(prt,:getPlotInfo("pt1"),guipar,"noReport")
else
    ucsFiles:save1DDData(guipar,tAxis,sumData/scan,"data")
endif
ucsFiles:incrementExperiment(guipar)

# Save the processing parameters
:saveProcPar(guipar,ph0)

# Pack the data into a structure
result = struct()
result->tx = tAxis
result->ty = sumData/scan
result->fx = fAxisDisp
result->fy = spectrum/scan
result->par = struct(guipar)

# Return result
return(result)

endproc("execpp") # Don't remove argument

procedure(getPlotInfo,plotRegion)
    info = ["pt1","fid.pt1","pt2","spectrum.pt1"]
    if(plotRegion == "all")
        return(info)
    endif
endprocedure

```

```

endif
idx = getlistindex(info,plotRegion)
if(idx != -1)
    return(info[idx+1])
endif
endproc(null)

procedure(updateProgress, scans, guipar)

# Define progress/timing expressions
if(isvar("progressCtrl"))
    if(isvar("wvUpdateProgressCtrl"))
        if(wvUpdateProgressCtrl == 0)
            return
        endif
    endif
    assignlist(guiPar)

# Define progress/timing expressions
totTime = nrScans*repTime/1000
expTime = (scans+1)*repTime/1000
remTime = totTime - expTime
progress = 100*expTime/totTime

# Update controls
ucsCtrl:updateProgress(scans+1,progress,totTime,expTime,remTime)

endif

endproc()

procedure(expectedDuration, guipar)
    assignstruct(guiPar)
    totScans = nrScans + useStartDelay
    duration = (totScans*repTime)/1000
endproc(duration)

procedure(saveProcPar,guiPar,p0)
    assignlist(guiPar)
    procpAr = ["apodizationFunction = \"$filterType$\"",
        "baseLineCorrectionMethod = \"None\"",
        "displayInPPM = \"$usePPMScale$\"",
        "ftOrigin = \"Start\"",
        "ftType = \"Complex\"",
        "p0Phase = $p0$",
        "p1Phase = 0",
        "p1Pivot = 0",
        "p1FixedPhase = 360",
        "phaseMethod = \"p0, p1 fixed phase\"",
        "ppmOffset = $wvPPMOffset1H$",
        "zeroFill = 1"]
    if(expNr != "")
        cd("$dataDirectory$\\$expName$\\$expNr$")
    else
        cd("$dataDirectory$\\$expName$")
    endif
    if(isfile("proc.par"))
        par = load("proc.par")
        procpAr = mergelists(procpAr,par)
    endif
    save("proc.par",procpAr)
    if(isfile("proc_temp.par"))
        rmfile("proc_temp.par")
    endif
endproc()

procedure(getAmpTable,nSteps,cutFac,a180Amp)

```



```

# Procedure for generation of shaped Gaussian pulse

# Convert dB attenuation (set for experiment) to linear attenuation
amp = 10^(a180Amp/20)

# Convert cutoff percentage to a truncation factor between 0 and 1
truncFac = sqrt(log(0.5)/log(cutFac/100))

# (Ideal) Gaussian shaped pulse in linear amplitude scale with nSteps and a truncation factor of truncFac
gaussLin = exp(-4*log(2)*linvec(-0.5,0.5,nSteps)^2/truncFac^2)*amp

# Corrected linear Gaussian scaled to 14 bit number
ampTable = round(2^14*gaussLin)-1

endproc(ampTable)

```

Macro n°3 – Default parameters

```

90pulseLength31P = 67
90Amplitude31P = -6.6
180pulseLength31P = 10000
180HpulseLength31P = 134
180Amplitude31P = -37
180HAmplitude31P = -6.6
accumulate = "yes"
acqDelay = 20
acqPoints = 65536
acqTime = 1
b1Freq1H = 80.5239842999999950d
b1Freq31P = 32.59946139999999810d
bandwidth = 50
bkgdCorr = 0
corPoints = 1
cutFac = 1
dAcqDelay = 20
dataDirectory = ""
dispRange = 0
dispRangeMaxPPM = 100
dispRangeMinPPM = 30
dwellTime = 20
experiment = "P_SHARPER_withNOE_LAT01"
expName = ""
expNr = ""
exptName = "P_SHARPER_withNOE_LAT01"
fdPhaseCorr = "autophase"
filter = "yes"
filterType = "exponential"
flatFilter = "yes"
incExpNr = "no"
noeAmp = -20
noeDelay = 3000
nrPnts = 50
nrScans = 7
nSteps = 1000
nucleus = "31P"
position = [-1,-1]
PPMOffset31P = 64.75
pulseLengthH180 = 274.4
remImag = 0
repTime = 9000
rxChannel = "31P"
rxGain = 34
rxPhase = -3
saveData = "true"
softwareVersion = "1.41.22"
specID = ""

```

```

specType = ""
spoilAmp = 10000
spoilDur = 500
usePhaseCycle = "yes"
usePPMScale = "yes"
windowSize = "small"
zf = 2

```

Macro n°4 – User interface

```

procedure(status)
endproc("readonly")

```

```

procedure(interfaceDescription)
interface = [
    "nucleus", "Nucleus", "tb", "readonly_string", "",
    "b1Freq31P", "B1 Frequency (MHz)", "tbw", "double", "[1,400]",
    "PPMOffset31P", "Offset Frequency (ppm)", "tbw", "float", "",
    "repTime", "Repetition time (ms)", "tbw", "float", "[1,1e+008]",
    "b1Freq1H", "1H frequency (MHz)", "tb", "double", "[1,400]",
    "noeDelay", "NOE delay time (ms)", "tb", "float", "[1,1e+008]",
    "noeAmp", "NOE power (dB)", "tb", "float", "[-85,0]",
    "pulseLengthH180", "1H 180 pulse length (us)", "tb", "float", "[0.5,1000]",
    "acqDelay", "Pulse acqu. delay (us)", "tb", "float", "[2,327670]",
    "90Amplitude31P", "90 Pulse amplitude (dB)", "tb", "float", "[-85,0]",
    "180HAmplitude31P", "180 Pulse amplitude (dB)", "tb", "float", "[-85,0]",
    "180Amplitude31P", "180 sel-Pulse amp (dB)", "tb", "float", "[-85,0]",
    "90pulseLength31P", "90 Pulse length (us)", "tb", "float", "[0.5,1000]",
    "180HpulseLength31P", "180 Pulse length (us)", "tb", "float", "[0.5,1000]",
    "180pulseLength31P", "Sel-Pulse length (us)", "tb", "float", "[0.1,10000]",
    "nSteps", "Num. steps in sel-Pulse", "tb", "integer", "[1,1e8]",
    "cutFac", "Gaussian truncation (%)", "tb", "float", "[0.1,50]",
    "spoilAmp", "Homospoil amplitude (?)", "tbw", "float", "[0,50000]",
    "spoilDur", "Homospoil duration (us)", "tbw", "float", "[2,327670]",
    "dAcqDelay", "Pulse acqu. delay (us)", "tb", "float", "[2,327670]",
    "acqPoints", "total number of points", "tm", "integer", "[128,256,512,1024,2048,4096,8192,16384,32768]",
    "corPoints", "removed points", "tb", "integer", "[1,1e8]",
    "remImag", "remove imaginary", "tm", "integer", "[1,0]",
    "acquDiv", "Acquisition", "dv", "", "",
    "rxGain", "Receiver gain", "tm", "integer", "[\"-20\", \"-17\", \"-14\", \"-11\", \"-8\", \"-5\", \"-2\", \"1\", \"4\", \"7\", \"10\", \"13\", \"16\", \"19\", \"22\", \"25\", \"28\", \"31\", \"34\", \"37\", \"40\", \"43\", \"46\", \"49\", \"52\", \"55\", \"58\", \"61\", \"64\", \"67\", \"70\"]",
    "rxChannel", "Receiver channel", "tm", "string", "[\"1H\", \"13C\", \"15N\", \"19F\", \"29Si\", \"31P\", \"X\"]",
    "rxPhase", "Receiver phase", "tb", "float", "[-360,360]",
    "nrPnts", "Number of points", "tm", "integer", "[\"4\", \"8\", \"16\", \"32\", \"64\", \"128\", \"256\", \"512\", \"1024\", \"2048\", \"4096\", \"8192\", \"16384\", \"32768\"]",
    "dwellTime", "Dwell time (us)", "tm", "float", "[\"1\", \"2\", \"5\", \"10\", \"20\", \"50\", \"100\", \"200\", \"500\", \"1000\", \"2000\"]",
    "nrScans", "Number of scans", "tb", "float", "[1,1e8]",
    "flatFilter", "Flat filter", "cb", "string", "no,yes",
    "accumulate", "Accumulate data", "cb", "string", "no,yes",
    "usePhaseCycle", "Phase cycle", "cb", "string", "no,yes",
    "bandwidth", "Bandwidth (kHz)", "tb2", "float", "",
    "acqTime", "Acquisition time (ms)", "tb", "float", "",
    "procDiv", "Processing", "dv", "", "",
    "zf", "Zero fill factor?", "tm", "integer", "[\"1\", \"2\", \"4\", \"8\", \"16\"]",
    "filter", "Apodisation filter?", "cb", "string", "no,yes",
    "filterType", "Filter type", "tm", "string", "[\"none\", \"exp:1\", \"exponential\", \"sinebellsquared\"]",
    "fdPhaseCorr", "Freq. domain phasing", "tm", "string", "[\"autophase\", \"mag\", \"none\"]",
    "dispDiv", "Display", "dv", "", "",
    "usePPMScale", "Use ppm scale?", "cb", "string", "no,yes",
    "dispRangeMinPPM", "Minimum ppm value", "tb", "float", "[-2000,2000]",
    "dispRangeMaxPPM", "Maximum ppm value", "tb", "float", "[-2000,2000]",
    "dispRange", "Display range (Hz)", "tb", "float", "[0,2e6]",
    "fileDiv", "Files", "dv", "", ""
]

```

```

"saveData","Save data?","cb","string","false,true"]
endproc(interface)

procedure(plot_run_layout)
    layout = ["pt1";
              "pt2"]
endproc(layout)

procedure(plot_load_layout)
    layout = ["name=pt1, type=fid";
              "name=pt2, type=spectrum"]
endproc(layout)

procedure(processing_controls)
    layout = struct(buttonLabel = "SNR",    plotName = "pt1", macroToRun = "snrSpectrum()",      toolTip =
    = "Calculate FID signal to noise ratio.";
                  buttonLabel = "FT",    plotName = "pt1", macroToRun = "apodizeNTransform(\"pt1\\\", \"pt2\\\")",
    toolTip = "Reprocess the FID data (Fourier transform).";
                  buttonLabel = "Phase",  plotName = "pt2", macroToRun = "manualPhase1DSpecial()",      toolTip =
    = "Phase complex data.";
                  buttonLabel = "Apodize", plotName = "pt2", macroToRun = "apodizeFreq()",          toolTip =
    "Apply time domain window function.";
                  buttonLabel = "Baseln", plotName = "pt2", macroToRun = "baseLineCorrect1D()",      toolTip =
    "Baseline correct data.";
                  buttonLabel = "SNR",    plotName = "pt2", macroToRun = "snrSpectrum()",          toolTip =
    "Calculate spectrum signal to noise ratio.";
                  buttonLabel = "ppm/Hz", plotName = "pt2", macroToRun = "togglePPM_Hz(1)",        toolTip =
    = "Switch between ppm and Hz axis.";
                  buttonLabel = "Calib.", plotName = "pt2", macroToRun = "calibrateXAxis()",        toolTip =
    "Set spectral reference frequency in PPM.";
                  buttonLabel = "MNova",  plotName = "pt1", macroToRun = "exportMNova(\"pt1\\\")",    toolTip =
    = "Export FID to MNova for processing.";
                  buttonLabel = "MNova",  plotName = "pt2", macroToRun = "exportMNova(\"pt1\\\")",    toolTip =
    = "Export FID to MNova for processing.")
endproc(layout)

```

Macro n°5 – Spectrometer ASM file (selected section)

```

PARAM_BASE    equ    *    ; Memory for pulse program parameters
RXG1          ds     1    ; 00 - Receiver gain block 1
RXG2          ds     1    ; 01 - Receiver gain block 2
DEC1          ds     1    ; 02 - Decimation for CIC1
DEC5          ds     1    ; 03 - Decimation for CIC5
DECFIR        ds     1    ; 04 - Decimation for FIR
ATT1          ds     1    ; 05 - Attenuation for CIC1
DELAYFIR      ds     1    ; 06 - Delay for CIC5
ATTFIR        ds     1    ; 07 - Attenuation for FIR
Ntaps         ds     1    ; 08 - Taps for FIR
TXF10         ds     1    ; 09 - Tx Ch 1 frequency word 0
TXF11         ds     1    ; 10 - Tx Ch 1 frequency word 1
RXSETCHANNEL  ds     1    ; 11 - RxAmp set channel code
RXSETGAIN     ds     1    ; 12 - RxAmp set gain code
RXF00         ds     1    ; 13 - Rx Frequency word 0
RXF01         ds     1    ; 14 - Rx Frequency word 1
TXF20         ds     1    ; 15 - Tx Ch 2 frequency word 0
TXF21         ds     1    ; 16 - Tx Ch 2 frequency word 1
RXP0          ds     1    ; 17 - Rx Phase word 0
NRSCANS       ds     1    ; 18 - Number of scans to perform
EXPDELAY      ds     1    ; 19 - Delay between experiments
PGO           ds     1    ; 20 - Pulse gate overhead delay
GRADRESET     ds     1    ; 21 - 1 if gradients are to be reset
LFRXAMP       ds     1    ; 22 - 1 if low frequency Kea
SKIPPNTS      ds     1    ; 23 - Points to skip at start of acquisition
JITTER_CH1    ds     1    ; 24 - DDS channel 1 antiphase jitter parameter
JITTER_CH2    ds     1    ; 25 - DDS channel 2 antiphase jitter parameter
SoftVersion   ds     1    ; 26 - FPGA software version return

```

UseTrigger ds 1 ; 27 - Use the trigger input (0/1)

Pulse program info

NRDataPnts ds 1 ; 28 - Number DataPnts
FXreq1H_0 ds 1 ; 29 - Frequency req1H word 0
FXreq1H_1 ds 1 ; 30 - Frequency req1H word 1
FXreq31P_0 ds 1 ; 31 - Frequency req31P word 0
FXreq31P_1 ds 1 ; 32 - Frequency req31P word 1
NRNOE ds 1 ; 33 - Number NOE
TXANOE ds 1 ; 34 - Tx amplitude NOE word 0
TXP4 ds 1 ; 35 - Tx phase 4
DELAY270 ds 1 ; 36 - Delay 270
TXP3 ds 1 ; 37 - Tx phase 3
DELAY360 ds 1 ; 38 - Delay 360
DELAY180 ds 1 ; 39 - Delay 180
DELAY90 ds 1 ; 40 - Delay 90
DELAYAcq ds 1 ; 41 - Delay Acq
TXA90Amp ds 1 ; 42 - Tx amplitude 90Amp word 0
TXP1 ds 1 ; 43 - Tx phase 1
DELAY90Dur ds 1 ; 44 - Delay 90Dur
DELAY6 ds 1 ; 45 - Delay 6
NRchunkhalf ds 1 ; 46 - Number chunkhalf
NRSHARPER ds 1 ; 47 - Number SHARPER
DELAY5 ds 1 ; 48 - Delay 5
TXA180HAmp ds 1 ; 49 - Tx amplitude 180HAmp word 0
TXP2 ds 1 ; 50 - Tx phase 2
DELAY180HDur ds 1 ; 51 - Delay 180HDur
NRchunk ds 1 ; 52 - Number chunk
NRlastchunk ds 1 ; 53 - Number lastchunk

5.6. Macro of sel-SHARPER sequence with NOE

Macro n°1 – Pulse program

#procedure(pulse_program,dir,mode,pars)

procedure(pulse_program,dir,mode)

Interface description (name, label, ctrl, vartype)

```
interface = ["nucleus",      "Nucleus",      "tb", "readonly_string";
             "b1Freq31P",    "B1 Frequency (MHz)",    "tbw", "freq";
             "PPMOffset31P",  "Offset Frequency (ppm)",  "tbw", "float";
             "repTime",      "Repetition time (ms)",    "tbw", "reptime";
             "b1Freq1H",     "1H frequency (MHz)",     "tb", "freq";
             "noeDelay",     "NOE delay time (ms)",    "tb", "reptime";
             "noeAmp",       "NOE power (dB)",      "tb", "pulseamp";
             "pulseLengthH180", "1H 180 pulse length (us)", "tb", "pulselength";
             "acqDelay",     "Pulse acqu. delay (us)",  "tb", "sdelay";
             "90Amplitude31P", "90 Pulse amplitude (dB)", "tb", "pulseamp";
             "180HAmplitude31P", "180 Pulse amplitude (dB)", "tb", "pulseamp";
             "180Amplitude31P", "180 sel-Pulse amp (dB)", "tb", "pulseamp";
             "90pulseLength31P", "90 Pulse length (us)", "tb", "pulselength";
             "180HpulseLength31P", "180 Pulse length (us)", "tb", "pulselength";
             "180pulseLength31P", "Sel-Pulse length (us)", "tb", "float,[0.1,10000]";
             "nSteps",       "Num. steps in sel-Pulse", "tb", "integer";
             "cutFac",       "Gaussian truncation (%)", "tb", "float,[0.1,50]";
             "spoilAmp",     "Homospoil amplitude (?)", "tbw", "float,[0,50000]";
             "spoilDur",     "Homospoil duration (us)", "tbw", "sdelay";
             "dAcqDelay",    "Pulse acqu. delay (us)", "tb", "sdelay";
             "acqPoints",    "total number of points", "tm",
             "integer,[128,256,512,1024,2048,4096,8192,16384,32768]";
             "corPoints",    "removed points", "tb", "integer";
             "remImag",     "remove imaginary", "tm", "integer,[1,0]"]
```

Relationships to determine remaining variable values

```
relationships = ["b1Freq      = b1Freq31P",
                 "nDataPnts = nrPnts",
                 "centerFreqPPM = PPMOffset31P",
                 "waltzDuration = WALTZ16:duration(pulseLengthH180/2,pgo)",
                 "nNOE        = trunc(1000*noeDelay/waltzDuration)+1",
                 "aNOE        = noeAmp",
                 "d180        = pulseLengthH180",
                 "d90         = pulseLengthH180/2",
                 "d270        = 3*pulseLengthH180/2",
                 "d360        = 2*pulseLengthH180",
                 "offFreq31P  = (centerFreqPPM-wvPPMOffset31P)*b1Freq31P",
                 "freq31P     = double(b1Freq31P)+double(offFreq31P/1e6d)",
                 "freq1H      = double(b1Freq1H)",
                 "w1          = noeDelay*1000",
                 "dAcq        = acqDelay",
                 "nSHARPER    = trunc(acqPoints/(2*nrPnts)-0.5)",
                 "nchunk      = 2*nrPnts+corPoints",
                 "nchunkhalf  = nrPnts",
                 "nlastchunk  = acqPoints - 2*nrPnts*(nSHARPER) - nrPnts+corPoints",
                 "n2 = xshim",
                 "n3 = yshim",
                 "n4 = zshim",
                 "n5 = xshim-(spoilAmp*xshim/(abs(xshim)+1))",
                 "n6 = yshim-(spoilAmp*yshim/(abs(yshim)+1))",
                 "n7 = zshim-(spoilAmp*zshim/(abs(zshim)+1))",
                 "a90Amp      = 90Amplitude31P",
                 "d90Dur      = 90pulseLength31P",
                 "a180HAmp    = 180HAmplitude31P",
                 "d180HDur    = 180HpulseLength31P",
                 "a180Amp     = 180Amplitude31P",
                 "d180Dur     = 180pulseLength31P/nSteps",
                 "t1 = P_selSHARPER_withNOE_LAT01:getAmpTable(nSteps,cutFac,a180Amp)",
                 "t2 = t1*0",
```

```

    "d4 = spoilDur",
    "d5 = dAcqDelay-pgo",
    "d6 = dAcqDelay+rxLat",
    "totPnts = acqPoints",
    "O1 = (PPMOffset31P-wvPPMOffset31P)*b1Freq31P",
    "totTime = dwellTime*acqPoints/1000"]

# Define the tabs and their order
groups = ["Pulse_sequence", "Progress", "Acquisition",
          "Processing_Std", "Display_Std", "File_Settings"]

# These parameters may be changed between experiments
variables = [""]

# Pulse sequence
initpp(dir)

cleardata(nDataPnts)
settxfreqs(freq1H, freq31P)
delay(5000)
loop(12, nNOE)
    WALTZ16(1, aNOE, d90, d180, d270, d360, p4, p5, 1, 1)
endloop(12)
delay(dAcq)

pulse(2, a90Amp, p1, d90Dur) # 90 hard pulse

shim16(1, n5) # x
shim16(2, n6) # y
shim16(0, n7) # z
delay(d4) # homospoil delay
shim16(1, n2) # x
shim16(2, n3) # y
shim16(0, n4) # z
delay(d5)

shapedrf(2, t1, t2, p2, nSteps, d180Dur) # 180 selective pulse

shim16(1, n5) # x
shim16(2, n6) # y
shim16(0, n7) # z
delay(d4) # homospoil delay
shim16(1, n2) # x
shim16(2, n3) # y
shim16(0, n4) # z
delay(d6)

acquire("append", nchunkhalf)

loop(11, nSHARPER)
    delay(d5)
    pulse(2, a180HAmp, p3, d180HDur)
    delay(d6)
    acquire("append", nchunk)
endloop(11)

delay(d5)
pulse(2, a180HAmp, p3, d180HDur)
delay(d6)
acquire("append", nlastchunk)

parList = endpp(mode)

# Phase cycle list
phaseList = [0, 2, 0, 2;
             1, 3, 1, 3;
             3, 1, 3, 1;
             0, 0, 2, 2;

```

```
2,2,0,0;
0,2,0,2]
```

```
endproc(parList,groups,interface,relationships,variables,null,phaseList)
```

```
procedure(getFactoryBasedParameters, par)
  specPar = SpinsolveParameterUpdater:readDSPPar(null)
  if(specPar == null)
    return(null)
  endif
  assignlist(specPar)
  modelPar = ucsUtilities:getModelBasedParameters("31P",specPar)
  par = ["rxGain      = $modelPar->rxGain$",
        "b1Freq31P   = $Frequency_X$"]
endproc(par)
```

Macro n°2 – Experiment control

```
procedure(P_selSHARPER_withNOE_LAT01, parameters=null)
  macroLocation = getmacropath()
  parentPath = getbasepath(macroLocation)
  ppGroup = getbasedir(parentPath)
  if(iskeypressed("shift"))
    PulseProgramCompiler(guiwinnr(),null,parentPath,"P_selSHARPER_withNOE_LAT01")
  elseif(iskeypressed("control"))
    gView->showExperimentHelp("P_selSHARPER_withNOE_LAT01")
  else
    gExpt->addExperiment(ppGroup,"P_selSHARPER_withNOE_LAT01",parameters)
  endif
endproc()
```

```
procedure(backdoor, guipar)
  seqInfo = :getseqpar()
  r = gSeq->initAndRunPP(getmacropath(), getmacroname(), guipar, seqInfo)
endproc(r)
```

```
procedure(getseqpar)
  rel = ["b1Freq      = b1Freq31P",
        "nDataPnts   = nrPnts",
        "centerFreqPPM = PPMOffset31P",
        "waltzDuration = WALTZ16:duration(pulseLengthH180/2,pgo)",
        "nNOE        = trunc(1000*noeDelay/waltzDuration)+1",
        "aNOE        = noeAmp",
        "d180         = pulseLengthH180",
        "d90          = pulseLengthH180/2",
        "d270         = 3*pulseLengthH180/2",
        "d360         = 2*pulseLengthH180",
        "offFreq31P   = (centerFreqPPM-wvPPMOffset31P)*b1Freq31P",
        "freq31P      = double(b1Freq31P)+double(offFreq31P/1e6d)",
        "freq1H       = double(b1Freq1H)",
        "w1           = noeDelay*1000",
        "dAcq         = acqDelay",
        "nSHARPER     = trunc(acqPoints/(2*nrPnts)-0.5)",
        "nchunk       = 2*nrPnts+corPoints",
        "nchunkhalf   = nrPnts",
        "nlastchunk   = acqPoints - 2*nrPnts*(nSHARPER) - nrPnts+corPoints",
        "n2 = xshim",
        "n3 = yshim",
        "n4 = zshim",
        "n5 = xshim-(spoilAmp*xshim/(abs(xshim)+1))",
        "n6 = yshim-(spoilAmp*yshim/(abs(yshim)+1))",
        "n7 = zshim-(spoilAmp*zshim/(abs(zshim)+1))",
        "a90Amp       = 90Amplitude31P",
        "d90Dur       = 90pulseLength31P",
```

```

    "a180HAmp = 180HAmplitude31P",
    "d180HDur = 180HpulseLength31P",
    "a180Amp = 180Amplitude31P",
    "d180Dur = 180pulseLength31P/nSteps",
    "t1 = P_selSHARPER_withNOE_LAT01:getAmpTable(nSteps,cutFac,a180Amp)",
    "t2 = t1*0",
    "d4 = spoilDur",
    "d5 = dAcqDelay-pgo",
    "d6 = dAcqDelay+rxLat",
    "totPnts = acqPoints",
    "O1 = (PPMOffset31P-wvPPMOffset31P)*b1Freq31P",
    "totTime = dwellTime*acqPoints/1000"]
var = [""]
pp_list =
["nDataPnts","freq1H","freq31P","nNOE","l2","aNOE","p5","d270","p4","d360","d180","d90","dAcq","a90Amp",
"p1","d90Dur","n5","n6","n7","d4","n2","n3","n4","d5","t1","t2","p2","nSteps","d180Dur","d6","nchunkhalf","nS
HARPER","l1","a180HAmp","p3","d180HDur","nchunk","nlastchunk"]
pp_name = "P_selSHARPER_withNOE_LAT01.p"
phase_list = [0,2,0,2;1,3,1,3;3,1,3,1;0,0,2,2;2,2,0,0;0,2,0,2]
seqInfo = struct(rel,var,pp_list,pp_name,phase_list)
endproc(seqInfo)

procedure(execcpp,guipar,ppList,pcList,pcIndex,varIndex)

# Make all gui parameters available
assignlist(guipar)

# Calculate pulse sequence parameters
nSHARPER = trunc(acqPoints/(2*nrPnts)-0.5)
nchunk = 2*nrPnts
nchunkhalf = nrPnts
nlastchunk = acqPoints - 2*nrPnts*(nSHARPER) - nrPnts
ngetPoints = nchunkhalf + (nchunk+corPoints)*nSHARPER + nlastchunk + corPoints
pr nSHARPER
pr nchunk
pr nchunkhalf
pr nlastchunk
pr ngetPoints

# Allocate space for output data
sumData = cmatrix(totPnts)

# Calculate suitable time and frequency axes
tAxis = ([0:1:totPnts-1]/totPnts)*totTime*1000 # ms
fAxis = [-totPnts*zf/2:totPnts*zf/2-1]/(totTime*zf)*1000 # Hz

# Time domain filter
if(filter == "yes")
    flt = filters:get_filter(filterType,"FTFid",totPnts)
else
    flt = matrix(totPnts)+1
endif

# Get plot regions
(prt,prf) = ucsPlot:getPlotRegions(guipar,2,wvPP)

# First order phase correction
guipar = guipar + ["firstOrderCorr = 2*pi"]

# Handle ppm scale
if(usePPMScale == "yes")
    fAxisDisp = single(double(fAxis)/b1Freq31P)+PPMOffset31P
    prf->axes->xdirection("reversed")
    prf->axes->xppmscale("true")
    fAxisLabel = "Frequency (ppm)"
else
    prf->axes->xdirection("reversed")
    prf->axes->xppmscale("false")

```



```

fAxisDisp = fAxis
fAxisLabel = "Frequency (Hz)"
endif

# Initilise progress bar
:updateProgress(-1,guipar)

if nrScans > 1
    allData = cmatrix(totPnts,nrScans)
endif

# Accumulate scans
for(scan = 0 to nrScans-1)

    # Check timing
    t1 = time()

    # Set phases for this scan
    (ppList,pAcq) = ucsRun:setPPPhase(ppList,scan,pcList,pcIndex)

    # Send phase parameters to DSP
    dspwrite("x",0x00,ppList)

    # Run the pulse program and collect the data
    ucsUtilities:suspendLock()
    (status,data) = ucsRun:getData(ngetPoints,guipar)
    ucsUtilities:resumeLock()

    # See if stop button/escape key pressed
    if(status != "ok")
        return(0)
    endif

    # Process chunked data to remove extra point as start of each chunk
    procData = cmatrix(totPnts)
    procData[0:nchunkhalf-1] = data[0:nchunkhalf-1]
    count0 = nchunkhalf # index in output array
    count1 = nchunkhalf+corPoints # index in data array
    for (sharp = 0 to nSHARPER-1)
        procData[count0:(count0+nchunk-1)] = data[count1:(count1+nchunk-1)]
        count0 = count0+nchunk
        count1 = count1+nchunk+corPoints
    next(sharp)
    procData[count0:(count0+nlastchunk-1)] = data[count1:(count1+nlastchunk-1)]

    # Accumlate the data
    if bkgdCorr == 1
        sumData = sumData + procData
        sumDataR = real(sumData) + i*matrix(totPnts)
    else
        sumData = ucsRun:accumulate(accumulate,pAcq,sumData,procData)
        sumDataR = real(sumData) + i*matrix(totPnts)
    endif
    if nrScans > 1
        allData[:,scan] = procData*round(exp(i*pAcq/16384*pi/2))
    endif
    if remImag == 1

        # Process data
        (phasedTimeData,spectrum,ph0) =
ucsRun:transformData(zeroFill(sumDataR.*flt,zf*totPnts,"end"),fAxis,guipar,"fid")

        # Plot the data
        if bkgdCorr == 1
            ucsPlot:graphTimeAndFreq(prt,prf,tAxis,sumDataR,fAxisDisp,spectrum,0,guipar,
                "Time data","Spectral data",
                "Time (ms)","Amplitude (\G(m)V)",
                fAxisLabel,"Amplitude")
        endif
    endif
endfor

```

```

else
    ucsPlot:graphTimeAndFreq(prt,prf,tAxis,sumDataR,fAxisDisp,spectrum,scan,guipar,
        "Time data","Spectral data",
        "Time (ms)","Amplitude (\G(m)V)",
        fAxisLabel,"Amplitude")
endif
else

    # Process data
    (phasedTimeData,spectrum,ph0) =
ucsRun:transformData(zeroFill(sumData.*flt,zf*totPnts,"end"),fAxis,guipar,"fid")

    # Plot the data
    if bkgdCorr == 1
        ucsPlot:graphTimeAndFreq(prt,prf,tAxis,sumData,fAxisDisp,spectrum,0,guipar,
            "Time data","Spectral data",
            "Time (ms)","Amplitude (\G(m)V)",
            fAxisLabel,"Amplitude")
    else
        ucsPlot:graphTimeAndFreq(prt,prf,tAxis,sumData,fAxisDisp,spectrum,scan,guipar,
            "Time data","Spectral data",
            "Time (ms)","Amplitude (\G(m)V)",
            fAxisLabel,"Amplitude")
    endif
endif

    # Update progress bar
    :updateProgress(scan,guipar)

# Save the data
if(isvar("wvUsingExpertGUI"))
    ucsFiles:savePlot(prt,:getPlotInfo("pt1"),guipar,"noReport")
    ucsFiles:savePlot(prf,:getPlotInfo("pt2"),guipar,"noReport")
    ucsFiles:saveMNOvaData(prt,"",guipar,"noReport",phase0=ph0)
    if bkgdCorr == 1
        ucsFiles:save1DDData(guipar,tAxis,sumData,"dataRaw")
        ucsFiles:save1DDData(guipar,tAxis,sumDataR,"dataProc")
    else
        ucsFiles:save1DDData(guipar,tAxis,sumData/(scan+1),"dataRaw")
        ucsFiles:save1DDData(guipar,tAxis,sumDataR/(scan+1),"dataProc")
    endif
    if nrScans > 1
        ucsFiles:save2DDData(guipar,allData,"allData")
    endif
else
    ucsFiles:save1DDData(guipar,tAxis,sumData/scan,"data")
endif

# Save the processing parameters
:saveProcPar(guipar,ph0)

# Check timing
check = ucsRun:checkTimeAndAbort(guipar,t1,scan,pcList,"ignoreLastScan")
if(check == "abort")
    return(0)
elseif(check == "finish")
    scan = scan+1
    exitfor()
endif

next(scan)

# Save the data
if(isvar("wvUsingExpertGUI"))
    ucsFiles:savePlot(prt,:getPlotInfo("pt1"),guipar,"noReport")
    ucsFiles:savePlot(prf,:getPlotInfo("pt2"),guipar,"noReport")
    ucsFiles:saveMNOvaData(prt,:getPlotInfo("pt1"),guipar,"noReport")
else

```

```

        ucsFiles:save1DDData(guiapar,tAxis,sumData/scan,"data")
    endif
    ucsFiles:incrementExperiment(guiapar)

# Save the processing parameters
    :saveProcPar(guiapar,ph0)

# Pack the data into a structure
    result = struct()
    result->tx = tAxis
    result->ty = sumData/scan
    result->fx = fAxisDisp
    result->fy = spectrum/scan
    result->par = struct(guiapar)

# Return result
    return(result)

endproc("execpp")

procedure(getPlotInfo,plotRegion)
    info = ["pt1","fid.pt1","pt2","spectrum.pt1"]
    if(plotRegion == "all")
        return(info)
    endif
    idx = getlistindex(info,plotRegion)
    if(idx != -1)
        return(info[idx+1])
    endif
endproc(null)

procedure(updateProgress, scans, guipar)

# Define progress/timing expressions
    if(isvar("progressCtrl"))
        if(isvar("wvUpdateProgressCtrl"))
            if(wvUpdateProgressCtrl == 0)
                return
            endif
        endif
        assignlist(guiapar)

# Define progress/timing expressions
        totTime = nrScans*repTime/1000
        expTime = (scans+1)*repTime/1000
        remTime = totTime - expTime
        progress = 100*expTime/totTime

# Update controls
        ucsCtrl:updateProgress(scans+1,progress,totTime,expTime,remTime)

    endif

endproc()

procedure(expectedDuration, guipar)
    assignstruct(guiapar)
    totScans = nrScans + useStartDelay
    duration = (totScans*repTime)/1000
endproc(duration)

procedure(saveProcPar,guiapar,p0)
    assignlist(guiapar)
    procpa = ["apodizationFunction = \"$filterType$\"",
        "baseLineCorrectionMethod = \"None\"",
        "displayInPPM = \"$usePPMScale$\"",
        "ftOrigin = \"Start\"",
        "ftType = \"Complex\""]

```

```

        "p0Phase = $p0$",
        "p1Phase = 0",
        "p1Pivot = 0",
        "p1FixedPhase = 360",
        "phaseMethod = \"p0, p1 fixed phase\"",
        "ppmOffset = $wvPPMOffset1H$",
        "zeroFill = 1"]
if(expNr != "")
    cd("$dataDirectory$\$expName$\$expNr$")
else
    cd("$dataDirectory$\$expName$")
endif
if(isfile("proc.par"))
    par = load("proc.par")
    procpar = mergelists(procpar,par)
endif
save("proc.par",procpar)
if(isfile("proc_temp.par"))
    rmfile("proc_temp.par")
endif
endproc()

procedure(getAmpTable,nSteps,cutFac,a180Amp)

# Procedure for generation of shaped Gaussian pulse

# Convert dB attenuation (set for experiment) to linear attenuation
amp = 10^(a180Amp/20)

# Convert cutoff percentage to a truncation factor between 0 and 1
truncFac = sqrt(logc(0.5)/logc(cutFac/100))

# (Ideal) Gaussian shaped pulse in linear amplitude scale with nSteps and a truncation factor of truncFac
gaussLin = exp(-4*logc(2)*linvec(-0.5,0.5,nSteps)^2/truncFac^2)*amp

# Corrected linear Gaussian scaled to 14 bit number
ampTable = round(2^14*gaussLin)-1

endproc(ampTable)

```

Macro n°3 – Default parameters

```

90pulseLength31P = 67
90Amplitude31P = -6.6
180pulseLength31P = 5000
180HpulseLength31P = 134
180Amplitude31P = -31
180HAmplitude31P = -6.6
accumulate = "yes"
acqDelay = 20
acqPoints = 65536
acqTime = 0.8
b1Freq1H = 80.5239075000000070d
b1Freq31P = 32.59943029999999950d
bandwidth = 20
bkgdCorr = 0
corPoints = 1
cutFac = 1
dAcqDelay = 50
dataDirectory = ""
dispRange = 0
dispRangeMaxPPM = 90
dispRangeMinPPM = 40
dwellTime = 50
experiment = "P_selSHARPER_withNOE_LAT01"
expName = ""

```

```

expNr = ""
exptName = "P_selSHARPER_withNOE_LAT01"
fdPhaseCorr = "autophase"
filter = "yes"
filterType = "exponential"
flatFilter = "yes"
incExpNr = "no"
noeAmp = -19.1
noeDelay = 2000
nrPnts = 16
nrScans = 16
nSteps = 1000
nucleus = "31P"
position = [-1,-1]
PPMOffset31P = 49.3
pulseLengthH180 = 274.4
remImag = 0
repTime = 25000
rxChannel = "31P"
rxGain = 34
rxPhase = -2.5
saveData = "true"
softwareVersion = "1.41.22"
specID = ""
specType = ""
spoilAmp = 10000
spoilDur = 600
usePhaseCycle = "yes"
usePPMScale = "yes"
windowSize = "small"
zf = 2

```

Macro n^o4 – User interface

```

procedure(status)
endproc("readonly")

```

```

procedure(interfaceDescription)
  interface = [
    "nucleus","Nucleus","tb","readonly_string","",
    "b1Freq31P","B1 Frequency (MHz)","tbw","double","[1,400]",
    "PPMOffset31P","Offset Frequency (ppm)","tbw","float","",
    "repTime","Repetition time (ms)","tbw","float","[1,1e+008]",
    "b1Freq1H","1H frequency (MHz)","tb","double","[1,400]",
    "noeDelay","NOE delay time (ms)","tb","float","[1,1e+008]",
    "noeAmp","NOE power (dB)","tb","float","[-85,0]",
    "pulseLengthH180","1H 180 pulse length (us)","tb","float","[0.5,1000]",
    "acqDelay","Pulse acqu. delay (us)","tb","float","[2,327670]",
    "90Amplitude31P","90 Pulse amplitude (dB)","tb","float","[-85,0]",
    "180HAmplitude31P","180 Pulse amplitude (dB)","tb","float","[-85,0]",
    "180Amplitude31P","180 sel-Pulse amp (dB)","tb","float","[-85,0]",
    "90pulseLength31P","90 Pulse length (us)","tb","float","[0.5,1000]",
    "180HpulseLength31P","180 Pulse length (us)","tb","float","[0.5,1000]",
    "180pulseLength31P","Sel-Pulse length (us)","tb","float","[0.1,10000]",
    "nSteps","Num. steps in sel-Pulse","tb","integer","[1,1e8]",
    "cutFac","Gaussian truncation (%)","tb","float","[0.1,50]",
    "spoilAmp","Homospoil amplitude (?)","tbw","float","[0,50000]",
    "spoilDur","Homospoil duration (us)","tbw","float","[2,327670]",
    "dAcqDelay","Pulse acqu. delay (us)","tb","float","[2,327670]",
    "acqPoints","total number of points","tm","integer","[128,256,512,1024,2048,4096,8192,16384,32768]",
    "corPoints","removed points","tb","integer","[1,1e8]",
    "remImag","remove imaginary","tm","integer","[1,0]",
    "acquDiv","Acquisition","dv","",
    "rxGain","Receiver gain","tm","integer","[\"-20\", \"-17\", \"-14\", \"-11\", \"-8\", \"-5\", \"-2\", \"-1\", \"4\", \"7\", \"10\", \"13\", \"16\", \"19\", \"22\", \"25\", \"28\", \"31\", \"34\", \"37\", \"40\", \"43\", \"46\", \"49\", \"52\", \"55\", \"58\", \"61\", \"64\", \"67\", \"70\"]",

```

```

"rxChannel","Receiver channel","tm","string","[\"1H\", \"13C\", \"15N\", \"19F\", \"29Si\", \"31P\", \"X\"]",
"rxPhase","Receiver phase","tb","float", "[-360,360]",
"nrPnts","Number of
points","tm","integer","[\"4\", \"8\", \"16\", \"32\", \"64\", \"128\", \"256\", \"512\", \"1024\", \"2048\", \"4096\", \"8192\", \"16384\", \"32768\"]",
"dwellTime","Dwell time
(us)","tm","float","[\"1\", \"2\", \"5\", \"10\", \"20\", \"50\", \"100\", \"200\", \"500\", \"1000\", \"2000\"]",
"nrScans","Number of scans","tb","float", "[1,1e8]",
"flatFilter","Flat filter","cb","string", "no,yes",
"accumulate","Accumulate data","cb","string", "no,yes",
"usePhaseCycle","Phase cycle","cb","string", "no,yes",
"bandwidth","Bandwidth (kHz)","tb2","float", "",
"acqTime","Acquisition time (ms)","tb","float", "",
"procDiv","Processing","dv", "", "",
"zf","Zero fill factor?","tm","integer","[\"1\", \"2\", \"4\", \"8\", \"16\"]",
"filter","Apodisation filter?","cb","string", "no,yes",
"filterType","Filter type","tm","string","[\"none\", \"exp:1\", \"exponential\", \"sinebellsquared\"]",
"fdPhaseCorr","Freq. domain phasing","tm","string","[\"autophase\", \"mag\", \"none\"]",
"dispDiv","Display","dv", "", "",
"usePPMScale","Use ppm scale?","cb","string", "no,yes",
"dispRangeMinPPM","Minimum ppm value","tb","float", "[-2000,2000]",
"dispRangeMaxPPM","Maximum ppm value","tb","float", "[-2000,2000]",
"dispRange","Display range (Hz)","tb","float", "[0,2e6]",
"fileDiv","Files","dv", "", "",
"saveData","Save data?","cb","string", "false,true"]
endproc(interface)

procedure(plot_run_layout)
    layout = ["pt1";
              "pt2"]
endproc(layout)

procedure(plot_load_layout)
    layout = ["name=pt1, type=fid";
              "name=pt2, type=spectrum"]
endproc(layout)

procedure(processing_controls)
    layout = struct(buttonLabel = "SNR",    plotName = "pt1", macroToRun = "snrSpectrum()",          toolTip =
    "Calculate FID signal to noise ratio.";
                  buttonLabel = "FT",     plotName = "pt1", macroToRun = "apodizeNTransform(\"pt1\", \"pt2\")",
    toolTip = "Reprocess the FID data (Fourier transform).";
                  buttonLabel = "Phase",   plotName = "pt2", macroToRun = "manualPhase1DSpecial()",        toolTip =
    "Phase complex data.";
                  buttonLabel = "Apodize", plotName = "pt2", macroToRun = "apodizeFreq()",             toolTip =
    "Apply time domain window function.";
                  buttonLabel = "Baseline", plotName = "pt2", macroToRun = "baseLineCorrect1D()",         toolTip =
    "Baseline correct data.";
                  buttonLabel = "SNR",     plotName = "pt2", macroToRun = "snrSpectrum()",             toolTip =
    "Calculate spectrum signal to noise ratio.";
                  buttonLabel = "ppm/Hz",  plotName = "pt2", macroToRun = "togglePPM_Hz(1)",           toolTip =
    "Switch between ppm and Hz axis.";
                  buttonLabel = "Calib.",   plotName = "pt2", macroToRun = "calibrateXAxis()",           toolTip =
    "Set spectral reference frequency in PPM.";
                  buttonLabel = "MNOVA",   plotName = "pt1", macroToRun = "exportMNOVA(\"pt1\")",          toolTip =
    "Export FID to MNOVA for processing.";
                  buttonLabel = "MNOVA",   plotName = "pt2", macroToRun = "exportMNOVA(\"pt1\")",          toolTip =
    "Export FID to MNOVA for processing.")
endproc(layout)

```

Macro nº5 – Spectrometer ASM file (selected section)

```

PARAM_BASE    equ    *      ; Memory for pulse program parameters
RXG1          ds     1      ; 00 - Receiver gain block 1
RXG2          ds     1      ; 01 - Receiver gain block 2
DEC1          ds     1      ; 02 - Decimation for CIC1

```

DEC5 ds 1 ; 03 - Decimation for CIC5
 DECFIR ds 1 ; 04 - Decimation for FIR
 ATT1 ds 1 ; 05 - Attenuation for CIC1
 DELAYFIR ds 1 ; 06 - Delay for CIC5
 ATTFIR ds 1 ; 07 - Attenuation for FIR
 Ntaps ds 1 ; 08 - Taps for FIR
 TXF10 ds 1 ; 09 - Tx Ch 1 frequency word 0
 TXF11 ds 1 ; 10 - Tx Ch 1 frequency word 1
 RXSETCHANNEL ds 1 ; 11 - RxAmp set channel code
 RXSETGAIN ds 1 ; 12 - RxAmp set gain code
 RXF00 ds 1 ; 13 - Rx Frequency word 0
 RXF01 ds 1 ; 14 - Rx Frequency word 1
 TXF20 ds 1 ; 15 - Tx Ch 2 frequency word 0
 TXF21 ds 1 ; 16 - Tx Ch 2 frequency word 1
 RXP0 ds 1 ; 17 - Rx Phase word 0
 NRSCANS ds 1 ; 18 - Number of scans to perform
 EXPDELAY ds 1 ; 19 - Delay between experiments
 PGO ds 1 ; 20 - Pulse gate overhead delay
 GRADRESET ds 1 ; 21 - 1 if gradients are to be reset
 LFRXAMP ds 1 ; 22 - 1 if low frequency Kea
 SKIPPTS ds 1 ; 23 - Points to skip at start of acquisition
 JITTER_CH1 ds 1 ; 24 - DDS channel 1 antiphase jitter parameter
 JITTER_CH2 ds 1 ; 25 - DDS channel 2 antiphase jitter parameter
 SoftVersion ds 1 ; 26 - FPGA software version return
 UseTrigger ds 1 ; 27 - Use the trigger input (0/1)

Pulse program info

NRDataPnts ds 1 ; 28 - Number DataPnts
 FXreq1H_0 ds 1 ; 29 - Frequency req1H word 0
 FXreq1H_1 ds 1 ; 30 - Frequency req1H word 1
 FXreq31P_0 ds 1 ; 31 - Frequency req31P word 0
 FXreq31P_1 ds 1 ; 32 - Frequency req31P word 1
 NRNOE ds 1 ; 33 - Number NOE
 TXANOE ds 1 ; 34 - Tx amplitude NOE word 0
 TXP5 ds 1 ; 35 - Tx phase 5
 DELAY270 ds 1 ; 36 - Delay 270
 TXP4 ds 1 ; 37 - Tx phase 4
 DELAY360 ds 1 ; 38 - Delay 360
 DELAY180 ds 1 ; 39 - Delay 180
 DELAY90 ds 1 ; 40 - Delay 90
 DELAYAcq ds 1 ; 41 - Delay Acq
 TXA90Amp ds 1 ; 42 - Tx amplitude 90Amp word 0
 TXP1 ds 1 ; 43 - Tx phase 1
 DELAY90Dur ds 1 ; 44 - Delay 90Dur
 NR5 ds 1 ; 45 - Number 5
 NR6 ds 1 ; 46 - Number 6
 NR7 ds 1 ; 47 - Number 7
 DELAY4 ds 1 ; 48 - Delay 4
 NR2 ds 1 ; 49 - Number 2
 NR3 ds 1 ; 50 - Number 3
 NR4 ds 1 ; 51 - Number 4
 DELAY5 ds 1 ; 52 - Delay 5
 TABLE1 ds 1 ; 53 - Table 1
 TABLE2 ds 1 ; 54 - Table 2
 TXP2 ds 1 ; 55 - Tx phase 2
 NRSteps ds 1 ; 56 - Number Steps
 DELAY180Dur ds 1 ; 57 - Delay 180Dur
 DELAY6 ds 1 ; 58 - Delay 6
 NRchunkhalf ds 1 ; 59 - Number chunkhalf
 NRSHARPER ds 1 ; 60 - Number SHARPER
 TXA180HAmp ds 1 ; 61 - Tx amplitude 180HAmp word 0
 TXP3 ds 1 ; 62 - Tx phase 3
 DELAY180HDur ds 1 ; 63 - Delay 180HDur
 NRchunk ds 1 ; 64 - Number chunk
 NRlastchunk ds 1 ; 65 - Number lastchunk

5.7. X-ray structure determination

X-ray quality crystals were selected in Fomblin YR-1800 perfluoroether (Alfa Aesar) at low temperature. Diffraction data were collected at 123(2) K on a Bruker Kappa APEX II Duo diffractometer using Mo-K α radiation for [Rh(DPPB)(η^6 -ethylbenzene)]BF $_4$ or Cu-K α radiation for [Rh(DPPB)] $_2$ (BF $_4$) $_2$. The structures were solved by direct methods (SHELXS-97)⁷⁰ and refined by full matrix least square techniques against F 2 (SHELXL-2014)⁷¹. Semi-empirical absorption corrections were applied (SADABS/Bruker).⁷² The non-hydrogen atoms were refined anisotropically. The hydrogen atoms were placed into theoretical positions and were refined by using the riding model. DIAMOND (Crystal Impact GbR) was used for structure representations.

Crystallographic data (excluding structure factors) for the structures reported in this paper have been deposited at the Cambridge Crystallographic Data Centre. Copies of the data can be obtained free of charge on application to CCDC, 12 Union Road, Cambridge, CB21EZ, UK (fax: int. code + (1223) 336-033; e-mail: deposit@ccdc.cam.ac.uk).

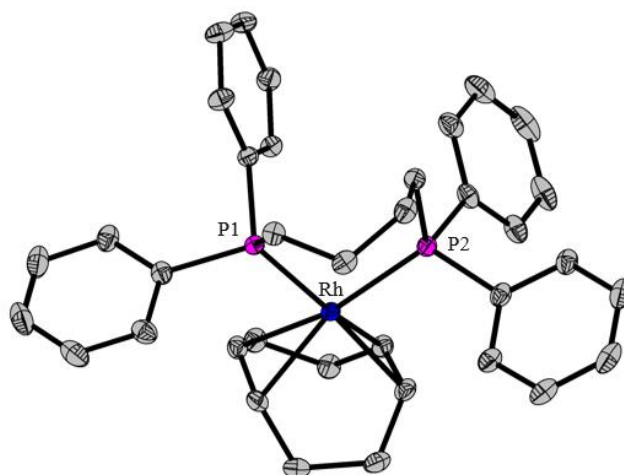


Figure A1. Molecular structure of the cation of [Rh(DPPB)(COD)]BF $_4$ (Scheme 2). Thermal ellipsoids are set at 30% probability. For clarity, hydrogen atoms are omitted. The structure of the crystal obtained is in agreement with the one that has already been reported.⁷³

Table A1. Crystallographic details of [Rh(DPPB)(COD)]BF₄ (Figure A1); [Rh(DPPB)]₂(BF₄)₂ (Figure 35); [Rh(DPPB)(η^6 -ethylbenzene)]BF₄ (Figure 39).

Compound	[Rh(DPPB)(COD)]BF ₄	[Rh(DPPB)] ₂ (BF ₄) ₂	[Rh(DPPB)(η^6 -ethylbenzene)]BF ₄
Chem. Formula	C ₃₆ H ₄₀ BF ₄ P ₂ Rh	C ₅₆ H ₅₆ B ₂ F ₈ P ₄ Rh ₂	2 C ₃₆ H ₃₈ BF ₄ P ₂ Rh· C ₂ H ₄ Cl ₂
Formula weight [g/mol]	724.34	1232.32	1543.60
Color	red	red	orange
Crystal system	monoclinic	triclinic	triclinic
Space group	C2c	$P\bar{1}$	$P\bar{1}$
<i>a</i> [Å]	30.2570(9)	10.4716(3)	10.8807(8)
<i>b</i> [Å]	10.1979(3)	11.5268(4)	18.0412(12)
<i>c</i> [Å]	26.7303(7)	11.9925(4)	18.9332(13)
α [°]	90	83.230(2)	79.853(2)
β [°]	128.868(2)	85.023(2)	81.350(2)
γ [°]	90	63.014(2)	73.532(2)
<i>V</i> [Å ³]	6421.7(3)	1280.03(7)	3488.5(4)
<i>Z</i>	8	1	2
$\rho_{\text{calcd.}}$ [g/cm ³]	1.498	1.599	1.470
μ [mm ⁻¹]	0.680	6.973	0.705
<i>T</i> [K]	150(2)	150(2)	150(2)
Measured reflections	45374	13825	126646
Independent reflections	7012	4572	13725
Reflections with <i>I</i> > 2 σ (<i>I</i>)	6432	3918	10810
<i>R</i> _{int}	0.0169	0.0586	0.0676
<i>F</i> (000)	2976	624	1580
<i>R</i> ₁ (<i>R</i> [<i>F</i> ² > 2 σ (<i>F</i> ²)])	0.0268	0.0466	0.0382
w <i>R</i> ₂ (<i>F</i> ²)	0.0749	0.1269	0.1015
GooF	1.120	1.037	1.027
No. of Parameters	445	325	831
Largest difference peak and hole (e/Å ⁻³)	0.806/ -0.342	1.720/-1.091	1.209/-0.863
CCDC #	n.a.	n.a.	2206998

5.8. On-line registration of gas consumption under isobaric conditions

The device used allow to monitor the hydrogen uptake (a constant pressure of 1.0 bar of molecular hydrogen is being maintained).⁷⁴ With respect to my customized flow setup (Figure 18), it has a wider surface between the liquid and the gas phase, and the reaction solution is never flowing in any capillary. For these reasons, it is likely that the hydrogen is more quickly getting in contact with the reagent. All the experiments (Table A2) are indeed showing a faster reaction time. Unfortunately, partial oxidation of the DPPB ligand has been observed in these experiments, as confirmed by sampling the solution at the end of the reaction and performing a static HF $^{31}\text{P}\{^1\text{H}\}$ NMR.

Table A2. Experiments for the monitoring of the hydrogen uptake (Figure A2) of the hydrogenation of styrene in methanol, in the presence of $[\text{Rh}(\text{DPPB})(\text{MeOH})_2]\text{BF}_4$ (ratio $[\text{Rh}]/\text{styrene}$ 1:100, Scheme 8).

#	Time (h)	[Rh] (mM)	Conditions	Notes from $^{31}\text{P}\{^1\text{H}\}$ NMR spectra
A	0.5	0.65	-	2% ligand oxidation
B	1.5	12.2	Fast stirring (\approx 700 -100 RPM)	1% ligand oxidation
C	2.5	12.2	Slow stirring (\approx 100 -200 RPM)	New unidentified species appearing after drying the sample and adding $\text{MeOH}-d_4$

A lower concentration of $[\text{Rh}(\text{DPPB})(\text{MeOH})_2]\text{BF}_4$ leads to a faster reaction (A). This could be explained by substrate or product inhibition, which occurs the moment a higher initial concentration of styrene in methanol is chosen. Interestingly, two experiments with different stirring speed of the reaction mixture have been performed (B,C). In particular, a faster stirring (B) leads to a faster reaction, probably because of better dissolution of molecular hydrogen into solution.

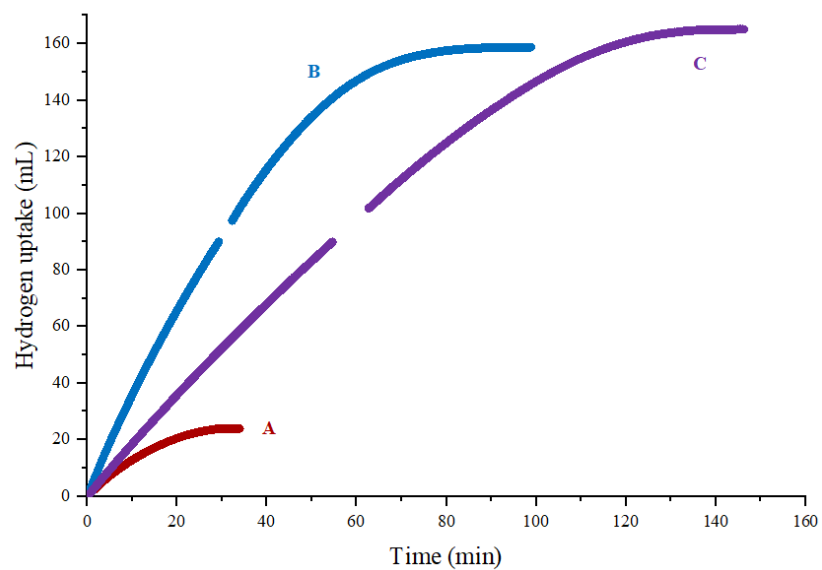


Figure A2. Volumetric curve of the experiments described in Table A2. The last two experiments (B,C) have an interrupted curve. This is due to a setup limitation, for which the analysis needed to be interrupted and could be restarted after a delay.

5.9. Additional HF NMR spectra in static conditions

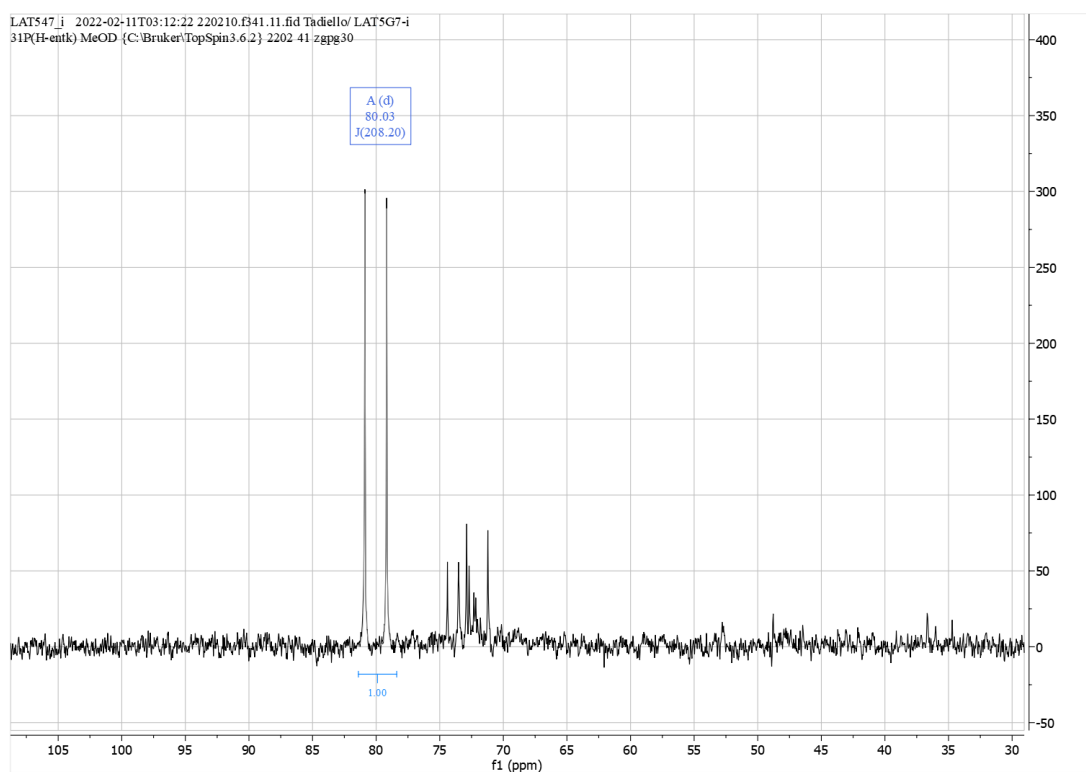


Figure A3. Static HF $^{31}\text{P}\{^1\text{H}\}$ NMR spectrum (methanol- d_4 , 122 MHz) of the complex $[\text{Rh}((R,R)\text{-DIPAMP})(\text{MeOH})_2]\text{BF}_4$ (doublet at 80.0 ppm) and the corresponding the η^6 -arene rhodium dinuclear species (signals between 70–75 ppm and 81–84 ppm overlapping with the signal of the solvent complex).

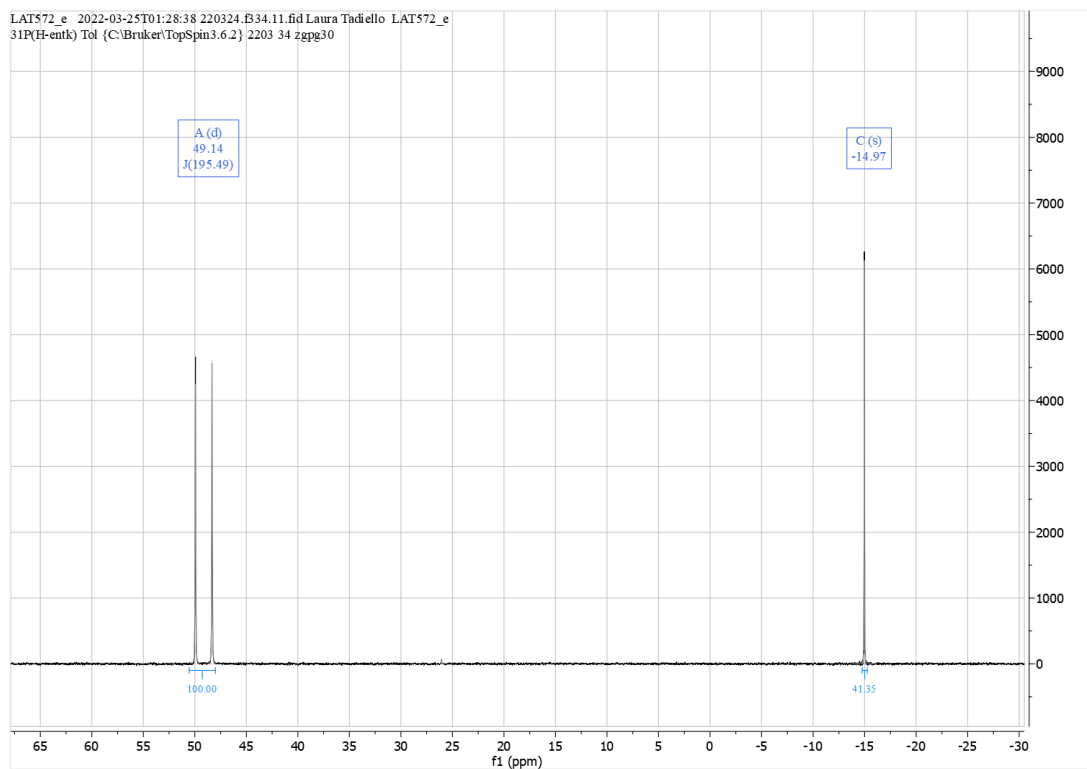


Figure A4. Static HF $^{31}\text{P}\{^1\text{H}\}$ NMR spectrum (toluene + toluene- d_8 , 122 MHz) of the complex $[\text{Rh}((R)\text{-BINAP})(\mu\text{-Cl})_2]$ in the presence of excess of BINAP. Negligible amount of oxidized BINAP could be found at 27 ppm.

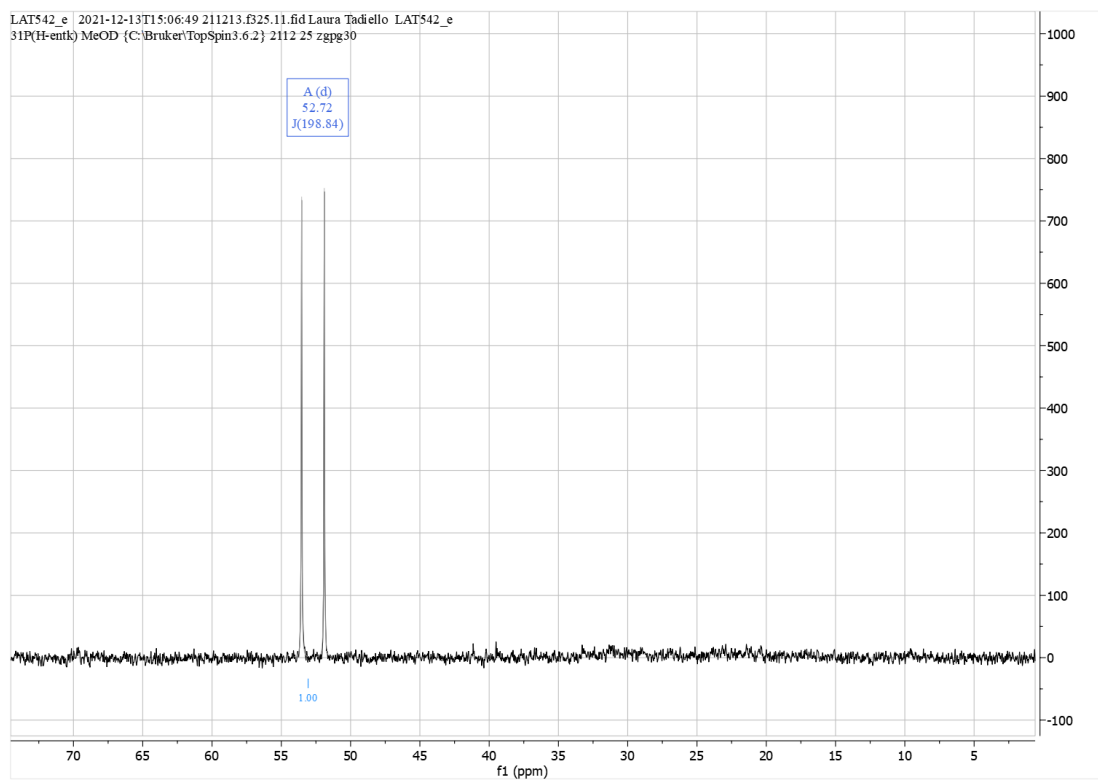


Figure A5. Static HF $^{31}\text{P}\{^1\text{H}\}$ NMR (methanol- d_4 , 122 MHz) of the complex $[\text{Rh}(\text{DPPB})(\text{MeOH})_2]\text{BF}_4$.

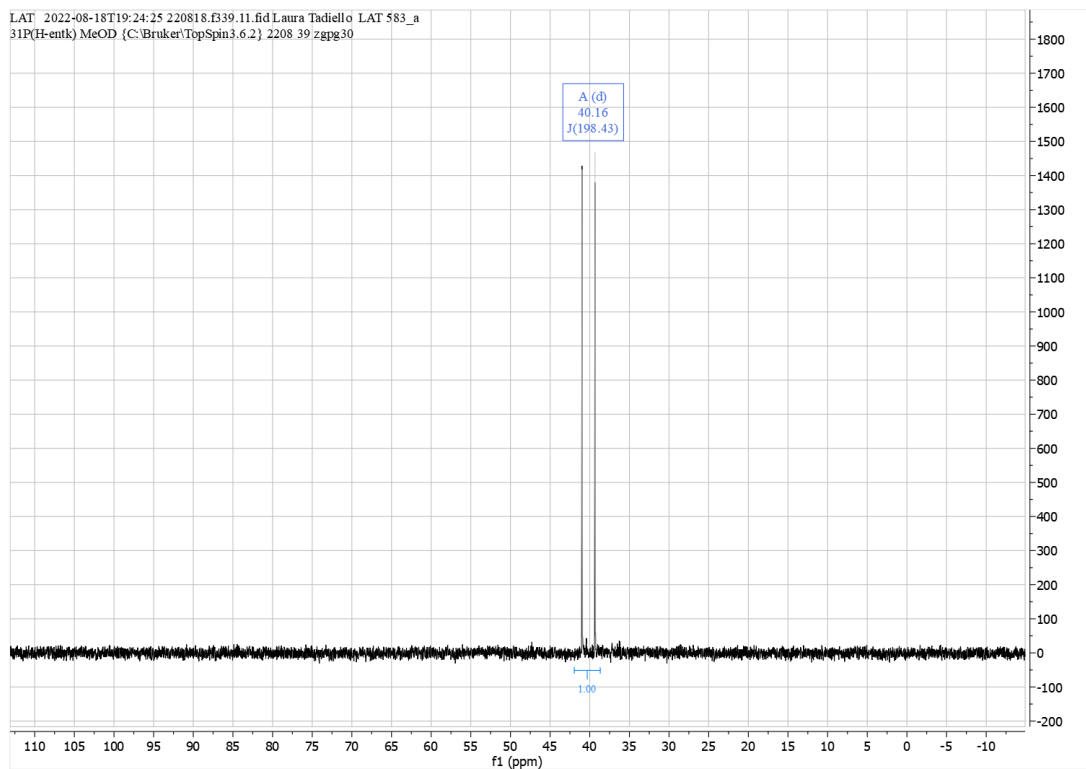


Figure A6. Static HF $^{31}\text{P}\{\text{}^1\text{H}\}$ NMR spectrum (MeOH + methanol- d_4 , 162 MHz) of the complex $[\text{Rh}(\text{DPPB})(\eta^6\text{-styrene})]\text{BF}_4$ generated in a solution of $[\text{Rh}(\text{DPPB})(\text{MeOH})_2]\text{BF}_4$ and styrene.

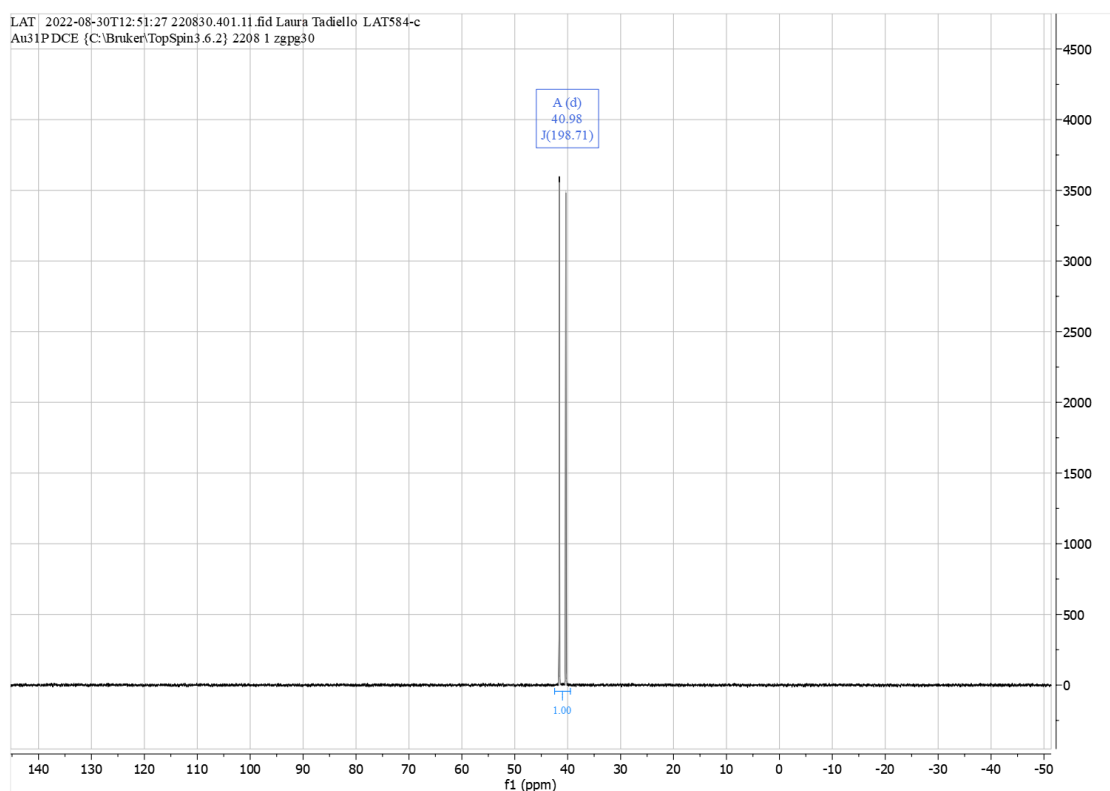


Figure A7. Static HF $^{31}\text{P}\{\text{}^1\text{H}\}$ NMR spectrum (1,2-DCE + 1,2-DCE- d_4 , 162 MHz) of the complex $[\text{Rh}(\text{DPPB})(\eta^6\text{-ethylbenzene})]\text{BF}_4$.

5.10. Parameter screening – Presaturation power

On the Spinsolve software, up to three saturation frequencies can be set. The parameters that can be tuned are the saturation power, in decibels, and the saturation period. Figure A8 shows the influence of the different powers of the saturation, while keeping constant the saturation time (3 s). The NMR sample under analysis contains [Rh(DPPB)(NBD)]BF₄ in methanol, with a large excess of free COD ligand (ratio [Rh]/COD 1:99). The complex is not clearly visible in the ¹H NMR spectrum but the solvent peaks as well as the two peaks of the COD ligand are assigned (Figure A8A). A relatively weak saturation power (-65 dB), led to a soft attenuation of both COD and solvent peaks (Figure A8B, Figure A9). And intermediate one (-55 dB), gave the best compromise between attenuation of solvent peaks and retention of the COD peaks (Figure A8C). Higher saturation power (-45 dB and -35 dB) led to much stronger impact on the COD peaks, which is undesired (Figure A8D,E).

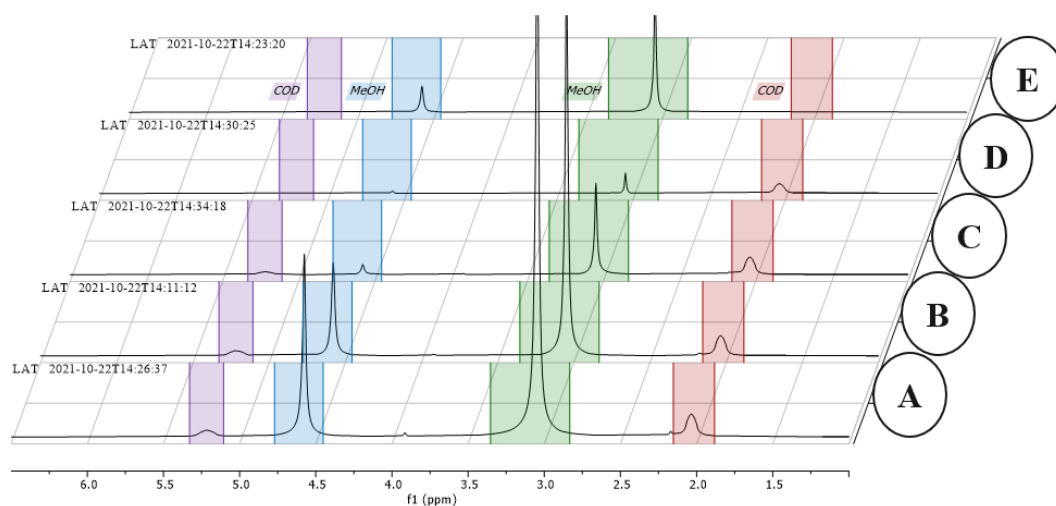


Figure A8. Low-Field static ¹H NMR spectra with and without presaturation of [Rh(DPPB)(NBD)]BF₄ (MeOH, 80 MHz, [Rh] = 39 mM) in the presence of excess of COD ligand: ¹H NMR spectrum without presaturation (A); ¹H NMR spectrum with presaturation with a power of -65 dB (B); ¹H NMR spectrum with presaturation with a power of -55 dB (C); ¹H NMR spectrum with presaturation with a power of -45 dB (D); ¹H NMR spectrum with presaturation with a power of -35 dB (E). The stacked plot is tilted for a clearer visualisation.

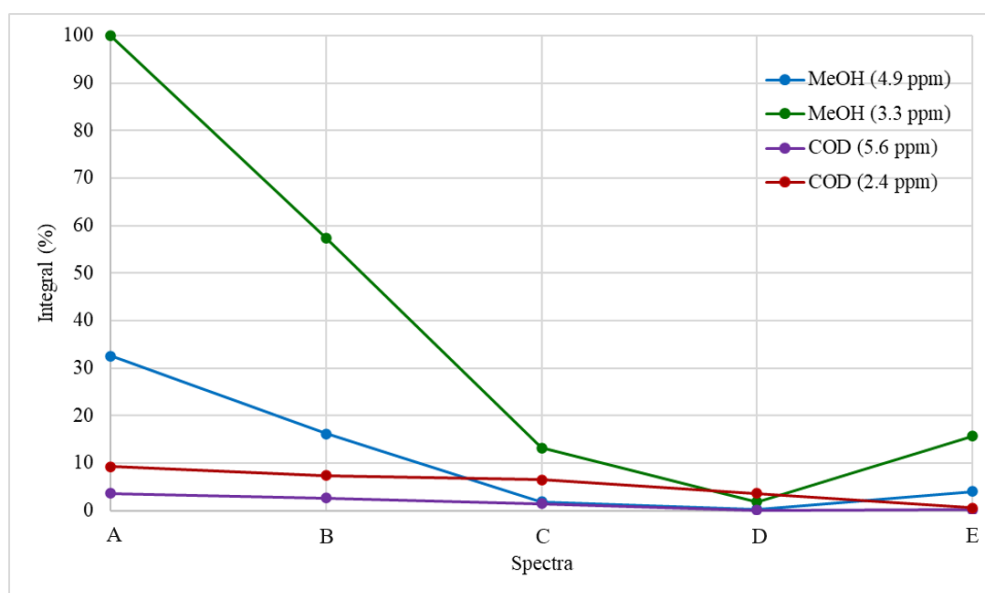


Figure A9. Plot of relative integrals for each spectrum (Figure A8). The integral of the highest peak of the solvent is set to 100 as reference in the ^1H NMR spectrum without presaturation.

5.11. Parameter screening – Echo time

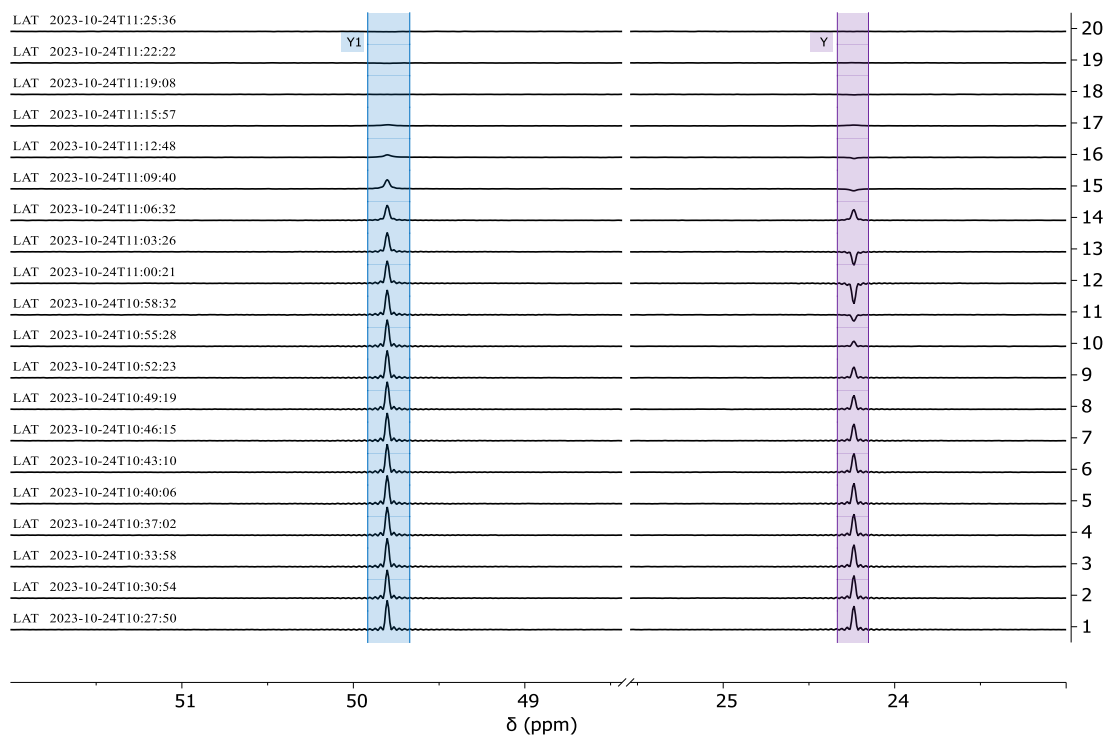


Figure A10. MR-SHARPER ^{31}P NMR of a mixture of $[\text{Rh}((R,R)\text{-DIPAMP})(\text{NBD})]\text{BF}_4$ (107 mM in $\text{DCM-}d_2$, in blue) and $[\text{Rh}(\text{DPPB})(\text{COD})]\text{BF}_4$ (106 mM in $\text{DCM-}d_2$, in purple): selected experiments for echo time screening. Phase correction has been applied to the peak corresponding to the complex $[\text{Rh}((R,R)\text{-DIPAMP})(\text{NBD})]\text{BF}_4$.

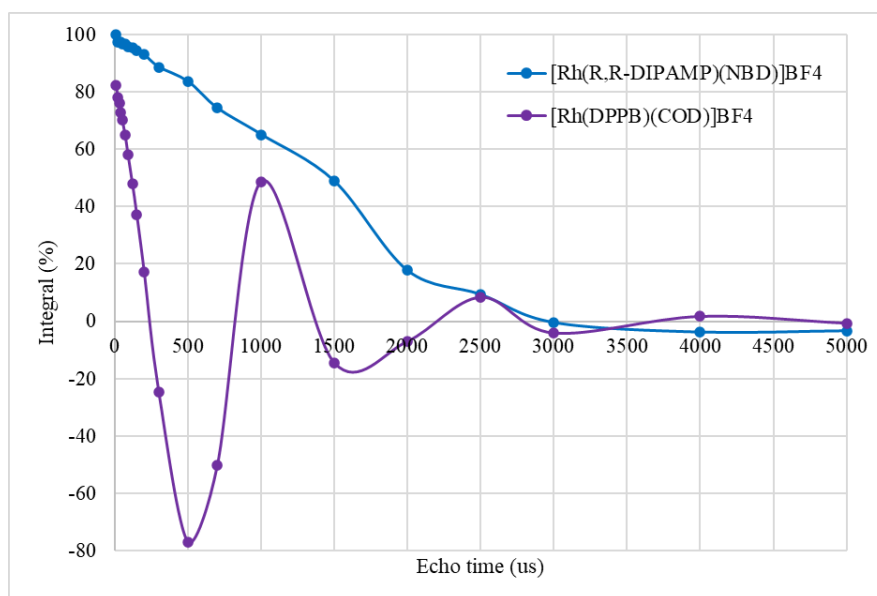


Figure A11. Plot of relative integrals against echo time (Figure A10). The integral of the complex $[\text{Rh}((R,R)\text{-DIPAMP})(\text{NBD})]\text{BF}_4$ (in blue) is compared to the integral of the complex $[\text{Rh}(\text{DPPB})(\text{COD})]\text{BF}_4$ (in purple).

5.12. Parameters screening in flow conditions

Abbreviations used: total number of points (TP); number of points (NP); dwell time (DW); number of scans (NS); acquisition time (AT); repetition time (RT); removed points (RP); imaginary part not removed from FID (RI0) vs imaginary part removed from FID (RI1); echo time (ET); chunk length (CL).

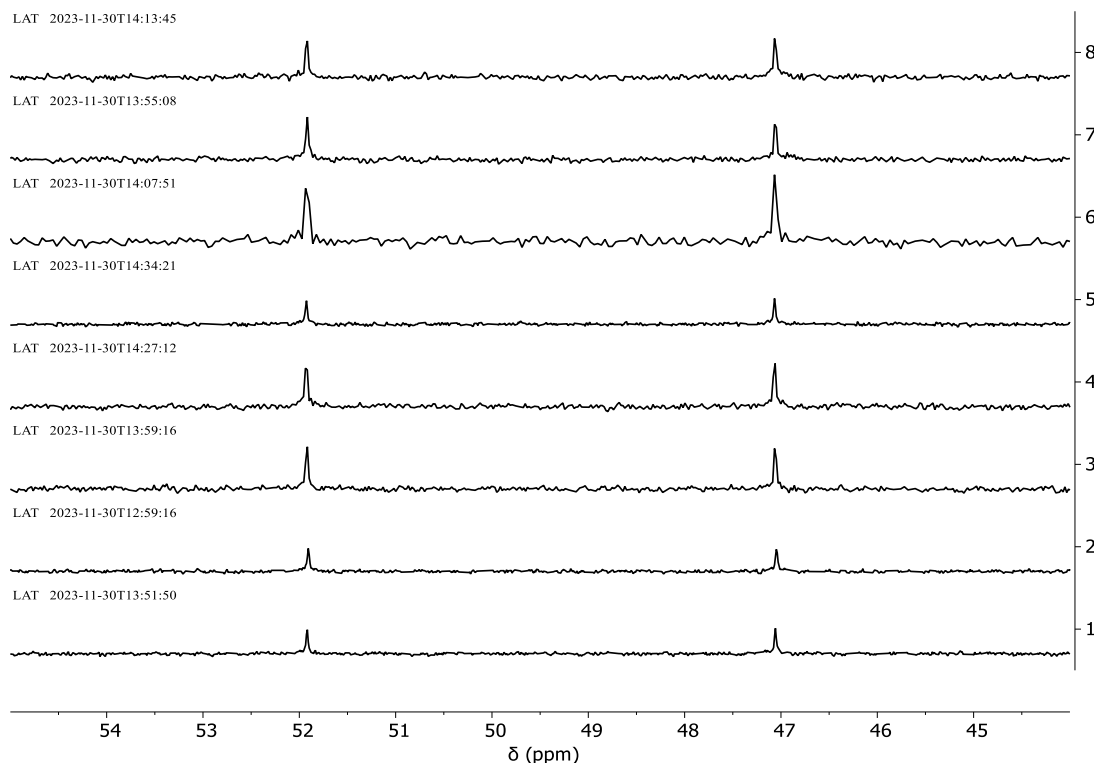


Figure A12. $^{31}\text{P}\{^1\text{H}\}$ NMR spectra of $[\text{Rh}((R,R)\text{-DIPAMP})(\text{NBD})]\text{BF}_4$ (23 mM in MeOH): selected experiments in flow conditions for parameters screening (Table A3).

Table A3. Parameters of NMR spectra in Figure A12. Common parameters: flow rate of 3.5 mL min^{-1} ; zero filling to 128k points; exponential line broadening of 0.2 Hz; noise region of 100–200 ppm.

#	Offset (ppm)	NP	DW (μs)	NS	AT (ms)	RT (s)	Exp. time	Peak region (ppm)	SNR	Peak region' (ppm)	SNR'
8	65	16k	50	32	0.8	5	2min40s	46-48	11.9	51-53	11.8
7	65	33k	25	32	0.8	5	2min40s	46-48	13.6	51-53	11.9
6	65	16k	25	32	0.4	4	2min7s	46-48	11.5	51-53	13.6
5	65	66k	25	32	1.6	5.6	2min57s	46-48	13.1	51-53	14.2
4	65	66k	12	32	0.8	5.2	2min40s	46-48	13.2	51-53	14.2
3	65	33k	25	32	0.8	4.5	2min8s	46-48	13.7	51-53	12.5
2	65	66k	25	32	1.6	15	7min51s	46-48	12.6	51-53	12.2
1	65	66k	25	32	1.6	6	2min40s	46-48	13.8	51-53	14.3

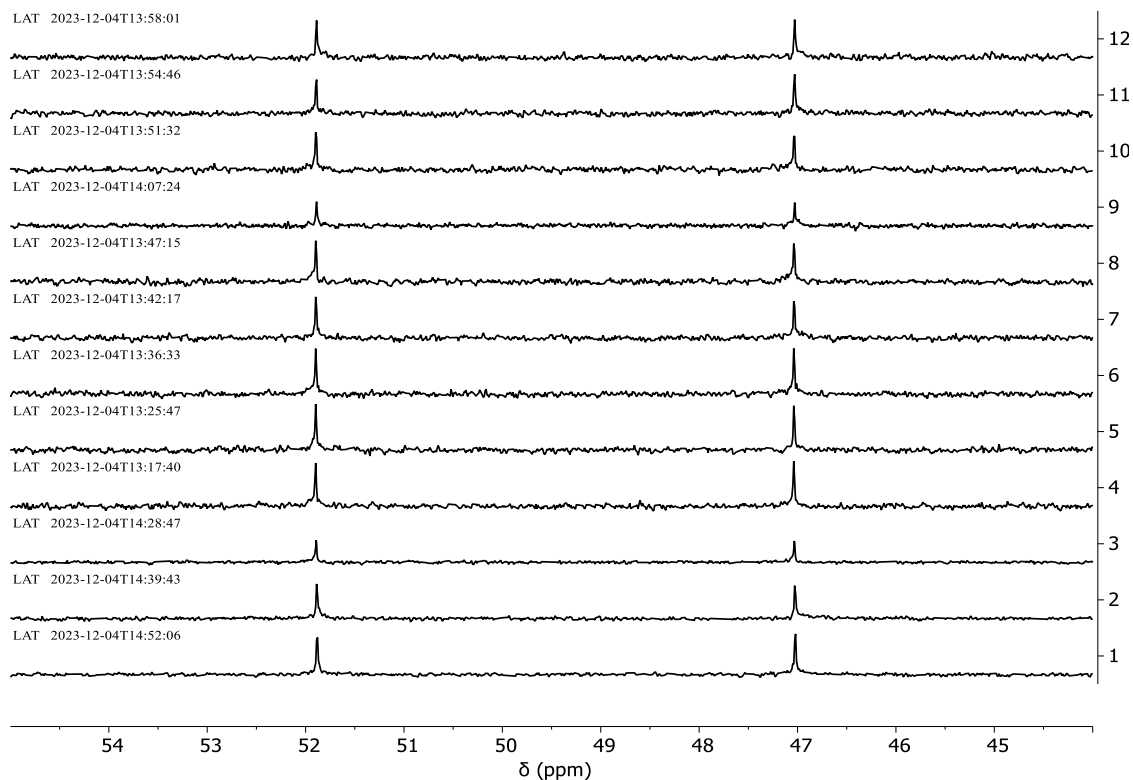


Figure A13. $^{31}\text{P}\{^1\text{H}\}$ NMR spectra of $[\text{Rh}((R,R)\text{-DIPAMP})(\text{NBD})]\text{BF}_4$ (23 mM in MeOH): selected experiments in flow conditions for parameters screening (Table A4).

Table A4. Parameters of NMR spectra in Figure A13. Common parameters: zero filling to 128k points; exponential line broadening of 0.2 Hz; noise region of 100–200 ppm.

#	Offset (ppm)	NP	DW (μs)	NS	AT (ms)	RT (s)	Exp. time	Flow rate (mL min^{-1})	Peak region (ppm)	SNR	Peak region' (ppm)	SNR'
12	65	66k	25	30	1.6	5.9	2min56s	1.5	46-48	12	51-53	12
11	65	66k	25	30	1.6	5.9	2min56s	1.7	46-48	11	51-53	12
10	65	66k	25	30	1.6	5.9	2min56s	1.9	46-48	12	51-53	11
9	65	66k	25	15	3.2	12	2min53s	2.1	46-48	10	51-53	10
8	65	66k	25	30	1.6	5.9	2min56s	2.1	46-48	13	51-53	12
7	65	66k	25	30	1.6	5.9	2min56s	2.3	46-48	13	51-53	12
6	65	66k	25	30	1.6	5.9	2min56s	2.6	46-48	14	51-53	14
5	65	66k	25	30	1.6	5.9	2min56s	3.0	46-48	14	51-53	14
4	65	66k	25	30	1.6	5.9	2min56s	3.5	46-48	14	51-53	14
3	65	66k	50	32	3.3	15	7min51s	static	46-48	14	51-53	13
2	65	66k	25	80	1.6	6	7min59s	static	46-48	18	51-53	17
1	65	66k	25	80	1.6	6	7min59s	3.5	46-48	20	51-53	22

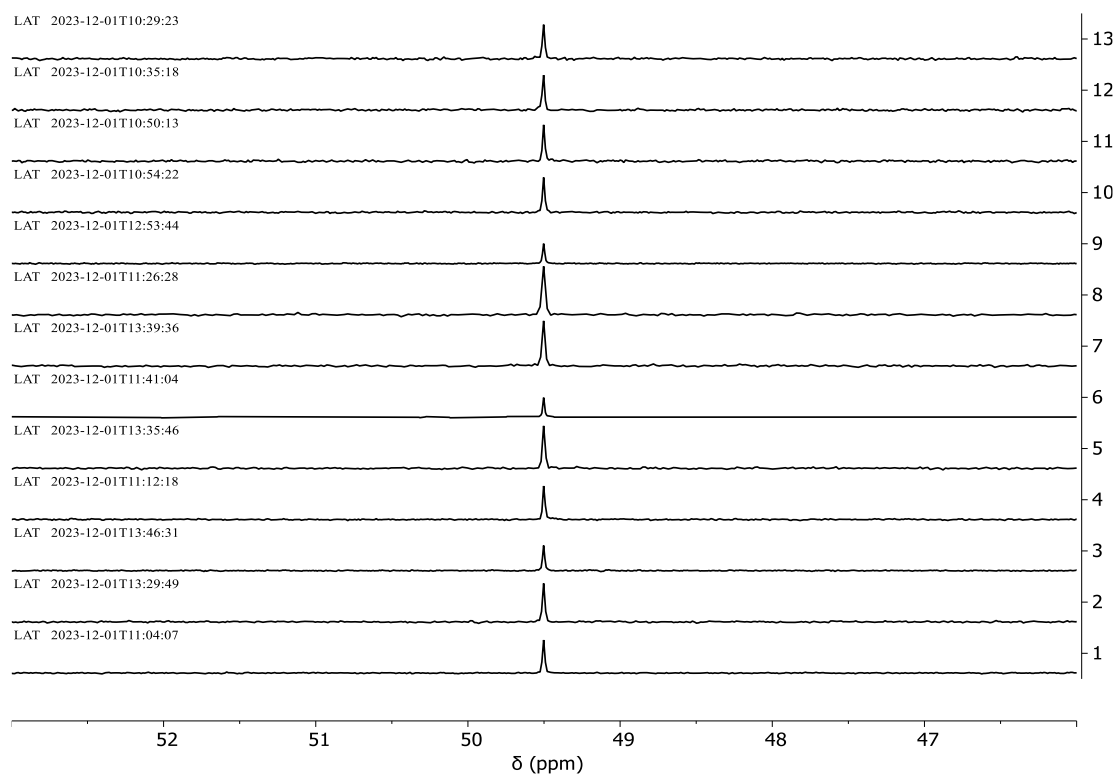


Figure A14. SHARPER ^{31}P NMR spectra of $[\text{Rh}((R,R)\text{-DIPAMP})(\text{NBD})]\text{BF}_4$ (23 mM in MeOH): selected experiments in flow conditions for parameters screening (Table A5).

Table A5. Parameters of NMR spectra in Figure A14. Common parameters: flow rate of 3.5 mL min^{-1} ; zero filling to 128k points; exponential line broadening of 0.2 Hz; noise region of 100–200 ppm; peak region of 49–50 ppm.

#	Offset (ppm)	TP	NP	DW (μs)	NS	CL (ms)	RT (s)	Exp. time	Others	SNR
13	49.5	66k	60	20	8	2.4	25	2min59s	RP1 RI0; ET20	29.5
12	49.5	66k	50	20	8	2.0	25	2min59s	RP1 RI0; ET20	30.6
11	49.5	66k	50	20	8	2.0	15	1min49s	RP1 RI0; ET20	30.9
10	49.5	66k	50	20	12	2.0	15	2min49s	RP1 RI0; ET20	36.2
9	49.5	66k	50	30	20	3.0	9	2min55s	RP1 RI0; ET20	37.6
8	49.5	33k	50	20	20	2.0	9	2min55s	RP1 RI0; ET20	41.2
7	49.5	66k	84	12	20	2.0	9	2min55s	RP1 RI0; ET20	41.9
6	49.5	131k	50	20	15	2.0	12	2min54s	RP1 RI0; ET20	42.3
5	49.5	66k	72	14	20	2.0	9	2min55s	RP1 RI0; ET20	44.4
4	49.5	66k	50	20	20	2.0	9	2min55s	RP1 RI0; ET20	44.7
3	49.5	66k	36	28	20	2.0	9	2min55s	RP1 RI0; ET20	45.6
2	49.5	66k	59	17	20	2.0	9	2min55s	RP1 RI0; ET20	46.0
1	49.5	66k	50	20	32	2.0	9	4min36s	RP1 RI0; ET20	56.6

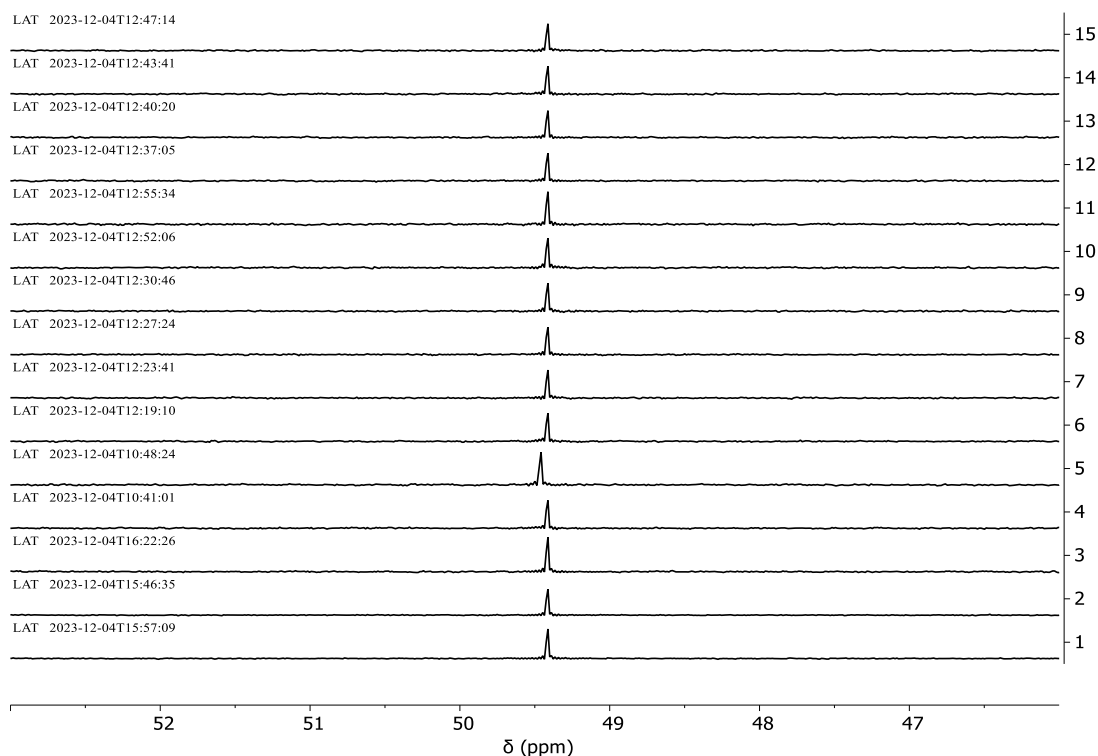


Figure A15. SHARPER ^{31}P NMR spectra of $[\text{Rh}((R,R)\text{-DIPAMP})(\text{NBD})]\text{BF}_4$ (23 mM in MeOH): selected experiments in flow conditions for parameters screening (Table A6).

Table A6. Parameters of NMR spectra in Figure A15. Common parameters: TP of 66k; zero filling to 128k points; exponential line broadening of 0.2 Hz; noise region of 100–200 ppm; peak region of 49–50 ppm.

#	Offset (ppm)	NP	DW (μs)	NS	CL (ms)	RT (s)	Exp. time	Others	SNR
15	64.75	50	20	20	2	9	2min55s	static; RP1 RI0; ET20	40.1
14	64.75	50	20	20	2	9	2min55s	1.5 mL min ⁻¹ ; RP1 RI0; ET20	41.7
13	64.75	50	20	20	2	9	2min55s	1.7 mL min ⁻¹ ; RP1 RI0; ET20	40.4
12	64.75	50	20	20	2	9	2min55s	1.9 mL min ⁻¹ ; RP1 RI0; ET20	41.5
11	64.75	50	20	12	2	15	2min49s	2.1 mL min ⁻¹ ; RP1 RI0; ET20	37.4
10	64.75	50	20	15	2	12	2min52s	2.1 mL min ⁻¹ ; RP1 RI0; ET20	38.2
9	64.75	50	20	20	2	9	2min55s	2.1 mL min ⁻¹ ; RP1 RI0; ET20	42.6
8	64.75	50	20	20	2	9	2min55s	2.3 mL min ⁻¹ ; RP1 RI0; ET20	42.1
7	64.75	50	20	20	2	9	2min55s	2.6 mL min ⁻¹ ; RP1 RI0; ET20	41.3
6	64.75	50	20	20	2	9	2min55s	3.0 mL min ⁻¹ ; RP1 RI0; ET20	42.7
5	64.75	59	17	20	2	9	2min55s	3.5 mL min ⁻¹ ; RP1 RI0; ET20	42.1
4	64.75	50	20	20	2	9	2min55s	3.5 mL min ⁻¹ ; RP1 RI0; ET20	42.5
3	64.75	50	20	20	2	25	7min59s	static; RP1 RI0; ET20	51.2
2	64.75	50	20	54	2	9	8min1s	static; RP1 RI0; ET20	65.1
1	64.75	50	20	54	2	9	8min1s	3.5 mL min ⁻¹ ; RP1 RI0; ET20	72.0

5.13. Additional LF NMR spectra in static conditions

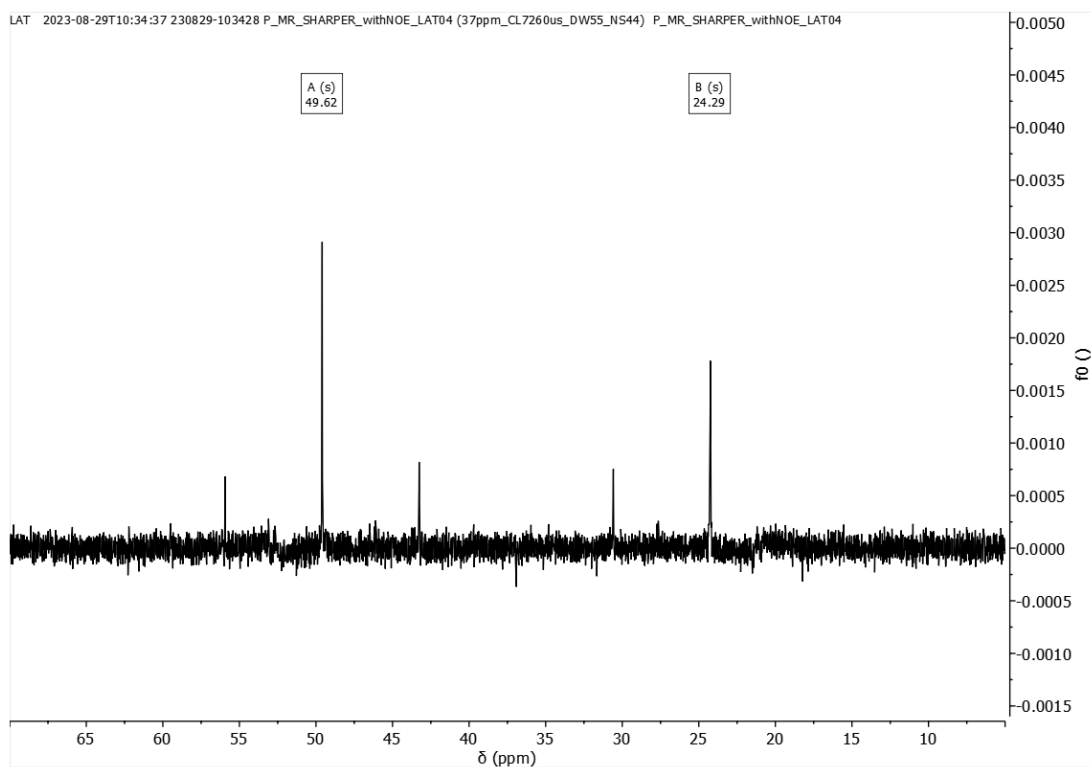


Figure A16. MR-SHARPER ^{31}P NMR spectrum of a mixture of $[\text{Rh}((R,R)\text{-DIPAMP})(\text{NBD})]\text{BF}_4$ (107 mM in $\text{DCM-}d_2$) and $[\text{Rh}(\text{DPPB})(\text{COD})]\text{BF}_4$ (106 mM in $\text{DCM-}d_2$). One of the most distorted spectra I have recorded with a relatively long chunk length ($\text{CL} = 7.26$ ms).

5.14. Additional parameters of SHARPER and traditional ^{31}P NMR spectra

Abbreviations used: total number of points (TP); number of points (NP); dwell time (DW); number of scans (NS); acquisition time (AT); repetition time (RT); removed points (RP); imaginary part not removed from FID (RI0) *vs* imaginary part removed from FID (RI1); homospoil amplitude (HA); homospoil duration (HD); acquisition delay (AD); echo time (ET); chunk length (CL).

Table A7. Experimental and processing parameters.

Figure	#	Experimental parameters									Processing parameters								
		Offset (ppm)	TP	NP	DW (μs)	NS	AT (s) /CL (ms)	RT (s)	Experiment time	Others	Zero filling	Exp. Apod. (Hz)	Noise region (ppm)	Peak region (ppm)	SNR	Factor	Peak region' (ppm)	SNR'	Factor'
45	I	49.66	66k	16	50	8	1.6	25	2min58s	RP1 RI0	2 (128K)	0.2	100-200	49-50	316	9	-	-	-
	H	49.66	66k	16	50	8	1.6	25	2min58s	RP1 RI0	2 (128K)	0.2	100-200	49-50	242	7	-	-	-
	G	49.7	66k	16	50	8	1.6	25	2min58s	gaussian 5ms - 31dB; HA10k, HD600us; AD50us; RP1 RI0	2 (128K)	0.2	100-200	49-50	215	6	-	-	-
	F	49.66	66k	16	50	8	1.6	25	2min58s	gaussian 5ms - 31dB; HA10k, HD600us; AD50us; RP1 RI0	2 (128K)	0.2	100-200	49-50	177	5	-	-	-
	E	49.7	66k	16	50	8	1.6	25	2min58s	gaussian 10ms - 37.5dB; HA10k, HD600us; AD50us; RP1 RI0	2 (128K)	0.2	100-200	49-50	116	3	-	-	-
	D	49.66	66k	16	50	8	1.6	25	2min58s	gaussian 10m - 37.5dB; HA10k, HD600us; AD50us; RP1 RI0	2 (128K)	0.2	100-200	49-50	97	3	-	-	-
	C	50	-	66k	25	8	1.7	15	1min50s	-	2 (128K)	0.2	100-200	46-53	34	1	-	-	-
	B	37	-	66k	25	8	1.7	15	1min50s	-	2 (128K)	0.2	100-200	46-53	27	-	-	-	-
	A	37	-	66k	25	8	1.7	15	1min50s	-	2 (128K)	0.2	100-200	46-53	n.a.	-	-	-	-

Table A7. (continued).

Figure	#	Experimental parameters										Processing parameters							
		Offset (ppm)	TP	NP	DW (μs)	NS	AT (s) /CL (ms)	RT (s)	Experiment time	Others	Zero filling	Exp. Apod. (Hz)	Noise region (ppm)	Peak region (ppm)	SNR	Factor	Peak region' (ppm)	SNR'	Factor'
46	D	49.67	66k	11	55	8	1.21	25	2min58s	RP1 RI0	2 (128K)	0.2	100-200	49-50	326	10	-	-	-
	C	36.97	66k	22	55	8	2.42	25	2min58s	RP1 RI0	2 (128K)	0.2	100-200	49-50	192	6	-	-	-
	B	24.27	66k	22	55	8	2.42	25	2min58s	RP1 RI0	2 (128K)	0.2	100-200	49-50	137	4	-	-	-
	A	50	-	66k	50	8	3.3	15	1min50s	-	2 (128K)	0.2	100-200	46-53	34	1	-	-	-
47	D	36.92	66k	60	20	8	2.4	25	2min58s	RP1 RI0	4 (256K)	0.3	100-200	49-50	206	4	23.5-24.5	202	4
	C	24.27	66k	40	15	8	1.2	25	2min58s	RP1 RI0	4 (256K)	0.3	100-200	49-50	145	3	23.5-24.5	226	5
	B	49.66	66k	40	15	8	1.2	25	2min58s	RP1 RI0	4 (256K)	0.3	100-200	49-50	261	5	23.5-24.5	190	4
	A	37	-	66k	-	8	3.3	15	1min50s	-	4 (256K)	0.3	100-200	46-53	52	1	20-28	45	1
48	G	64.56	66k	72	14	52	2.02	25	21min19s	RP1 RI0; ET20	2 (128K)	0.3	100-200	49-50	62	-	-	-	-
	F	65	-	66k	50	52	3.3	15	12min51s	-	2 (128K)	0.3	100-200	46-53	15	-	-	-	-
	E	64.56	66k	72	14	32	2.02	25	13min0s	RP1 RI0; ET20	2 (128K)	0.3	100-200	49-50	48	-	-	-	-
	D	65	-	66k	50	32	3.3	15	7min50s	-	2 (128K)	0.3	100-200	46-53	12	-	-	-	-
	C	64.56	66k	72	14	20	2.02	25	7min59s	RP1 RI0; ET20	2 (128K)	0.3	100-200	49-50	36	-	-	-	-
	B	65	-	66k	50	14	3.3	15	3min50s	-	2 (128K)	0.3	100-200	46-53	7	-	-	-	-
	A	64.56	66k	72	14	10	2.02	25	3min49s	RP1 RI0; ET20	2 (128K)	0.3	100-200	49-50	27	-	-	-	-
49	B	65	-	66k	50	32	3.3	15	7min50s	-	4 (256K)	0.3	100-200	46-53	10	-	manual selection	5	-
	A	64.56	66k	72	14	20	2.02	25	7min59s	RP1 RI0; ET20	4 (256K)	0.3	100-200	49-50	36	4	79-80	21	4

Table A7. (continued).

Figure	#	Experimental parameters										Processing parameters							
		Offset (ppm)	TP	NP	DW (μs)	NS	AT (s) /CL (ms)	RT (s)	Experiment time	Others	Zero filling	Exp. Apod. (Hz)	Noise region (ppm)	Peak region (ppm)	SNR	Factor	Peak region' (ppm)	SNR'	Factor'
50	B	65	-	66k	50	4	3.3	15	51s	-	4 (256K)	0.3	100-200	46-53	n.a.	-	76-84	n.a.	-
	A	64.56	66k	72	14	3	2.02	25	54s	RP1 RI0; ET20	4 (256K)	0.3	100-200	49-50	12	n.a.	79-80	9	n.a.
51	D	64.75	66k	50	20	20	2.0	9	2min55s	RP1 RI0; ET20	2 (128K)	0.2	100-200	49-50	42.5	-	-	-	-
	C	64.75	66k	59	17	20	2.0	9	2min55s	RP1 RI0; ET20	2 (128K)	0.2	100-200	49-50	42.1	-	-	-	-
	B	49.5	66k	50	20	20	2.0	9	2min55s	RP1 RI0; ET20	2 (128K)	0.2	100-200	49-50	44.7	-	-	-	-
	A	49.5	66k	59	17	20	2.0	9	2min55s	RP1 RI0; ET20	2 (128K)	0.2	100-200	49-50	46.0	-	-	-	-
52	B	65	-	66k	25	10	1.6	6	59s	flow	2 (128K)	0.2	100-200	46-53	n.a.	-	76-84	n.a.	-
	A	64.75	66k	50	20	7	2.02	9	58s	RP1 RI0; ET20; flow	2 (128K)	0.2	100-200	49-50	26.2	-	79.5-80.5	11.9	-

5.15. Academic Curriculum Vitae

Laura Tadiello

Address Breesen 31, 18299 Laage, Germany

E-mail laura.tadi96@gmail.com

Date of birth May 6th, 1996

Nationality Italian

WORK EXPERIENCE

Apr 2021 – Jun 2024 PhD student in chemistry

Leibniz Institute for Catalysis (LIKAT), Albert-Einstein-Straße 29A, 18059 Rostock, Germany

Method development for reaction monitoring (inorganic and analytical chemistry).

Adaptability (engineering, catalysis, programming) and autonomy.

Relationship with stakeholders and organization with collaboration partners.

Responsibility as PhD and postdoc representative.

May 2023 – Jul 2023 Visiting PhD student

University of York, YO10 5DD York, United Kingdom

Advanced pulse programming (benchtop NMR spectrometer).

Oral and poster presentations at international conferences and symposia.

Nov 2020 – Mar 2021 Research scientist

Leibniz Institute for Catalysis (LIKAT), Albert-Einstein-Straße 29A, 18059 Rostock, Germany

Finalization of the Erasmus project on homogeneous catalysis.

EDUCATION

Oct 2018 – Oct 2020 Master of Science in chemistry – Mark 110/110 cum laude

University of Milan (UNIMI), via Golgi 19, 20133 Milan, Italy

Homogeneous catalysis for chemo- and enantioselective transformations.

Schlenk and glovebox techniques, high pressure autoclaves manipulation.

Jun 2020 – Sep 2020 Erasmus student

Leibniz Institute for Catalysis (LIKAT), Albert-Einstein-Straße 29A, 18059 Rostock, Germany

Catalysis with abundant metal complexes.

Communication skills in an international environment.

Oct 2016 – Dec 2018 Bachelor of Science in chemistry – Mark 107/110 cum laude

University of Milan (UNIMI), via Golgi 19, 20133 Milan, Italy

Synthesis of intermediate and final products for catalytic applications.

Analytical chemistry (*e.g.*, GC, HPLC, IR, MS, NMR).

PUBLICATIONS

Manuscripts L. Tadiello, M. E. Halse, T. Beweries, Improved *on-line* benchtop ³¹P NMR reaction monitoring *via* multi resonance SHARPER, submitted manuscript.

L. Tadiello, H.-J. Drexler, T. Beweries, Low-field flow ³¹P NMR spectroscopy for organometallic chemistry: *on-line* analysis of rhodium diphosphine complexes, *Organometallics* **2022**, *41*, 2833–2843.

L. Tadiello, T. Gandini, B. M. Stadler, S. Tin, H. Jiao, J. G. de Vries, L. Pignataro, C. Gennari, Regiodivergent reductive opening of epoxides by catalytic hydrogenation promoted by a (cyclopentadienone)iron complex, *ACS Catal.* **2022**, *12*, 235–246.

CONFERENCES

Awards & Honours Poster prize, issued by 17. Koordinationschemie-Treffen, Jena (Germany), September **2022**.

Oral presentations L. Tadiello, M. Halse, T. Beweries, Low-field flow ^{31}P NMR for organometallic chemistry, Small Molecule NMR (SMASH) conference, Baveno (Italy), September **2023**.

L. Tadiello, M. Halse, T. Beweries, Low-field flow ^{31}P NMR reaction monitoring of highly air-sensitive organometallic complexes, RSC NMR Discussion Group (NMRDG) meeting, Leicester (United Kingdom), June **2023**.

L. Tadiello, B. M. Stadler, S. Tin, J. G. De Vries, L. Pignataro, C. Gennari, Catalytic hydrogenation promoted by (cyclopentadienone)iron complexes for the reductive opening of epoxides, ACS Spring meeting 2021, online, April **2021**.

Poster presentations L. Tadiello, H.-J. Drexler, M. Halse, T. Beweries, Low-Field Flow ^{31}P NMR Reaction Monitoring of Highly Air-Sensitive Organometallic Complexes, Small Molecule NMR (SMASH) conference, Baveno (Italy), September **2023**.

L. Tadiello, H.-J. Drexler, T. Beweries, Low-field flow ^{31}P NMR spectroscopy for *on-line* analysis of highly air-sensitive organometallic complexes, Quantitative NMR Methods for Reaction and Process Monitoring (NMRPM) symposium, Kaiserslautern (Germany), May **2023**.

L. Tadiello, H.-J. Drexler, T. Beweries, Low-field flow ^{31}P NMR spectroscopy for organometallic chemistry: *on-line* analysis of rhodium diphosphine complexes, 17. Koordinationschemie-Treffen, Jena (Germany), September **2022**.

L. Tadiello, H.-J. Drexler, T. Beweries, Low-field flow ^{31}P NMR spectroscopy for organometallic chemistry: *on-line* analysis of rhodium diphosphine complexes, International Conference on Organometallic Chemistry (ICOMC), Prague (Czech Republic), July **2022**.

L. Tadiello, H.-J. Drexler, T. Beweries, Low-field flow ^{31}P NMR spectroscopy for organometallic chemistry: *on-line* analysis of rhodium diphosphine complexes, ComBioCat symposium, Rostock (Germany), June **2022**.

L. Tadiello, B. M. Stadler, S. Tin, J. G. de Vries, L. Pignataro, C. Gennari, Catalytic hydrogenation promoted by (cyclopentadienone)iron complexes for the reductive opening of epoxides, Jahrestreffen Deutscher Katalytiker, online, March **2021**.

SKILLS

Languages Italian (native), English (fluent), German (intermediate).

Personal skills Initiative, flexibility and willingness to learn, fundamental for growing in my future role.
Communication and presentation skills in intercultural contexts, crucial for delivering clear and meaningful ideas.
Prioritization of milestones and mediation, key for achieving shared goals.

Certificates Leadership skills (in German), Graduate Academy of Rostock, March **2024**.
Project management (in German), Graduate Academy of Rostock, February **2023**.
Presentation skills (in English), Graduate Academy of Rostock, November **2022**.

Lab skills Inert conditions for highly oxygen-sensitive organometallic complexes.
Synthesis and purification of organic and organometallic compounds.

Digital skills Chemistry programs: ChemDraw, MestReNova, TopSpin.
Computational chemistry programs: Gaussian; Gaussview, Titan, gNMR.
Programming language: Prospa.
Other programs: Word, Excel, Power Point, Origin.

6. References

- 1 Pellecchia, M.; Sem, D.; Wüthrich, K. *Nat. Rev. Drug. Discov.* **2002**, *1*, 211-219.
- 2 Hatzakis, E. *Compr. Rev. Food Sci. Food Saf.* **2019**, *18*, 189-220.
- 3 Moser, E.; Laistler, E.; Schmitt, F.; Kontaxis, G. *Front. Phys.* **2017**, *5*: 33.
- 4 van Beek, T. A. *Phytochem. Anal.* **2021**, *32*, 24-37.
- 5 Grootveld, M.; Percival, B.; Gibson, M.; Osman, Y.; Edgar, M.; Molinari, M.; Mather, M. L.; Casanova, F.; Wilson, P. B. *Anal. Chim. Acta* **2019**, *1067*, 11-30.
- 6 Danieli, E.; Perlo, J.; Blümich, B.; Casanova, F. *Angew. Chem. Int. Ed.* **2010**, *49*, 4133-4135.
- 7 Caramelli, D.; Granda, J. M.; Mehr, S. H. M.; Cambié, D.; Henson, A. B.; Cronin, L. *ACS Cent. Sci.* **2021**, *7*, 1821-1830.
- 8 Hoult, D. I. *J. Magn. Res.* **1976**, *21*, 337-347.
- 9 Mo, H.; Raftery, D. *J. Magn. Res.* **2008**, *190*, 1-6.
- 10 Berger, S.; Braun, S. *200 and More NMR Experiments, A Practical Course*, Wiley VCH, Weinheim, 2004, p. 506.
- 11 Gouilleux, B.; Charrier, B.; Akoka, S.; Giraudeau, P. *Magn. Res. Chem.* **2017**, *55*, 91-98.
- 12 Riegel, S. D.; Leskowitz, G. M. *Trends Anal. Chem.* **2016**, *83*, 27-38.
- 13 Isaac-Lam, M. F. *J. Chem. Educ.* **2014**, *91*, 1264-1266.
- 14 Giraudeau, P.; Felpin, F.-X. *React. Chem. Eng.* **2018**, *3*, 399-413.
- 15 Bornemann-Pfeiffer, M.; Wolf, J.; Meyer, K.; Kern, S.; Angelone, D.; Leonov, A.; Cronin, L.; Emmerling, F. *Angew. Chem. Int. Ed.* **2021**, *60*, 23202-23206.
- 16 Gouilleux, B.; Christensen, N. V.; Malmos, K. G.; Vosegaard, T. *Anal. Chem.* **2019**, *91*, 3035-3042.
- 17 Bogun, B.; Moore, S. *Forensic Sci. Int.* **2017**, *278*, 68-77.

- 18 Maschmeyer, T.; Yunker, L. P. E.; Hein, J. E. *React. Chem. Eng.* **2022**, *7*, 1061-1072.
- 19 Friebel, A.; von Harbou, E.; Münnemann, K.; Hasse, H. *Ind. Eng. Chem. Res.* **2019**, *58*, 18125-18133.
- 20 Neudert, R.; Ströfer, E.; Bremser, W. *Magn. Res. Chem.* **1986**, *24*, 1089-1092.
- 21 Foley, D. A.; Dunn, A. L.; Zell, M. T. *Magn. Res. Chem.* **2016**, *54*, 451-456.
- 22 Jacquemmoz, C.; Giraud, F.; Dumez, J.-N. *Analyst* **2020**, *145*, 478-485.
- 23 a) Scheithauer, A.; Brächer, A.; Grützner, T.; Zollinger, D.; Thiel, W. R.; von Harbou, E.; Hasse, H. *Ind. Eng. Chem. Res.* **2014**, *53*, 17589-17596; b) Buser, J. Y.; McFarland, A. D. *Chem. Commun.* **2014**, *50*, 4234-4237; c) Foley, D. A.; Wang, J.; Maranzano, B.; Zell, M. T.; Marquez, B. L.; Xiang, Y.; Reid, G. L. *Anal. Chem.* **2013**, *85*, 8928-8932; d) Christianson, M. D.; Tan, E. H. P.; Landis, C. R. *J. Am. Chem. Soc.* **2010**, *132*, 11461-11463; e) Bernstein, M. A.; Štefinović, M.; Sleight, C. J. *Magn. Res. Chem.* **2007**, *45*, 564-571; f) Maiwald, M.; Fischer, H. H.; Kim, Y.-K.; Albert, K.; Hasse, H. *J. Magn. Res.* **2004**, *166*, 135-146; g) Bayer, E.; Albert, K.; Nieder, M.; Grom, E.; Wolff, G.; Rindlisbacher, M. *Anal. Chem.* **1982**, *54*, 1747-1750; h) Bayer, E.; Albert, K.; Nieder, M.; Grom, E.; Keller, T. *J. Chromatogr. A* **1979**, *186*, 497-507.
- 24 Hall, A. M. R.; Chouler, J. C.; Codina, A.; Gierth, P. T.; Lowe, J. P.; Hintermair, U. *Catal. Sci. Technol.* **2016**, *6*, 8406-8417.
- 25 a) Bara-Estaún, A.; Lyall, C. L.; Lowe, J. P.; Pringle, P. G.; Kamer, P. C. J.; Franke, R.; Hintermair, U. *Faraday Discuss.* **2021**, *229*, 422-442; b) Vrijsen, J. H.; Thomlinson, I. A.; Levere, M. E.; Lyall, C. L.; Davidson, M. G.; Hintermair, U.; Junkers, T. *Polym. Chem.* **2020**, *11*, 3546-3550; c) Hall, A. M. R.; Dong, P.; Codina, A.; Lowe, J. P.; Hintermair, U. *ACS Catal.* **2019**, *9*, 2079-2090; d) Berry, D. B. G.; Codina, A.; Clegg, I.; Lyall, Catherine L.; Lowe, J. P.; Hintermair, U. *Faraday Discuss.* **2019**, *220*, 45-57.
- 26 Maschmeyer, T.; Prieto, P. L.; Grunert, S.; Hein, J. E. *Magn. Res. Chem.* **2020**, *58*, 1234-1248.
- 27 Bara-Estaún, A.; Harder, M. C.; Lyall, C. L.; Lowe, J. P.; Suturina, E.; Hintermair, U. *Chem. Eur. J.* **2023**, *29*, e202300215.
- 28 Baumann, B.; Mansel, S.; Heller, D.; Borns, S. *Magn. Res. Chem.* **1997**, *35*, 659-719.

- 29 Krüger, M. B.; Selle, C; Heller, D.; Baumann, W. *J. Chem. Eng. Data* **2012**, *57*, 1737-1744.
- 30 Hartwig, J. F., *Organotransition Metal Chemistry. From Bonding to Catalysis*. University Science Books, Sausalito, 2010.
- 31 Osborn, J. A.; Jardine, F. H.; Young, J. F.; Wilkinson, G. *J. Am. Chem Soc.* **1966**, 1711-1732.
- 32 Shapley, J. R.; Schrock, R. R.; Osborn, J. A. *J. Am. Chem. Soc.* **1969**, *91*, 2816-2817.
- 33 Crabtree, R. H.; Felkin, H.; Morris, G. E. *J. Organomet. Chem.* **1977**, *141*, 205-215.
- 34 Miyashita, A.; Yasuda, A.; Takaya, H.; Toriumi, K.; Ito, T.; Souchi, T.; Noyori, R. *J. Am. Chem. Soc.* **1980**, *102*, 7932-7934.
- 35 Noyori, R.; Ohkuma, T. *Angew. Chem. Int. Ed.* **2001**, *40*, 40-73.
- 36 Lubben, A. T.; McIndoe, J. S.; Weller, A. S. *Organometallics* **2008**, *27*, 3303-3306.
- 37 Muhr, M.; Heiß, P.; Schütz, M.; Bühler, R.; Gemel, C.; Linden, M. H.; Linden, H. B.; Fischer, R. A. *Dalton Trans.* **2021**, *50*, 9031-9036.
- 38 Glueck, D. S. *Coord. Chem. Rev.* **2008**, *252*, 2171-2179.
- 39 Jones, A. B.; Lloyd-Jones, G. C.; Uhrin, D. *Anal. Chem.* **2017**, *89*, 10013-10021.
- 40 Dickson, C. L.; Peat, G.; Rossetto, M.; Halse, M. E.; Uhrin, D. *Chem. Commun.* **2022**, *58*, 5534-5537.
- 41 Davy, M.; Dickson, C. L.; Wei, R.; Uhrin, D.; Butts, C. P. *Analyst* **2022**, *147*, 1702-1708.
- 42 Silva Terra, A. I.; Rossetto, M.; Dickson, C. L.; Peat, G.; Uhrin, D.; Halse, M. E. *ACS Meas. Sci. Au* **2023**, *3*, 73-81.
- 43 Gouilleux, B.; Farjon, J.; Giraudeau, P. *J. Magn. Res.* **2020**, *319*, 106810.
- 44 Zangger, K.; Sterk, H. *J Magn. Res.* **1997**, *124*, 486-489.
- 45 Castañar, L. *Magn. Res. Chem.* **2017**, *55*, 47-53.

- 46 Maschmeyer, T.; Russell, D. J.; Napolitano, J. G.; Hein, J. E. *Magn. Res. Chem.* **2023**, 1-13.
- 47 Tadiello, L.; Drexler, H.-J.; Beweries, T. *Organometallics* **2022**, 41, 2833-2843.
- 48 Alberico, E.; Möller, S.; Horstmann, M.; Drexler, H.-J.; Heller, D. *Catalysts* **2019**, 9, 582.
- 49 Meißner, A.; Alberico, E.; Drexler, H.-J.; Baumann, W.; Heller, D. *Catal. Sci. Technol.* **2014**, 4, 3409-3425.
- 50 Puts, G. J.; Crouse, P.; Ameduri, B. M. *Chem. Rev.* **2019**, 119, 1763-1805.
- 51 Saib, A.; Bara-Estaún, A.; Harper, O. J.; Berry, D. B. G.; Thomlinson, I. A.; Broomfield-Tagg, R.; Lowe, J. P.; Lyall, C. L.; Hintermair, U. *React. Chem. Eng.* **2021**, 6, 1548-1573.
- 52 Borys, A. M. *Organometallics* **2023**, 42, 182-196.
- 53 Meißner, A.; Preetz, A.; Drexler, H.-J.; Baumann, W.; Spannenberg, A.; König, A.; Heller, D. *ChemPlusChem* **2015**, 80, 169-180.
- 54 Heller, D.; Borns, S.; Baumann, W.; Selke, R. *Chem. Ber.* **1996**, 129, 85-89.
- 55 Cao, L.-Y.; Luo, J.-N.; Yao, J.-S.; Wang, D.-K.; Dong, Y.-Q.; Zheng, C.; Zhuo, C.-X. *Angew. Chem. Int. Ed.* **2021**, 60, 15254-15259.
- 56 Heller, D. *Habilitationsschrift*, E.-M.-Arndt-Universität Greifswald, 1998.
- 57 Laye, C.; Lusseau, J.; Robert, F.; Landais, Y. *Adv. Synth. Catal.* **2021**, 363, 3035-3043.
- 58 Fischer, C.; König, A.; Meißner, A.; Thede, R.; Selle, C.; Pribbenow, C.; Heller, D. *Eur. J. Inorg. Chem.* **2014**, 5849-5855.
- 59 Bunten, K. A.; Farrar, D. H.; Poë, A. J.; Lough, A. *Organometallics* **2002**, 21, 3344-3350.
- 60 Preetz, A.; Baumann, W.; Fischer, C.; Drexler, H.-J.; Schmidt, T.; Thede, R.; Heller, D. *Organometallics* **2009**, 28, 3673-3677.
- 61 Findeisen, M.; Brand, T.; Berger, S. *Magn. Res. Chem.* **2007**, 45, 175-178.
- 62 Hoffman, R. E. *Magn. Res. Chem.* **2006**, 44, 606-616.

- 63 Findeisen, M.; Berger, S. *50 and More Essential NMR Experiments, A Detailed Guide*, Wiley VCH, Weinheim, 2014, p. 257.
- 64 Brown, J. M.; Chaloner, P. A.; Kent, A. G.; Murrer, B. A.; Nicholson, P. N.; Parker, D.; Sidebottom, P. J. *J. Organomet. Chem.* **1981**, *216*, 263-276.
- 65 Preetz, A.; Fischer, C.; Kohrt, C.; Drexler, H.-J.; Baumann, W.; Heller, D., *Organometallics* **2011**, *30*, 5155-5159.
- 66 Halpern, J.; Riley, D. P.; Chan, A. S. C.; Pluth, J. J. *J. Am. Chem. Soc.* **1977**, *99*, 8055-8057.
- 67 Limited spectroscopic information could be found in: Anderson, M. P.; Pignolet, L. H. *Inorg. Chem.* **1981**, *20*, 4101-4107.
- 68 Similar complexes, with different diphosphine ligand, can be found in: a) McKay, A. I.; Barwick-Silk, J.; Savage, M.; Willis, M. C.; Weller, A. S. *Chem. Eur. J.* **2020**, *26*, 2883-2889; b) Fischer, C.; Thede R., Baumann, W.; Drexler, H.-J.; König, A.; Heller, D. *ChemCatChem* **2016**, *8*, 352-356; c) Pike, S. D.; Pernik, I.; Theron, R.; McIndoe, J. S.; Weller, A. S. *J. Organomet. Chem.* **2015**, *784*, 75-83; d) Fischer, C.; Thede, R.; Drexler, H.-J.; König, A.; Baumann, W.; Heller, D. *Chem. Eur. J.* **2012**, *18*, 11920-11928; e) Heller, D.; Drexler, H.-J.; Spannenberg, A.; Heller, B.; You, J.; Baumann, W. *Angew. Chem. Int. Ed.* **2002**, *41*, 777-780.
- 69 Selke, R.; Pracejus, H. *J. Mol. Catal.* **1986**, *37*, 213-225.
- 70 Sheldrick, G. M. "SHELXS 97, Program for the Solution of Crystal Structure," University of Göttingen, Göttingen, **1990**.
- 71 Sheldrick, G. M. *Acta Crystallogr.* **2015**, *C71*, 3-8.
- 72 Sheldrick, G. M. *SADABS Version 2*, University of Göttingen, Germany, **2004**.
- 73 Anderson, M. P.; Pignolet, L. H. *Inorg. Chem.* **1981**, *20*, 4101-4107.
- 74 For the method of *on-line* registration of gas consumption under isobaric conditions: de Vries, J. G.; Elsevier, C.J. *Handbook of Homogeneous Hydrogenation*, Wiley VCH, Weinheim, 2007, p. 257.